3-2006

Classification Characteristics of Carbon Nanotube Polymer Composite Chemical Vapor Detectors

Huynh A. Hinshaw

CLASSIFICATION CHARACTERISTICS OF CARBON NANOTUBE POLYMER COMPOSITE CHEMICAL VAPOR DETECTORS

THESIS

Huynh A. Hinshaw, Captain, USAF

AFIT/GOR/ENS/06-10

DEPARTMENT OF THE AIR FORCE
AIR UNIVERSITY

AIR FORCE INSTITUTE OF TECHNOLOGY

Wright-Patterson Air Force Base, Ohio

APPROVED FOR PUBLIC RELEASE; DISTRIBUTION UNLIMITED

AFIT/GOR/ENS/06-10

CLASSIFICATION CHARACTERISTICS OF CARBON NANOTUBE POLYMER COMPOSITE CHEMICAL VAPOR DETECTORS

THESIS

Presented to the Faculty

Department of Operational Sciences

Graduate School of Engineering and Management

Air Force Institute of Technology

Air University

Air Education and Training Command

In Partial Fulfillment of the Requirements for the

Degree of Master of Science in Operations Research

Huynh A. Hinshaw, B.S.

Captain, USAF

March 2006

AFIT/GOR/ENS/06-10

CLASSIFICATION CHARACTERISTICS OF CARBON NANOTUBE POLYMER COMPOSITE CHEMICAL VAPOR DETECTORS

Huynh A. Hinshaw, B.S.

Captain, USAF

Approved:

______________________________ ____________

Dr. Kenneth W. Bauer date

Thesis Advisor

______________________________ ____________

Dr. John O. Miller date

Committee Member

AFIT/GOR/ENS/06-10

Abstract

The first step in combating a chemical weapons threat is contamination avoidance. This is accomplished by the detection and identification of chemical agents. The Air Force has several instruments to detect chemical vapors, but is always looking for lighter, faster, and more accurate technology for a better capability.

This research is focused on using carbon nanotube polymer composite sensors for chemical detection. More specifically, models are developed to classify three sets of sensor data according to vapor using various multivariate techniques. Also, prediction models of a mixed sensor output are developed using neural networks and regression analysis. The classifiers developed are able to accurately classify three vapors for a specific set of data, but have problems when tested against data from aged sensors as well as data generated from a different set of new sensors. These results indicate that further research should be conducted to ensure accuracy in identifying chemical vapors using these types of sensors.

Acknowledgments

I would like to express my sincere appreciation to my advisor, Dr. Kenneth Bauer, for his guidance and encouragement throughout this entire process. His expertise and willingness to help were greatly appreciated. I would also like to thank Dr. J.O. Miller for being a reader on this "masterpiece" and for his help along the way. Much thanks also goes to Dr. Rajesh Naik and Dr. Liming Dai for giving me the idea for the thesis and to Dr. Lawrence Brott for providing much needed information, so I could understand the subject matter. I want to give special thanks to Dr. Wei Chen for his hard work in conducting the experiments that supplied the data for this effort. There would be no analysis and results if not for him. Additionally, thanks to Dr. Marcus Perry for his hours of help with regression.

I would like to also thank Apex Community Church and "The Least Squares" for caring for my spiritual health while here at AFIT. Additionally, I would like to express my gratitude to "The Council" for Tom Jones, Neil Diamond, and the other good times at AFIT.

Last, but not least, I would like to thank my Lord and Savior, Jesus Christ, for always reminding me of what I am in Him and for carrying me through this experience.

Huynh A. Hinshaw

Table of Contents

List of Figures

List of Tables

CLASSIFICATION CHARACTERISTICS OF CARBON NANOTUBE POLYMER COMPOSITE CHEMICAL VAPOR DETECTORS

1. Introduction

1.1 Background

Chemicals have been used in warfare for centuries. The earliest use of chemical gases against an enemy was seen during the Peloponnesian War when the Spartans gained control of an Athenian fort by directing smoke into it through "hollowed out" beams (Langford, 2004:211). Ancient Chinese writings describe the use of smoke, from burning mustard and toxic vegetable matter, to deter an enemy (Langford, 2004:212). Chemical weapons use was also witnessed in World War I, where mustard gas caused more deaths than any other chemical agent (Langford, 2004:216).

After viewing the effects of such weapons, the international community placed a stigma on the use of chemical weapons in conflict. In 1993, the Chemical Weapons Convention was opened for signature and has been signed by 186 countries, including the United States. The organization established to monitor the progress of the Convention is the Organization for the Prohibition of Chemical Weapons (OPCW). According to the OPCW:

> The Convention prohibits all development, production, acquisition, stockpiling, transfer, and use of chemical weapons. It requires each State Party to destroy chemical weapons and chemical weapons production facilities it possesses, as well as any chemical weapons it may have abandoned on the territory of another State Party (OPCW, 2005).

There are 8 countries, including Egypt, North Korea, and Syria, that have not signed the Convention.

While there is progress in disarmament, open source intelligence indicates that over twenty countries have either chemical weapons programs or stockpiles. The international community has taken a stand on this issue through the Convention, but it currently only addresses nation-states. The problem with this is that waging war has changed since the days of the World Wars. We are no longer fighting nation-states, but insurgents and international terrorist groups. Now, when we go into combat, we are engaging with a sometimes unknown enemy that does not fight conventionally. Terrorist groups have already shown their willingness to use chemical weapons to induce fear in a civilian population, as seen in the sarin attack on the Tokyo subway system in 1995. If they are willing to attack civilians in this fashion, they will have no qualms about using this same method to harm our military forces.

Chemical weapons can be blood, choking, nerve, blister, tear, vomiting, or incapacitating agents. They can be easily manufactured and specific chemicals, such as hydrogen cyanide and phosgene, can be purchased commercially. Due to the proliferation of chemical weapons, it is inevitable that our forces will encounter them. Senior leaders have shown that they believe this to be a significant threat, as seen by their increase in budget for weapons of mass destruction (WMD) countermeasures by $2.1 billion for FY06-11 (DoD, 2005).

The first step in battling the chemical weapons threat is "contamination avoidance" (DoD, 2005). Contamination avoidance includes the ability to detect a chemical agent and identify it. This thesis focuses on chemical agent vapor detection. The military has several devices that it currently uses to accomplish this. The Chemical Agent Monitor (CAM), Improved Chemical Agent Monitor (ICAM), Automatic Chemical Agent Detection Alarm (ACADA), HAPSITE, MINICAMS, TVA-1000, and various colorimetric devices are the current fielded capabilities. A device called the Joint Chemical Agent Detector (JCAD) was developed to provide a handheld detection capability to the warfighter and the Joint NBC Reconnaissance System (JNBCRS) was developed to provide reconnaissance in areas where NBC employment is suspected. These technologies will be fully discussed in Chapter 2.

An emerging technology that could also be used to address this issue is the use of carbon nanotube polymer composite sensors for detection. Their small size, low power consumption, and low cost make them a good option for research and development in this area. Figure 1 shows examples of how this technology could be potentially employed.

UAV

Hand-held Detector **Mobile Platform**

Figure 1. Potential carbon nanotube polymer composite sensor detector platforms (AFRL, 2005).

This research focuses on carbon nanotube polymer composite sensors, more specifically, identifying classifiers that will discriminate between different chemicals. The result is a study into whether this technology is a viable option for detecting and identifying chemical vapors.

1.2 Research Problem

While the Air Force has several capabilities available for chemical vapor detection, it continues to search for faster, lighter, and lower cost alternatives that provide better accuracy in the field. This thesis considered carbon nanotube polymer composite sensor technology as a possible alternative.

1.3 Research Objective

The objective of this thesis was to take existing sensor data for a number of chemicals that have interacted with different polymer sensors and develop algorithms to identify the chemical. The data was also used to investigate whether individual polymer sensor data sets can be used to predict the behavior of a mixed polymer sensor. Several multivariate analysis techniques, such as discriminant/classification analysis, neural networks, and regression analysis were considered.

1.4 Overview

Chapter 2 provides a literature review discussing current Air Force capabilities and previous research on the chemical detection capability of carbon nanotube polymer composite sensors. Chapter 3 discusses the methods used to classify and analyze the sensor data, while Chapter 4 provides the numerical analysis and results of the study. Chapter 5 presents the conclusion of the study, how this research is relevant to the Air Force, and recommendations for further research.

2. Literature Review

This chapter presents a literature review that focuses on chemical vapor detection technologies and multivariate analysis techniques. Section 2.1 focuses on the technologies currently being used or developed by the U.S. Air Force (USAF). Section 2.2 includes information on carbon nanotube polymer composite detectors and previous research into their chemical detection capability. Section 2.3 reviews discriminant analysis, Section 2.4 neural network techniques, and Section 2.5 regression analysis, and how they can be used to identify different chemicals.

2.1 Current and Developing Military Technology for Chemical Vapor Detection

Current detection devices are bulky and subject to false readings. Also, most do not provide information on the concentration of a detected chemical agent. Developing technology has attempted to resolve these issues, but several difficulties continue to exist.

2.1.1 Current Fielded Capability

The U.S. Air Force (USAF) currently uses the following technologies for chemical vapor detection: colorimetry, ion mobility spectrometry (IMS), gas chromatography with mass spectrometry (GC/MS), and photoionization/flame ionization.

Colorimetric sensors consist of litmus paper, or color spot, tests. This is the least expensive method, although rather slow for early warning detection, taking about 15-20 minutes to detect various agents (Hill and Martin, 2002:2283). These sensors are also lightweight and easy to use. They detect chemicals through the reaction of reagents, impregnated on the paper sensor, with the air. When a chemical agent is present, the reagent and chemical react and change the color of the paper. Since different reagents react to specific chemicals, a different sensor is required for each chemical to be detected. This is the main disadvantage of this technology, but it is also an advantage due to less false positives. The detector requires the human eye to act as the "signal (color) processor" (Sun and Ong, 2005:198). The problem with this is that each person's eye has a different sensitivity to color and some people have a degree of colorblindness (Sun and Ong, 2005:198). In addition, environmental factors, such as dim or bright light can inhibit the effectiveness of the sensor (Sun and Ong, 2005:198). This is why colorimetric detectors can, at best, be used for qualitative or semiqualitative analysis (Sun and Ong, 2005:198).

The current colorimetric detectors in use for vapor detection are the M256A1 Kit and the Draeger Civil Defense Simultest (CDS) Kit. The M256A1 Kit consists of M8 paper for liquid detection and M256A1 sampler detectors for vapor detection (DAF, 2003:43). The sampler detectors have pretreated test spots capable of detecting blister, blood, and nerve agents (DoD, 1999). There are two ampoules, filled with reagent, connected to each test spot via channels. When testing, the ampoules are broken and the reagents run down the channels to the pretreated test spots. The presence or absence of chemical agents can be seen by changes to the color of the test spots (DoD, 2005:A5).

The Draeger CDS Kit consists of a pump and two sets of detector tubes (Draeger, 2005). The pump is connected to the test sets and used to draw air into them. Each set contains “five different specially designed and calibrated detector tubes” (Drager, 2005). Specific color changes in the tubes will identify the presence of a chemical agent. The kit can detect nerve, blood, blister, and choking agents.

In IMS, ions are separated based on their drift velocity through an electric field (Sun and Ong, 2005:113). This detection process consists of “sample introduction, ionization, ionic drift, collision and diffusion, ion collection, and signal generation” (Sun and Ong, 2005:114). An IMS device usually contains a weak radioactive source to ionize a vapor sample once it has entered the system (Sun and Ong, 2005:118). These ions then enter the “drift region” where they move through an electric field. The time it takes them to move through the drift region depends on their shape, mass, and charge (Sun and Ong, 2005:113). While in the drift tube, ions collide with other molecules in the drift flow, which is opposite the ion flow. These collisions slow them down, but they are once again accelerated by the electric field gradient. Ions also undergo diffusion which causes the ions to disperse while in the drift tube. The ions eventually reach the ion collector where they lose their charges and a drift time is recorded. The drift time is the time it takes an ion to get to the ion collector after it has entered the drift region (Sun and Ong, 2005:121). At this time, an electrical current is generated, which is processed into a “signature” that correlates to the specific relative drift time (Sun and Ong, 2005:121). The detector compares this information to target information stored in its library and if it matches a target, an alarm is generated signifying detection of a chemical agent (Sun and Ong, 2005:115).

The advantages of IMS technology are that it can detect a chemical agent within seconds and at concentration levels as low as parts-per-billion (ppb) (Sun and Ong, 2005:113). It also can detect and identify many different vapors, even those not targeted, which can be a disadvantage due to false alarms (Sun and Ong, 2005:122). In addition, IMS devices can be small and lightweight, easy to operate since the microprocessor does most of the analysis, and purchased at low cost (Prelas and Ghosh, 2002:384).

Current IMS devices used by the USAF are the Chemical Agent Monitor (CAM), Improved Chemical Agent Monitor (ICAM), and Automatic Chemical Agent Detection Alarm (ACADA). The CAM and ICAM are both handheld devices that can detect and identify specific classes of nerve and blister agents, but ICAM is "300% more reliable, starts up 10 times faster, and the modular design is much less expensive to repair" (DoD, 2005:A2). ACADA is a man-portable system that can detect and identify all nerve agents, mustard, and lewisite (DoD, 2005:A7). It provides simultaneous detection of nerve and blister agents and can operate independently after start-up (JPEO-CBD, 2005).

GC/MS technology "uses a gas chromatograph to separate the materials in a sample into relatively pure chemical compounds, and then uses the mass spectrometer to identify the specific substance" (Langford, 2004:296). After the material is separated into different components by the GC, it will be ionized by an electron beam in the MS (EPA, 1998:iv). The ions are then subjected to an electric or magnetic field where they are further separated by mass (Langford, 2004:296). The resulting mass spectrum "serves as a molecular fingerprint that identifies the structure of the compound" (Langford, 2004:296). This technology allows for quick detection of chemical agents in the ppb to ppm range.

The HAPSITE Chemical Detection System is a portable GC/MS that is used by USAF. An agent is identified by its GC retention time and the comparison of its mass spectrum to a target compound library (EPA, 1998:6). The HAPSITE can detect, identify, and quantify chemical agents in the ppb to ppm range, but the cost of the device is in the tens of thousands and operational costs are hundreds of dollars a day (EPA, 1998:iv).

Another device used by the AF is the MINICAMS, which is a near real-time gas chromatography system. It operates by alternating between sampling, when air is pulled into the system, and analysis, when nitrogen is forced through the system to send captured analytes to the capillary column for separation (Utah, 1996:1). The separated analytes are then sent to the detector where the signal is analyzed to identify and quantify the chemical present (Utah, 1996:1). This process takes approximately three to ten minutes depending on system configuration (Utah, 1996:1). The MINICAMS can detect all nerve agents and specific blister agents in the ppb to ppm range (MINICAMS, 2006).

Lastly, photoionization/flame ionization detectors (PID/FID) identify the presence of a chemical agent by measuring the current generated by an ionized molecule (Sun and Ong, 2005:209). The difference in the two techniques is how they ionize the molecules. Photoionization does this through ultraviolet (UV) radiation, while flame ionization uses a hydrogen flame to burn molecules and produce ions (Sun and Ong, 2005:209). In both methods, the ions are subjected to an electrical field which forces them toward electrodes, where the ions release their charges on contact (Sun and Ong, 2005:209). This produces an electric current that is proportional to the amount of substance that enters the detector (Sun and Ong, 2005:212).

The USAF uses a dual PID/FID system called the TVA-1000 produced by the Foxboro Company. This equipment is used for gas survey monitoring through the sampling and measurement of the concentration of known gases. Before use, it must first be calibrated to the gas being measured (Foxboro, 1995). If the gas to be measured is different than the gas used to calibrate the system, a response factor must be used to calculate an accurate concentration reading (Foxboro, 1995). The disadvantage of this system is that it does not identify unknown gases, although a user can get an idea of what type of gas is being detected based on the different readings from the PID and FID (Foxboro, 1995).

2.1.2 Developing Capability

The Air Force has developed a sensor that makes use of Surface Acoustic Wave (SAW) technology. A piezoelectric plate is central to SAW technology. An electric field is applied to one end of the plate, which generates an acoustic wave on the surface of the plate (Hill and Martin, 2002:2282). The wave is detected at the other end of the plate and measured by the electric voltage it produces (Hill and Martin, 2002:2282). The plate itself is not capable of attracting chemicals to its surface, so a thin polymer film provides sorption sites for chemical agents (Sun and Ong, 2005:178). When a chemical sorbs onto the plate's surface, the acoustic wave's amplitude and phase changes (Hill and Martin, 2002:2282). This change is used to determine the amount of chemical deposited on the sensor. A detector can have several sensors, each with a different polymer on its surface. Each sensor will have a different response when exposed to a vapor. The chemical can be identified based on the response pattern generated from all the sensors (Sun and Ong, 2005:185). When a pattern matches one stored in the detector, the device will indicate the presence of a chemical agent (Sun and Ong, 2005:182). The SAW device is then subjected to flash heat, so the sorbed chemicals can be released and the process can start again (Sun and Ong, 2005:182).

The major advantages of this technology are that it can be made “small and portable” (Hill and Martin, 2002:2283), manufactured at low cost, and is able to detect chemicals at the ppb level (Sun and Ong, 2005:187). It is also very fast, developing a response to a detected chemical vapor within seconds (Sun and Ong, 2005:187).

A device developed that uses SAW technology is the Joint Chemical Agent Detector (JCAD). This detector uses a chemical sensor array made up of specific polymers that detect nerve, blister, and blood agent vapors (Laljer, 2005:5). It then uses a neural network algorithm to identify and quantify the detected agent (Laljer, 2005:5). When new chemical agents are discovered, the neural network algorithm can be updated with the new information to increase detection capability (Laljer, 2005:5).

Another new system, the Joint NBC Reconnaissance System (JNBCRS), is expected to be fielded in FY06. The JNBCRS detects chemical, as well as biological, radiological, and nuclear hazards and requires 3 people to operate: a driver, sensor operator, and surveyor (AFCESA, 2006). It is to be fielded as a reconnaissance system in areas where NBC weapons and toxic chemicals are suspected to have been employed (MCTSSA, 2006). The system currently carries the ACADA for chemical detection (Huber, 2006). The disadvantages of the JNBCRS are size and cost: a large vehicle is required and is costs have been quoted at approximately $900K per system and $138K for annual sustainment (AFCESA, 2006).

2.2 Carbon Nanotube Polymer Composite Sensors

Carbon nanotubes are "rolled up sheets of carbon atoms" (Nanotube, 2005). They were discovered in 1991 when Sumio Iijima was studying the deposits on a graphite cathode after arc evaporation (Harris, 1999:4). Since then, they have been involved in various research in several fields from physics to material science. Research in their use for chemical detection has been conducted since the early 2000s and continues today in various forms. Their unique electrical properties and high sensitivity allow them to detect gases and volatile organic compounds (Carbon, 2005).

Before delving into research concerning carbon nanotubes, another form of carbon must be discussed due to its contribution to chemical detection research. Carbon black is a form of carbon that is produced when materials containing carbon, such as oil or gas, are not burned completely due to lack of oxygen during the combustion process. Early research conducted with carbon black organic polymer sensors provided evidence that they had the potential to detect, identify, and quantify different organic vapors.

Research from Lonergan and associates showed that carbon black sensors could resolve common organic solvents. Their tests included taking "thin films of carbon black organic polymer composites" and placing them across two metallic leads to produce individual sensors (Lonergan et al., 1996:2298). Sensor arrays were constructed by using sensors made up of several different organic polymers to provide as much chemical diversity as possible. The carbon black supplied the electrical conductivity while the organic polymer provided the diversity to allow for detected chemical classification (Lonergan et al., 1996:2299). When a sensor was exposed to a vapor, the polymer would swell causing a change in resistance, but most interesting were the patterns in resistance change created by different vapors (Lonergan et al., 1996:2298). These patterns led to a fingerprint for each chemical that would allow for definitive classification and identification (Lonergan et al., 1996:2298). Before analysis, the team "normalized and autoscaled" the data (Lonergan et al., 1996:2305). The data was first normalized to correct for the differences in concentrations between exposures by calculating S_{ij}, the normalized signal

$$S_{ij} = \Delta R_{ij,\max} \Big/ \sum_j \Delta R_{ij,\max} \tag{1}$$

where $\Delta R_{ij,\max}$ is the maximum differential resistance change for the *j*th sensor to the *i*th exposure (Lonergan et al., 1996:2305). The normalized data was then autoscaled to account for the "differences in the dynamic ranges of the sensors" (Lonergan et al., 1996:2305). This resulted in features d_{ij} defined by

$$d_{ij} = (S_{ij} - \overline{S}_j) \big/ \sigma_j \tag{2}$$

where $\overline{S}_j$ and σ_j are the mean and standard deviation of the normalized responses (Lonergan et al., 1996:2305). The features were then analyzed using principal component analysis demonstrating that the sensors could effectively distinguish between different chemicals and their concentrations, as seen in Figure 2 (Lonergan et al., 1996:2307). Neural networks were identified as another possible option for differentiating the data.

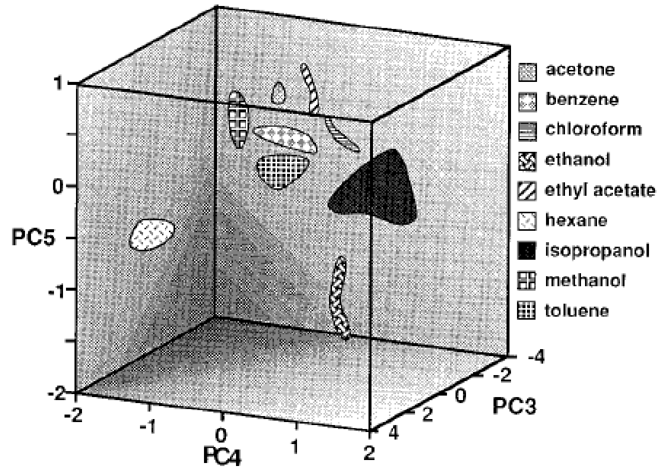

Figure 2. Results from the exposure of the 17-element array to nine solvents as represented in the third, fourth, and fifth dimensions of principal component space (Lonergan et al., 1996:2305).

Further research in 1998 focused on the sensor arrays and how they could be modified for better detection. Doleman and his team studied three areas (Doleman et al., 1998:4178):

- What vapors were not well-resolved by specific detector arrays, allowing for the change of array components to improve performance
- Optimal number of detectors needed in an array for the best performance in a specific task
- Performance of various types of detectors (bulk organic conducting polymers vs. carbon black polymer composites vs. tin oxide detectors)

Using the Fisher discriminant method, they found that the carbon black polymer composite type sensors performed best for the specific vapors tested and that for an unknown task, increasing the number of different detectors in the array will increase the array's ability to distinguish between different analytes (Doleman et al., 1998:4190).

Hopkins and Lewis also conducted tests using carbon black organic polymer composite sensors. They tested against the nerve agent simulants dimethylmethylphosphonate (DMMP) and diisopropylmethylphosponate (DIMP).

DMMP is considered a simulant for sarin and DIMP a simulant for soman (Hopkins and Lewis, 2001:887). Hopkins and Lewis found that the sensors could differentiate between these agents and other background analytes (benzene, toluene, diesel fuel, etc.) at limits of detection lower than the EC_{50} value for the nerve agents sarin and soman (Hopkins and Lewis, 2001:884). (EC_{50} is the concentration that would cause severe effects in 50% of a population exposed to the agents for 30 minutes.) They showed this was possible by performing principal component analysis, shown in Figure 3, as well as analyzing the data by pairs using Fisher linear discriminant analysis (Hopkins and Lewis, 2001:887).

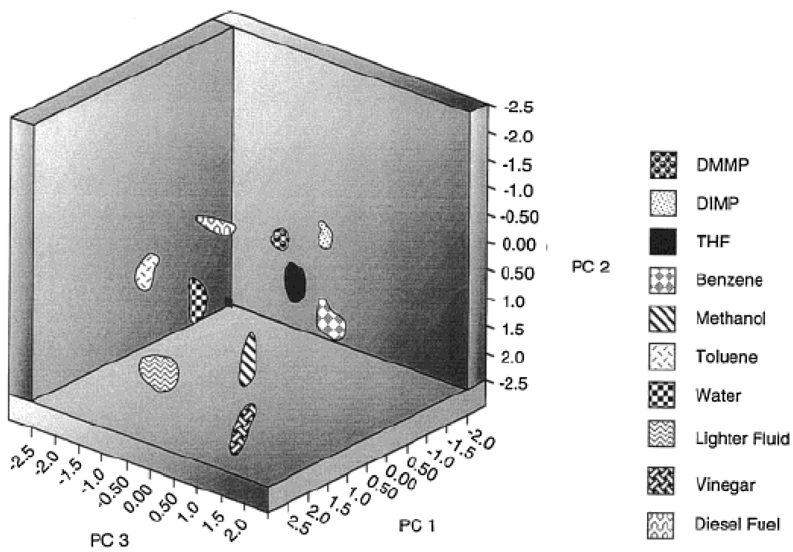

Figure 3. Data in principal component space of $\Delta R/R_b$ values produced when an eight-detector carbon black/polymer composite array was exposed to DMMP, DIMP, THF, benzene, methanol, toluene, water, lighter fluid, vinegar, or diesel fuel in an air background (Hopkins and Lewis, 2001:888).

Additionally, the Jet Propulsion Laboratory at the California Institute of Technology developed an electronic nose (ENose) using polymer-carbon black composite sensors to identify and quantify target compounds in the recycled air of spacecraft (Ryan et al., 2004:714). The ENose was composed of a 32-element sensor array with polymers chosen that could detect a set of specific compounds at exposure levels set by the National Aeronautics and Space Administration (NASA) (Ryan et al., 2004:714). The first-generation ENose used an algorithm based on Levenburg-Marquart nonlinear least-squares fitting to identify and quantify chemicals with a success rate of 85% for a single gas event (Ryan et al., 2004:719). This system was successfully tested on a space shuttle mission in 1998, but research has continued on optimizing the sensors and sensor array, as well as developing models to identify compounds the sensing arrays have not been trained for (Ryan et al., 2004:719).

In early 2000, the idea of using carbon nanotubes for chemical detection was introduced. Kong and associates showed that sensors composed of individual single-walled carbon nanotubes (SWNTs) could detect specific gases. Once exposed to nitrogen dioxide (NO_2) or ammonia (NH_3), the electrical resistance of the SWNT either dramatically increased, Figure 4a, or decreased, Figure 4b (Kong et al., 2000:622).

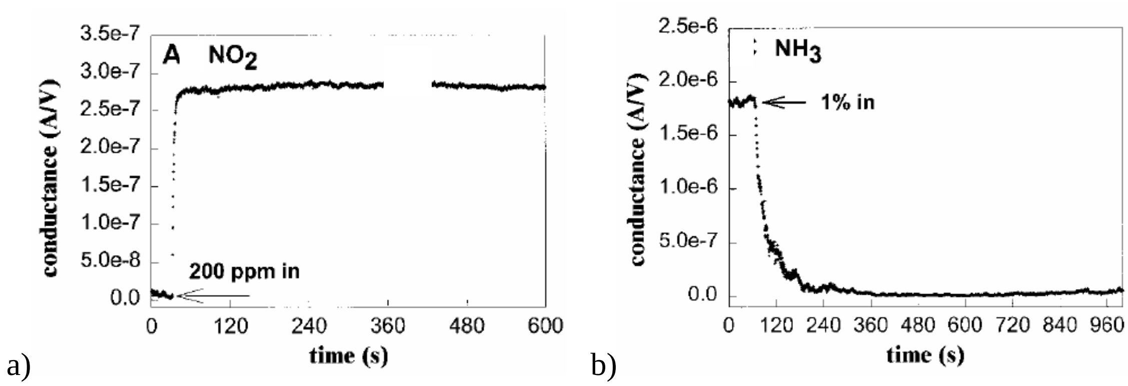

Figure 4. Electrical resistance of a semiconducting SWNT to gas molecules. (a) Conductance versus time in a 200-ppm flow. (b) Conductance versus time recorded with the same SWNT in a flow of argon (Ar) containing 1% NH_3 (Kong et al., 2000:624).

Shortly after, in 2003, a sensor platform that consisted of a network of SWNTs on interdigited electrodes (IDE) was developed for the detection of gases and organic vapors (Li et al., 2003:929). The sensors were exposed to NO_2 and nitrotoluene at different concentrations resulting in noticeable changes in resistance. Because these responses were linearly dependent on the concentrations, the detection limit of the sensors for each vapor was easily calculated by extrapolating the linear calibration curve to the point where the sensor response is considered to be the true signal, or when the signal equals three times the noise, shown in Figure 5 (Li et al., 2003:932). These sensors were found to be able to detect NO_2 and nitrotoluene to the ppb level (Li et al., 2003:932).

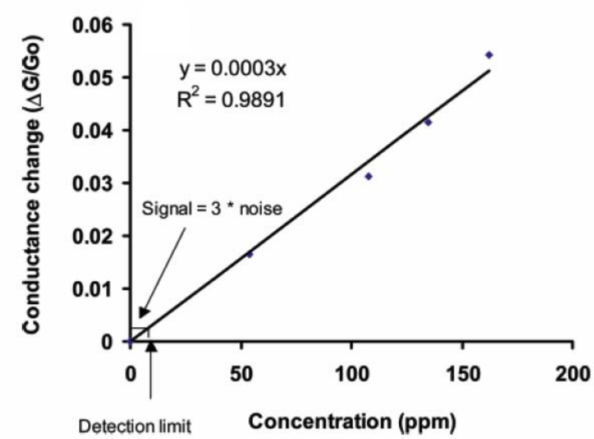

Figure 5. Calibration curve for nitrotoluene (Li et al., 2003:931).

Most recently, perpendicularly aligned carbon nanotube arrays have shown their worth as sensing materials. Wei and associates developed the sensors by dropping a polymer solution along the tube length of the aligned multiwall carbon nanotubes, as shown in Figure 6a (I) (Wei et al., 2006). The nanotube polymer composite film was then inverted (Figure 6a (II)) and gold electrodes were placed across the nanotube arrays (Figure 6a (III)) (Wei et al., 2006). The devices were then used to detect chemical vapors "through monitoring conductivity changes (Figure 6b) caused by charge-transfer interaction with gas molecules and/or inter-tube distance change induced by polymer swelling via gas adsorption" (Wei et al., 2006). Experiments conducted with these sensors showed that when exposed to various chemical vapors resistance changes occurred. The data from these tests were used for the classification studies in this thesis.

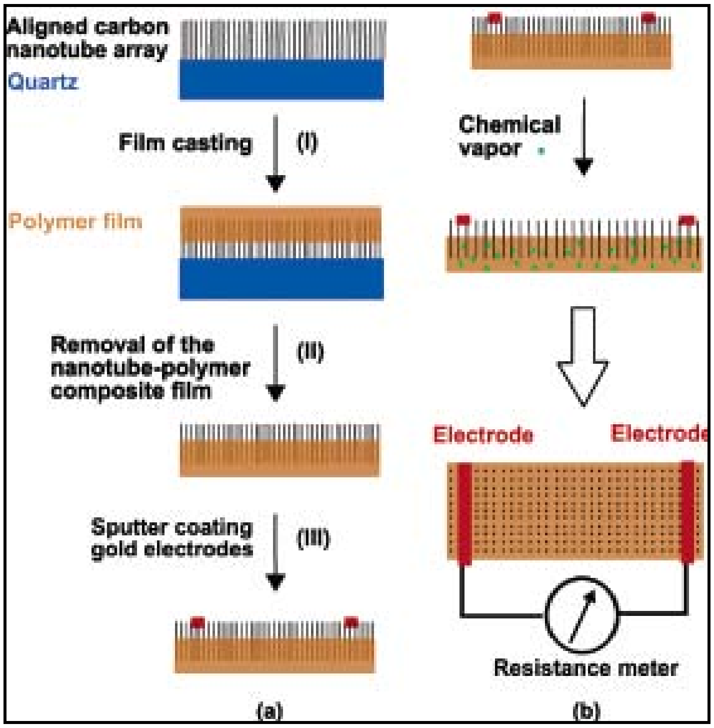

Figure 6. Schematic illustration of the procedures for (a) fabricating and (b) characterizing the aligned carbon nanotube-polymer composite chemical vapor sensor (Wei et al., 2006).

2.3 Discriminant Analysis

Discriminant Analysis is a technique for differentiating between individual observations based on their features. This is accomplished by developing a mathematical function and applying it to the features to separate the observations into mutually exclusive and exhaustive groups (Bauer, 2005a:58). The function assigns a score to each observation, so that each score (Bauer, 2005a:58)

- is a linear combination of the observation's attributes
- has average scores from the two groups as far apart as possible
- has a variance as small as possible

For the discrimination of two groups, A and B, a discriminant function **Y** is used to separate the groups. The discriminant score, Y, for each observation is calculated by multiplying the discriminant weight, b, by the observation's value on each independent variable, X_1 and X_2: **Y** = **b'X**, where **Y** is a 1 x n vector of discriminant scores, **b**' is a 1 x p vector of discriminant weights, and **X** is a p x n matrix containing the values for each of the n observations on the p independent variables (Dillon and Goldstein, 1984:361). Figure 7 shows a scatterplot of groups A, denoted by the dots, and B, denoted by the circles (Dillon and Goldstein, 1984:362). The straight line through the ellipses represents the smallest overlap between the univariate distributions *A'* and *B'* on the discriminant function graph (Dillon and Goldstein, 1984:362).

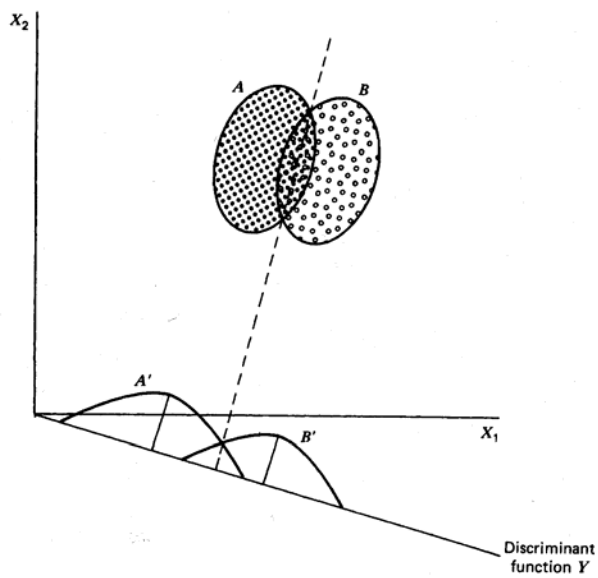

Figure 7. Graphical illustration of two-group discriminant analysis (Dillon and Goldstein, 1984:361).

The classification rules that allow the function to distinguish between groups are developed from a training set of data in which their groupings are known. This data is examined for differences and rules are developed so as to minimize misclassification (Johnson and Wichern, 2002:583).

2.3.1 Discriminant Analysis Methodology

There are several methods that can be used in discriminant analysis. For most methods, the populations are assumed to be multivariate normal. To test whether a data set originated from a multivariate normal population, each variable can be tested separately for univariate normality because if one variable is not normal, the entire vector is not multivariate normal (Rencher, 2002:92). Although this should not be the only approach since the normality of the individual variables does not ensure joint normality (Rencher, 2002:92).

The assumption of univariate normality can be tested by first putting the data in order according to magnitude, $x_{(1)} \leq x_{(2)} \leq \ldots \leq x_{(n)}$. Next, the probability levels (p) for the jth observation and the corresponding standard normal quantiles (q) can be calculated by (Johnson and Wichern, 2002:179):

$$P\left[Z \leq q_{(j)}\right] = p_{(j)} = \frac{j - \frac{1}{2}}{n} \tag{3}$$

where n is the total number of observations. The ordered data $x_{(j)}$ and the normal quantiles $q_{(j)}$ can then be plotted on a Q-Q plot and the "straightness" of the resulting plot should be examined. This can be measured by calculating the correlation coefficient, r_Q, of all points in the Q-Q plot (Johnson and Wichern, 2002:182):

$$r_Q = \frac{\sum_{j=1}^{n}\left(x_{(j)} - \overline{x}\right)\left(q_{(j)} - \overline{q}\right)}{\sqrt{\sum_{j=1}^{n}\left(x_{(j)} - \overline{x}\right)^2}\sqrt{\sum_{j=1}^{n}\left(q_{(j)} - \overline{q}\right)^2}} \tag{4}$$

If r_Q is less than the appropriate level of significance, α, we can reject the hypothesis of normality (Johnson and Wichern, 2002:182).

Testing multivariate normality is not as straightforward as testing univariate normality. If the sample is not large enough, it may not provide a good estimate of the actual distribution of the population (Rencher, 2002:97). Also, these tests may not be very powerful due to the sparseness of the data in space (Rencher, 2002:97).

One method that can be used to test multivariate normality is to calculate the standardized distance from each $\mathbf{x}_j$ to $\bar{\mathbf{x}}$ (Rencher, 2002:97; Johnson and Wichern, 2002:187):

$$d_j^2 = \left(\mathbf{x}_j - \bar{\mathbf{x}}\right)' \mathbf{S}^{-1} \left(\mathbf{x}_j - \bar{\mathbf{x}}\right) \tag{5}$$

If the data is multivariate normal, then

$$u_i = \frac{nD_i^2}{\left(n-1\right)^2} \tag{6}$$

has a beta distribution (Rencher, 2002:97). A Q-Q plot can also be constructed in this method, but the u_i values will instead be ranked in ascending order $u_{(1)} \leq u_{(2)} \leq \ldots \leq u_{(n)}$ and plotted against the quantiles v_i

$$v_i = \frac{i-\alpha}{n-\alpha-\beta+1} \tag{7}$$

where

$$\alpha = \frac{p-2}{2p} \tag{8}$$

$$\beta = \frac{n-p-3}{2(n-p-1)} \tag{9}$$

If the Q-Q plot has a nonlinear pattern, it is an indication that the data is not multivariate normal.

Once multivariate normality is established, it is necessary to determine whether the population covariance matrices are homogeneous. The covariance matrices (S) of each group should be calculated using (Bauer, 2005a:42):

$$S = \frac{1}{N-1}\left(\underline{X}' \underline{X} - \frac{1}{N} \underline{X}' 11' \underline{X} \right) \tag{10}$$

where N is the number of observations and $\underline{X}$ is the data matrix. These covariance matrices can then be tested for equality using Box's M-test. The hypothesis of all covariances being equal is tested by calculating (Rencher, 2002:257):

$$u = -2(1-c_1)\ln M \tag{11}$$

$$c_1 = \frac{(k+1)(2p^2+3p-1)}{6kv(p+1)} \tag{12}$$

$$\ln M = \frac{1}{2}\sum_{i=1}^{k} v_i \ln\left|S_i\right| - \frac{1}{2}\left(\sum_{i=1}^{k} v_i\right)\ln\left|S_{pl}\right| \tag{13}$$

where $v = n - 1$, p is the number of features in the covariance matrix, k is the number of groups to be separated, v_i is v of the i^{th} sample, $\mathbf{S}_i$ is the covariance matrix of the ith sample, and $\mathbf{S}_{pl}$ is the pooled sample covariance matrix (Rencher, 2002:256)

$$\mathbf{S}_{pl} = \frac{\sum_{i=1}^{k} v_i \mathbf{S}_i}{\sum_{i=1}^{k} v_i} \tag{14}$$

If $u > \chi^2_{\alpha}$, we can reject the hypothesis of all covariances being equal.

If the covariance matrices are equal, Fisher's Discriminant Function can be used to classify the data (Johnson and Wichern, 2002:609). The population does not need to be multivariate normal to use this method. Fisher's discriminant function finds a linear combination of the characteristics of a population so that the difference in means is maximized and the variance is minimized (Dillon and Goldstein, 1984:364). The linear combination in Equation 15 meets these requirements (Johnson and Wichern, 2002:610)

$$\hat{y} = \left(\bar{\mathbf{x}}_1 - \bar{\mathbf{x}}_2\right)' \mathbf{S}_{pooled}^{-1}\mathbf{x} \tag{15}$$

where $\mathbf{S}_{pooled}$ is the pooled sample covariance matrix. The midpoint of the maximal separation between the two populations $\hat{m} = \frac{1}{2}(\bar{\mathbf{x}}_1 - \bar{\mathbf{x}}_2)'\mathbf{S}_{pooled}^{-1}(\bar{\mathbf{x}}_1 + \bar{\mathbf{x}}_2)$ is used as the rule to classify new observations (Johnson and Wichern, 2002:611).

If the covariance matrices are not equal, quadratic discrimination scores should be calculated to identify classification rules. "Quadratic discriminant scores (D_q scores) are an approximation of the natural log of the likelihood estimators (Young, 2002:28)". The D_q scores are calculated using (Johnson and Wichern, 2002:617):

$$d_i^Q(\mathbf{x}) = -\frac{1}{2}\ln|\mathbf{S}_i| - \frac{1}{2}(\mathbf{x} - \bar{\mathbf{x}}_i)'\mathbf{S}_i^{-1}(\mathbf{x} - \bar{\mathbf{x}}_i) \tag{16}$$

where $\bar{\mathbf{x}}_i$ is the sample mean vector and $\mathbf{S}_i$ is the sample covariance matrix. Once the discriminant scores are calculated for each individual, the highest D_q score will determine which group the individual should be classified in.

After classification is accomplished, a confusion matrix can be created for n_1 observations from π_1 and n_2 observations from π_2 in the form (Johnson and Wichern, 2002:601)

Predicted membership

Actual membership		π_1	π_2
	π_1	N_{1C}	N_{1M}
	π_2	N_{2M}	N_{2C}

where

N_{1C} = number of π_1 items correctly classified as π_1 items
N_{1M} = number of π_1 items misclassified as π_2 items
N_{2C} = number of π_2 items correctly classified as π_2 items
N_{2M} = number of π_2 items misclassified as π_1 items

From the confusion matrix, the apparent error rate (APER) can be easily calculated

$$\text{APER} = \frac{N_{1M} + N_{2M}}{n_1 + n_2} \qquad (17)$$

The APER is based on the training set and therefore tends to underestimate the Actual Error Rate (AER) (Bauer, 2005a:85). To find a better estimate, the total sample is usually split into a training sample and a validation sample leading to separate confusion matrices (Johnson and Wichern, 2002:602). The training sample is used to construct the discriminant function while the validation data is used to evaluate it (Johnson and Wichern, 2002:602).

2.4 Artificial Neural Networks

Artificial Neural Networks (ANNs) are another method for classifying data. This technique was developed when scientists attempted to imitate the simple neuron functions that occur in the brain. A neuron, Figure 8, consists of a nucleus, dendrites that carry signals to the nucleus, and axons which carry signals away (Nelson and Illingworth, 1991:37). A synapse is the point where a neuron passes an impulse to another neuron, which allows for a “network” of communication throughout the brain. When a neuron receives an input, the input is “weighted” to either excite or inhibit the neuron to forward the signal (Nelson and Illingworth, 1991:39). Once the sum of the weighted inputs reaches a certain level, the neuron fires its output. This process is modeled in an ANN, which is “trained” to produce a specific output through the adjustment of the weights and network architecture.

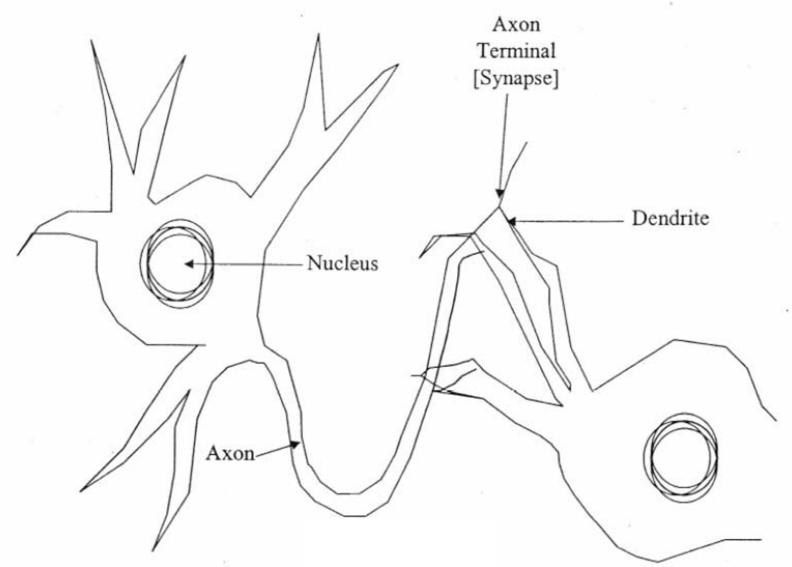

Figure 8. Biological neuron (Bauer, 2005b:1).

2.4.1 Artificial Neural Networks Definitions

The following are definitions of terms normally used when discussing ANNs (Bauer, 2005b:3):

- Artificial Neural Networks (ANN). An information processing system (algorithm) that operates on inputs to extract information and produces outputs corresponding to the extracted information.

- Architecture. The topological arrangements of neurons, layers, and connections which define the set of modeling equations available to the ANN.

- Backpropagation. A learning algorithm for updating weights in a feed-forward multilayer perceptron (MLP) ANN that minimizes the mean squared mapping error.

- Epoch. A complete presentation of the data set being used to train the MLP, or equivalently called a training cycle.

- Feature. In neural networks, features refer to the input vectors of information which are presumed to have some relation that might be helpful in distinguishing the various output classes. The vector of features is often called an Exemplar.

- Feed-forward Neural Networks. Multilayer ANNs whose connections exclusively feed inputs from lower to higher levels. In contrast to a feedback or recurrent ANN, a feed-forward ANN operates only until all the inputs propagate to the output layer. An example of a feed-forward ANN is the MLP.

- Hidden Units. The processing elements in MLP ANNs that are not included in the input or output layers. This is the part of the neural network located between the input and output layers.

- Neuron. The fundamental building block of an ANN. Normally, each neuron takes a weighted sum of its inputs to determine its net input. The net is then processed through its transfer function to produce a single valued output that is broadcast to "downstream" neurons.

- Training. The iterative process of updating the weights of each node to better fit the data.

- Weight: The values, associated with each connection, which signify its strength. The weights are combined to calculate the activations.

2.4.2 Artificial Neural Networks Paradigms

In the 1940s, the first neural network model was developed by Warren McCulloch and Walter Pitts. Their model, though, did not include the weighting of the inputs to the neuron. This was corrected in the 1950s when Frank Rosenblatt introduced the first perceptron model, Figure 9. This model was made up of three layers: sensory, association, and response (Smith, 1996:4). The sensory layer was connected to the association layer and the association layer to the response layer in a random manner (Smith, 1996:4). The response neuron with the strongest input would inhibit the other neurons and therefore provide the output for the network (Smith, 1996:5). The model was successful at "learning", but could only classify data correctly if it was linearly separable (Nelson and Illingworth, 1991:116).

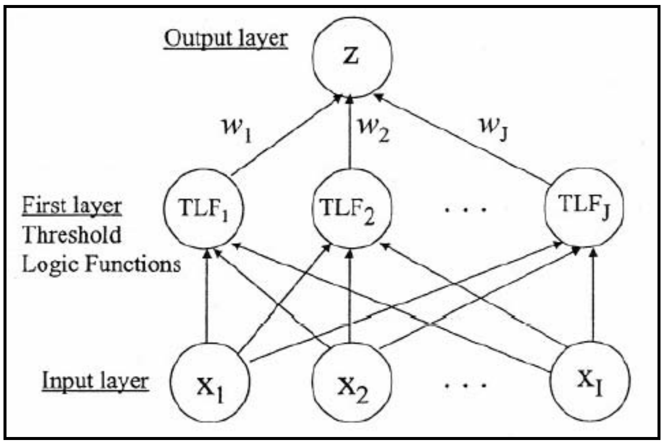

Figure 9. Rosenblatt's perceptron

Rosenblatt's Perceptron had a significant impact despite its problems. Several other models followed his, which led to the feedforward multilayer perceptron (MLP) in Figure 10. The output from one layer is fed forward to activate the next layer.

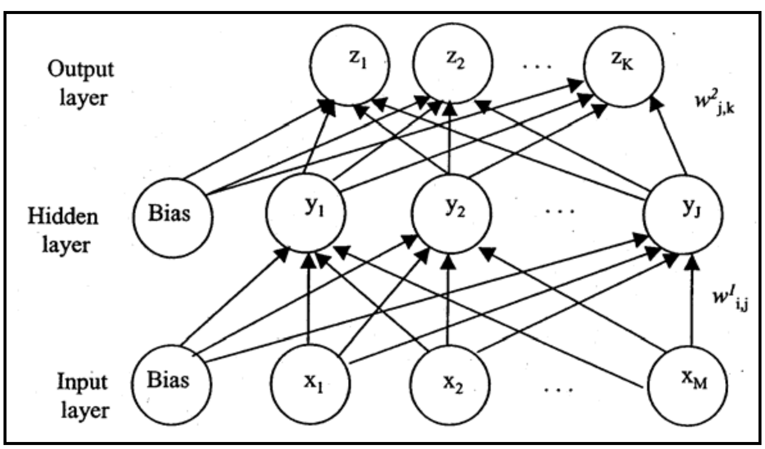

Figure 10. MLP ANN with bias

The first layer of the MLP is the input layer where the data is applied to the network. The last layer is the final output of the network. Between these two layers, there are hidden nodes. This research will include only one layer of hidden nodes in the network. The bias nodes, with values between zero and one, may be used to further inhibit the activity of certain neurons (Schalkoff, 1997:86).

The following equation describes the output for the nth exemplar (z^n) of the MLP ANN above (Bauer, 2005b:15):

$$k^{\text{th}} \text{ neural network output } = z^n{}_k = f\left(\sum_{j=1}^{J} w_{j,k}^2 x_j^1\right) \tag{18}$$

where

- J is the number of hidden nodes
- f(a) = 1/(1+e-a) for sigmoidal activation functions
- f(a) = a for linear activation functions
- $w_{j,k}^2$ is the weight from the hidden node j to output node k
- x_0^1 is the hidden layer bias term
- $x_j^1 = f\left(\sum_{i=1}^{M} w_{i,j}^1 x_i^n\right)$ is the output of hidden node j
- M is the number of input features
- $w_{i,j}^1$ is the weight from input node I to hidden node j
- x_0^n is the input layer bias term and is set equal to 1
- x_i^n is the *i*th input feature of the *n*th input vector

For the MLP to be useful, it must be able to learn patterns. Training algorithms such as the backwards propagation of errors method, or backpropagation, can accomplish this. Introduced in the mid-80s, it calculates the difference between the network output and the desired output and adjusts the weights of the neurons so as to minimize error. The instantaneous backpropagation algorithm for a single hidden layer feedforward network follows (Bauer, 2005b:19):

1. Randomly partition data into *training*, *training-test*, and *validation* sets.
2. Normalize the feature input data.
3. Initialize weights to small random values.
4. Present the network with a randomly selected vector from the training set, denoted x^n.
5. Calculate the network output z^n associated with the n^{th} training vector.
6. Update the weights.
7. If the training-test set error does not indicate sufficient convergence, go to Step 4.

Overfitting is training the data too closely and can become a problem while training an ANN. The problem is that it models the noise along with the actual population (Smith, 1996:113). This can be prevented by increasing the training sample size, by limiting the number of hidden nodes, by preventing the weights from getting too large, or by simply stopping training when overfitting begins (Smith, 1996:25). Limiting the training is the preferred method because of decreased computation time (Smith, 1996:117). This can be accomplished through early stopping. In early stopping, the data set is divided into a training set and a validation set. The training data error will continue to decrease as the training time increases, so the validation set error must be measured simultaneously. When the error on the validation set increases, overfitting has begun (Smith, 1996:126). At this time, training is stopped and the weights and biases that produced the lowest error on the validation set are used for the model (Smith, 1996:126).

2.4.3 Signal-to-Noise Ratios

The signal-to-noise ratio (SNR) saliency measure provides even more insight into the architecture of an ANN. This measure allows for the ranking of a population's features based on their usefulness to the network (Bauer et al., 2000:31). The SNR "directly compares the saliency of a feature to that of an injected noise feature":

$$SNR_i = 10 \log_{base10} \left(\frac{\sum_{j=1}^{J} \left(w_{i,j}^{1} \right)^2}{\sum_{j=1}^{J} \left(w_{N,j}^{1} \right)^2} \right) \tag{19}$$

where SNR_i is the value of the SNR saliency measure for feature i, J is the number of hidden nodes, $w_{i,j}^{1}$ is the first layer weight from node i to node j, and $w_{N,j}^{1}$ is the first layer weight from the injected noise node N to node j (Bauer et al., 2000:32). The injected noise feature is a Uniform (0, 1) random variable. If a feature is important to the network, the SNR saliency measure will be significantly larger than 0.0. If not, then the SNR will be close to or less than 0.0. The advantage of this method is that it may be completed in only one training run, whereas other methods require several.

2.5 Regression Analysis

Regression analysis is a statistical technique for modeling the relationship between predictor and response variables (Montgomery et al., 2001:1). A simple linear regression model consists of the mean function, $\mathrm{E}(Y|X = x) = \beta_0 + \beta_1 x$, and the variance function, $\mathrm{Var}(Y|X = x) = \sigma^2$ (Weisburg, 2005:19). The variance, σ^2, is usually a positive value, so the expected value of the *i*th response usually does not equal the observed value, y_i (Weisburg, 2005:19). The difference between the observed value and the expected value is the statistical error, ε_i, defined by $\varepsilon_i = y_i - \mathrm{E}(Y|X = x_i)$ (Weisburg, 2005:19).

A model with more than one predictor variable is a multiple linear regression model $y = \beta_0 + \beta_1 x_1 + \beta_2 x_2 + ... + \beta_k x_k + \varepsilon$ (Montgomery et al., 2001:68). The regression coefficients, β_k, can be estimated using several methods. One such method is the method of least squares, where the error term is assumed to have $\mathrm{E}(\varepsilon) = 0$, $\mathrm{Var}(\varepsilon) = \sigma^2$ and they are also assumed to be uncorrelated (Montgomery et al., 2001:71). Multiple regression models are easily expressed in matrix notation by

$$\mathbf{y} = \mathbf{X}\boldsymbol{\beta} + \boldsymbol{\varepsilon} \tag{20}$$

where **y** is an *n* x 1 vector of observations, $\mathbf{y} = \begin{bmatrix} y_1 \\ y_2 \\ \vdots \\ y_k \end{bmatrix}$, **X** is an *n* x *p* matrix of regressor variables, $\mathbf{X} = \begin{bmatrix} 1 & x_{11} & x_{12} & \cdots & x_{1k} \\ 1 & x_{21} & x_{22} & \cdots & x_{2k} \\ \vdots & \vdots & \vdots & & \vdots \\ 1 & x_{n1} & x_{n2} & \cdots & x_{nk} \end{bmatrix}$, **β** is a *p* x 1 vector of regression coefficients,

$\boldsymbol{\beta} = \begin{bmatrix} \beta_0 \\ \beta_1 \\ \vdots \\ \beta_k \end{bmatrix}$, and $\boldsymbol{\varepsilon}$ is an n x 1 vector of random errors, $\boldsymbol{\varepsilon} = \begin{bmatrix} \varepsilon_1 \\ \varepsilon_2 \\ \vdots \\ \varepsilon_k \end{bmatrix}$, for *n* observations and *p* = *k* + 1 (Montgomery et al., 2001:73). The observations, **y**, and the values of the regressor variables, **X**, are known, but the regressor coefficients, **β**, are unknown. The **β**'s can be estimated by finding least-squares estimators, $\hat{\boldsymbol{\beta}}$, that minimize the least-squares function S(**β**) = $\sum_{i=1}^{n} \varepsilon_i^2$ (Montgomery et al., 2001:74). Once the least-squares estimators are found, fitted values, $\hat{y}_i$, corresponding to the observed values, y_i, can be found using $\hat{\mathbf{y}} = \mathbf{X}\hat{\boldsymbol{\beta}}$ (Montgomery et al., 2001:75). The difference between these two values is called the residual, e_i, which can be expressed in matrix notation as $\mathbf{e} = \mathbf{y} - \hat{\mathbf{y}}$ (Montgomery et al., 2001:75).

2.5.1 Hypothesis Testing

Once the model has been estimated, a significance of regression test should be conducted to measure the accuracy of the model. The hypotheses used in this test are (Montgomery et al., 2001:87)

$$\begin{aligned} &H_0: \beta_1 = \beta_2 = \ldots = \beta_k = 0 \\ &H_1: \ \beta_j \neq 0 \text{ for at least one j} \end{aligned} \tag{21}$$

Rejection of the null hypothesis indicates that at least one regressor variable significantly contributes to the model (Montgomery et al., 2001:87). To test this, an analysis of variance (ANOVA) can be accomplished. An ANOVA table, in Table 1, is usually used to summarize the results of the test (Montgomery et al., 2001:88).

Table 1. ANOVA for Significance of Regression in Multiple Regression (Montgomery et al., 2001:88)

Source of Variation	Sum of Squares	Degrees of Freedom	Mean Square	F_0
Regression	SS_R	k	MS_R	MS_R / MS_{Res}
Residual	SS_{Res}	n-k-1	MS_{Res}	
Total	SS_T	n-1		

The total sum of squares, SST, measures the total variability in the observations and is made up of the sum of squares due to regression, SS_R, and the residual sum of squares, SS_{Res} (Montgomery et al., 2001:87)

$$SS_T = SS_R + SS_{Res} \tag{22}$$

It can also be calculated with the following equation (Montgomery et al., 2001:89):

$$SS_T = \mathbf{y}'\mathbf{y} - \frac{\left(\sum_{i=1}^{n} y_i\right)^2}{n} \tag{23}$$

The regression sum of squares is defined as

$$SS_R = \hat{\boldsymbol{\beta}}\mathbf{X}'\mathbf{y} - \frac{\left(\sum_{i=1}^{n} y_i\right)^2}{n} \tag{24}$$

and the residual sum of squares is (Montgomery et al., 2001:89)

$$SS_{Res} = \mathbf{y}'\mathbf{y} \text{ - } \hat{\boldsymbol{\beta}}'\mathbf{X}'\mathbf{y} \tag{25}$$

The regression mean square is found by dividing the regression sum of squares by its degrees of freedom

$$MS_R = SS_R / k \tag{26}$$

and the residual mean square, which is an unbiased estimator of the variance, is calculated by dividing the residual sum of squares by its degrees of freedom

$$MS_{\mathrm{Res}} = SS_{\mathrm{Res}} / n - p \tag{27}$$

where $p = k + 1$ (Perry, 2005). To test the null hypothesis, the test statistic F_0 must be calculated (Montgomery et al., 2001:90)

$$F_0 = MS_R / MS_{\mathrm{Res}} \tag{28}$$

If $F_0 > F_{\alpha,k,n-p}$, then the null hypothesis would be rejected implying that the regressor variables are related to the response, although this does not imply that the model is the best prediction of the relationship between the regressors and the response (Montgomery et al., 2001:90).

The above hypothesis test determines if at least one regressor is important to the model. To find which regressors are important, the significance of an individual regression coefficient can be tested. The hypotheses and test statistic are

$$\begin{aligned} H_0 &: \beta_j = 0 \\ H_1 &: \beta_j \neq 0 \end{aligned} \tag{29}$$

$$t_0 = \frac{\hat{\beta}_j}{\sqrt{\hat{\sigma}^2 C_{jj}}} \tag{30}$$

where C_{jj} is the diagonal element of $(\mathbf{X'X})^{-1}$ corresponding to $\hat{\beta}_j$ (Montgomery et al., 2001:91). The null hypothesis can be rejected if $|t_0| > t_{\alpha/2,n-k-1}$ (Montgomery et al., 2001:91). If it cannot be rejected, the regressor x_j can be removed from the model (Montgomery et al., 2001:91). The above procedure tests the contribution of x_j given all the other regressors are in the model (Montgomery et al., 2001:91).

To test the contribution of a specific subset of *r* regressors on a regression model with *k* regressors, the extra-sum-of-squares method can be used. In this method, the regression coefficients are partitioned into two sets

$$\boldsymbol{\beta} = \left[\frac{\boldsymbol{\beta}_1}{\boldsymbol{\beta}_2} \right]$$

where $\boldsymbol{\beta}_1$ is $(p - r) \times 1$ and $\boldsymbol{\beta}_2$ is $r \times 1$ (Montgomery et al., 2001:92). This partitioning leads to the following model (Montgomery et al., 2001:92)

$$\mathbf{y} = \mathbf{X_1}\,\boldsymbol{\beta}_1 + \mathbf{X_2}\,\boldsymbol{\beta}_2 + \boldsymbol{\varepsilon} \tag{31}$$

The hypotheses and test statistic are

$$\begin{aligned} H_0 &: \boldsymbol{\beta}_2 = 0 \\ H_1 &: \boldsymbol{\beta}_2 \neq 0 \end{aligned} \tag{32}$$

$$F_0 = \frac{SS_R\left(\boldsymbol{\beta}_2 \middle| \boldsymbol{\beta}_1\right)/r}{MS_{\mathrm{Res}}} \tag{33}$$

where $SS_R\left(\boldsymbol{\beta}_2 \middle| \boldsymbol{\beta}_1\right) = SS_R\left(\boldsymbol{\beta}\right) - SS_R\left(\boldsymbol{\beta}_1\right)$ (Montgomery et al., 2001:94). If $F_0 > F_{\alpha,r,n-p}$, the null hypothesis can be rejected implying that at least one of the regressors in $\mathbf{X_2}$ contributes significantly to the model (Montgomery et al., 2001:94).

2.5.2 Model Adequacy

After a model has been developed, the adequacy of the model should be examined. One way to do this is through residual analysis. It is good to use scaled residuals, as well as the original residuals, in this analysis because scaled residuals, such as studentized residuals, highlight observations that are outliers or extreme values.

Since the hypothesis tests depend on the normality of the errors, it is important to check on the validity of this assumption. This can be done by constructing normal probability plots of the residuals. The residuals should be ranked in increasing order $e_{[1]} < e_{[2]} < \cdots < e_{[n]}$ and then plotted against their cumulative probabilities $P_i = \left(i - \frac{1}{2}\right) \Big/ n$, i = 1, 2,…, n (Montgomery et al., 2001:138-139). If the resulting plotted points substantially depart from a straight line, the distribution is not normal (Montgomery et al., 2001:139). Figure 11 shows an example of an ideal normal probability plot.

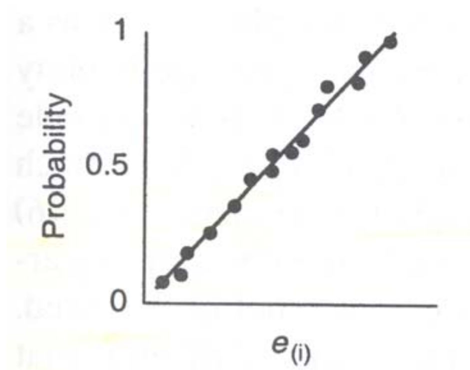

Figure 11. Ideal normal probability plot (Montgomery et al., 2001:139).

Another graphical analysis technique is to plot the residuals versus their corresponding fitted values $\hat{y}_i$, which allows for the detection of non-constant variance and nonlinearity. Figure 12 shows examples of an ideal residual plot (a) and those that indicate model deficiencies (b-d).

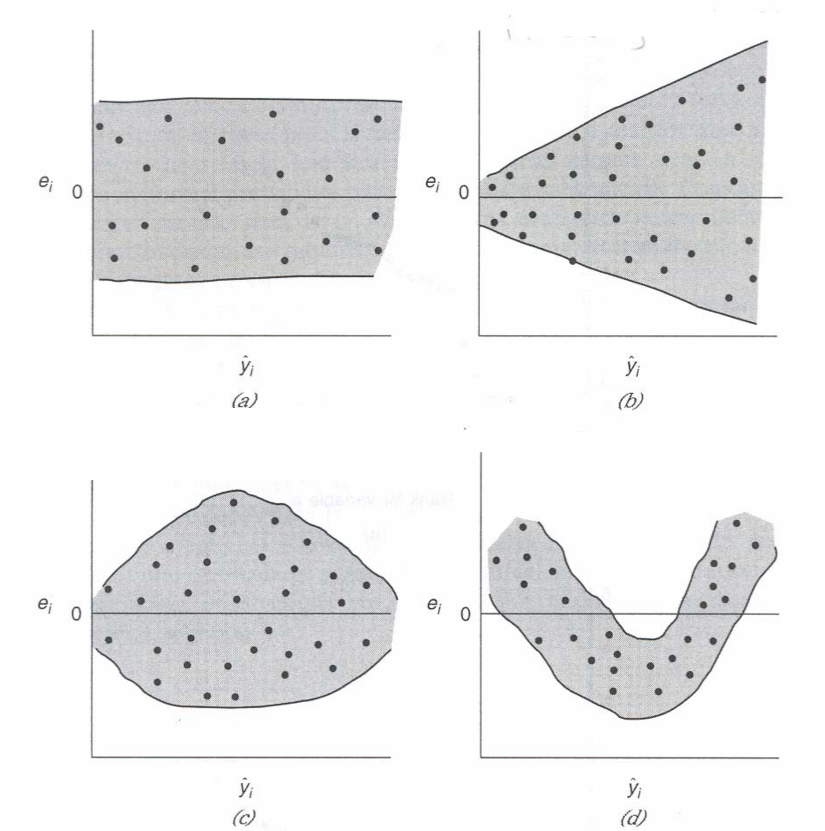

Figure 12. Patterns for residual plots: (a) satisfactory, constant variance; (b) increasing variance; (c) non-constant variance; (d) may indicate nonlinearity (Montgomery et al., 2001:142; Perry, 2005).

If residual analysis indicates non-constant variance or nonnormality in the error terms, or nonlinearity of the model, data transformations can be used to correct these problems. Analytical methods, such as Box-Cox and Box-Tidwell, can be used to select the correct transformation needed.

The Box-Cox method can be used to correct nonnormality and/or nonconstant variance (Montgomery et al., 2001:186). The power transformation y^{λ} is used in this method where λ is to be determined (Montgomery et al., 2001:186). The procedure for the Box-Cox method follows (Perry, 2005; Montgomery et al., 2001:187)):

1. Select a value for λ.
    a. Compute the temporary scaled response $y^{(\lambda)}$

$$y^{(\lambda)} = \begin{cases} \dfrac{y^{\lambda}-1}{\lambda \dot{y}^{\lambda-1}}, & \lambda \neq 0 \\ \dot{y} \ln y, & \lambda = 0 \end{cases} \tag{34}$$

$$\dot{y} = \exp\left[\frac{1}{n} \left(\sum_{i=1}^{n} \ln y_i \right) \right] \tag{35}$$

    b. Use the scaled response to fit the model

$$\mathbf{y}^{(\lambda)} = \mathbf{X}\boldsymbol{\beta} + \boldsymbol{\varepsilon} \tag{36}$$

    c. Calculate $SS_{\text{Res}}(\lambda)$

2. Repeat Step 1 for various λ's. Typically, 10-20 values are needed to estimate an optimum value.

3. Plot the $SS_{\text{Res}}(\lambda)$ versus λ to find the value of λ that minimizes $SS_{\text{Res}}(\lambda)$.

4. Fit the model using y^{λ} as the response if $\lambda \neq 0$. If $\lambda = 0$, then use ln y.

If the relationship between y and its regressors is nonlinear, but the assumptions of normality and constant variance are satisfied, the Box-Tidwell method can be used to select a transformation on the regressor variables (Montgomery et al., 2001:190). The steps for the Box-Tidwell method are as follows (Perry, 2005; Montgomery et al., 2001:191):

0. Assume that the response y is related to a power of the regressor x', where

$$x' = \begin{cases} \ln x, & \alpha = 0 \\ x^{\alpha}, & \alpha \neq 0 \end{cases} \tag{37}$$

1. Fit $\hat{y} = \hat{\beta}_0 + \hat{\beta}_1 x$ by least squares.

2. Define another regressor $w = x \ln x$ and fit $\hat{y} = \hat{\beta}_0 + \hat{\beta}_1 x + \hat{\gamma} w$ by least squares.

3. Define $\hat{\alpha}_j = \frac{\hat{\gamma}}{\hat{\beta}_1} + 1$, where *j* is the number of iterations.

4. Replace *x* with $x' = x^{\hat{\alpha}}$ and *w* with $w' = x' \ln x'$. Return to Step 1.

This procedure usually converges quickly, so a single iteration often gives a satisfactory estimate of *α* (Montgomery, 2001:192).

The nonconstant variance problem can also be addressed by fitting the model using the weighted least squares method. The variance of the errors are said to be uncorrelated and unequal with a covariance matrix of (Montgomery et al., 2001:195)

$$\sigma^2 V = \sigma^2 \begin{bmatrix} \frac{1}{w_1} & & & 0 \\ & \frac{1}{w_2} & & \\ & & \ddots & \\ 0 & & & \frac{1}{w_n} \end{bmatrix} \tag{38}$$

The weighted least-squares estimator is (Montgomery et al., 2001:196)

$$\hat{\boldsymbol{\beta}} = \left(\mathbf{X}'\mathbf{W}\mathbf{X}\right)^{-1} \mathbf{X}'\mathbf{W}\mathbf{y} \tag{39}$$

where $\mathbf{W} = \mathbf{V}^{-1}$. The weights w_i must be known and residual analysis can sometimes give an indication of what they are (Montgomery et al., 2001:196). For example, the variance could be a function of one of the regressors, $Var(\varepsilon_i) = \sigma^2 x_{ij}$, so that $w_i = 1/x_{ij}$ (Montgomery et al., 2001:196). Most often, the weights will have to be estimated, the analysis performed, and the weights reestimated based on the results, which may take several iterations (Montgomery et al., 2001:196).

3. Methodology

This chapter describes the methods used to detect and identify chemical agents. Section 3.1 provides background information on the data used for this study. Section 3.2 outlines the different phases of analysis and the assumptions used. Section 3.3 presents the specific methods used to classify the data.

3.1 Background Information

The data used for this study was generated through several experiments conducted at The University of Dayton by Dr. Wei Chen. These chemical detection experiments were conducted on carbon nanotube polymer composite sensors composed of multi-walled carbon nanotubes embedded in a polymer film, as seen in Figure 13.

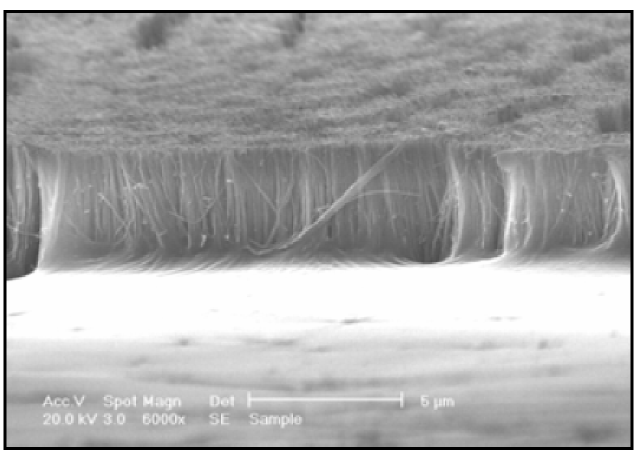

Figure 13. Scanning electron microscope (SEM) image of an aligned carbon nanotube array in a polymer matrix (Wei et al., 1006)

Three different sensors, made of the following polymers, were used: (1) polyisopropene (PI), (2) poly(vinyl acetate) (PVAc), and (3) a 1:1, by weight, mixture of the two (PI-

PVAc). These 3 sensors were individually exposed to 3 different chemical vapors: (1) cyclohexane, (2) ethanol, and (3) tetrahydrofuran (THF).

Once the chemical was exposed to the sensor, the resistance was measured by a multimeter and a change in relative resistance was calculated with the following equation:

$$\frac{(R - R_0)}{R_0} * 100 \tag{40}$$

where R is the resistance after exposure in kiloohms (kΩ) and R_0 is the initial resistance in kΩ (Wei, 2006). The experimental error was about 5% in terms of relative resistance (Wei, 2006).

The experiment began by exposing each sensor to air for 110 seconds. Each sensor was then exposed to a chemical from 120 to 230 seconds. After this, the sensor was once again exposed to air for another 120 seconds thus beginning the cycle of exposure to air and chemical. This cycle continued for approximately 30 minutes.

3.2 Phases of Analysis and Assumptions

Three different sets of data were used in this research. The initial set was from sensors that had approximately 20 experiments conducted on them. The second data set was from identical sensors that had been "aged" seven to nine months and had about 50 experiments conducted on them. The last data set was from a new set of sensors that had no experiments conducted on them. Because of this, analysis consisted of four phases, as shown in Figure 14:

- Phase one: initial data set classified by vapor
- Phase two: initial data set sensor three predicted from sensors one and two
- Phase three: models developed from initial data set and validated by second data set
- Phase four: same models developed in phase three validated by last data set

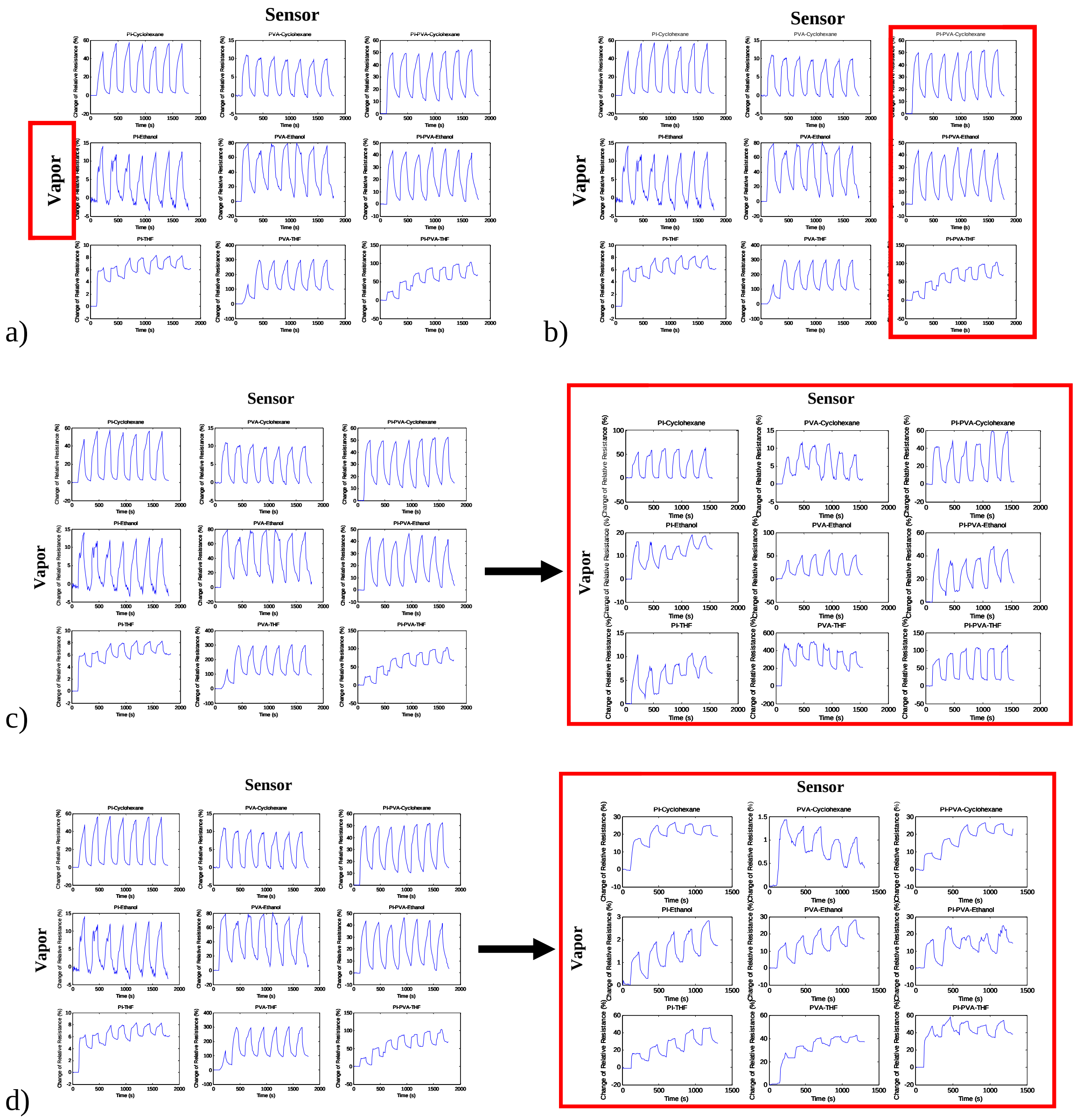

Figure 14. Phases of analysis (a) phase one, (b) phase two, (c) phase three, (d) phase four.

In the first phase Fisher's discriminant method, the quadratic discriminant scores method, and neural networks were used to classify the data by vapor. This would allow for the identification of an unknown vapor. During this phase, the sensors were assumed to be independent. Also, to use the quadratic discriminant scores method, we must assume the populations are multivariate normal. The second phase dealt with predicting the output of the mixture sensor from the poly(vinyl acetate) and polyisopropene sensor data using linear regression and neural networks. At this point, it was assumed that the output of the mixture was dependent on the interactions of the pure polymer data. Since a linear regression was used for prediction, it was also assumed that the relationship between the response and the regressors was approximately linear. Also, the errors were assumed to be independent random variables with a mean of zero and a constant variance. The same assumptions from phase one and two were applied to phases three and four.

3.3 Methods of Analysis

Analysis was split up into four phases with a specific methodology for each.

3.3.1 Phase One

For phase one, the initial set of data was used and classified according to vapor. All the data was split up by vapor and features (*F*) were calculated for each vapor *i*, sensor *j*, and exposure *k* using the following equation (Doleman et al., 1998:4180):

$$F_{ijk} = \left[\left(\frac{(R_{\max} - R_0)}{R_0} * 100 \right)_{ijk} - \bar{x}_{ijk} \right] / S_{ijk} \tag{41}$$

$$\frac{(R_{\max} - R_0)}{R_0} * 100 = \textit{maximum relative change in resistance}$$

$$\bar{x}_{ijk} = \frac{1}{n} \sum_{m=1}^{n} x_{ijk_m} = \textit{average relative change in resistance}$$

$$S_{ijk} = \sqrt{\frac{\sum_{m=1}^{n} \left(x_{ijk_m} - \bar{x}_{ijk} \right)^2}{n-1}} = \textit{standard deviation of relative change in resistance}$$

The classifier was trained against the first six exposures and the last exposure was used to test the prediction capability of the function.

The covariance matrices were equal, so Fisher's approach was used for classification. Quadratic discriminant scores were also calculated, using Equation 16, for comparison. Three scores, correlating to each vapor, were calculated for each observation. The scores were the discriminating feature of the vapors. For Fisher's approach, the same equations were used, but the individual covariance matrices for each vapor were replaced with the pooled covariance matrix.

Following this, a neural network analysis was performed using the Statistical Neural Network Analysis Package (SNNAP) software to validate the quadratic discriminate score method. A tutorial for using SNNAP is in Section 3.4 of this chapter.

After classification was completed, confusion matrices were created, for both methods, for n_1 observations from π_1, n_2 observations from π_2, and n_3 observations from π_3 in the form (Johnson, 2002:601)

Predicted membership

Actual membership

	π_1	π_2	π_3
π_1	n_{1C}	n_{1M2}	n_{1M3}
π_2	n_{2M1}	n_{2C}	n_{2M3}
π_3	n_{3M1}	n_{3M2}	n_{3C}

where

n_{1C} = number of π_1 items correctly classified as π_1 items
n_{1M2} = number of π_1 items misclassified as π_2 items
n_{1M3} = number of π_1 items misclassified as π_3 items
n_{2C} = number of π_2 items correctly classified as π_2 items
n_{2M1} = number of π_2 items misclassified as π_1 items
n_{2M3} = number of π_2 items misclassified as π_3 items
n_{3C} = number of π_3 items correctly classified as π_3 items
n_{3M1} = number of π_3 items misclassified as π_1 items
n_{3M2} = number of π_3 items misclassified as π_2 items

From the confusion matrix, the apparent error rate (APER) was calculated (Bauer, 2005a:85)

$$\text{APER} = \frac{n_{1M2} + n_{1M3} + n_{2M1} + n_{2M3} + n_{3M1} + n_{3M2}}{n_1 + n_2 + n_3} \tag{42}$$

Since the amount of data available was small, Lachenbruch's Holdout procedure was used to find an average error rate in classifying the data. To do this, the neural network was trained several times, each time leaving a different observation out of the training data set. For example, instead of using observation seven for validation, observation one and so on were held out and used. Once the procedure was completed, an expected actual error rate was calculated (Bauer, 2005a:86)

$$\mathrm{E(AER)} = \frac{\sum_h \sum_g I_{hg}}{HG} \tag{43}$$

where H is the total number of holdout procedures, G is the total number of gases classified, and

$$I_{hg} = \begin{cases} 1 \text{ if misclassified for holdout } h \text{, gas } g \\ 0 \text{ if classified correctly} \end{cases}$$

3.3.2 Phase Two

In phase two, rather than using features, the raw data from the initial data set was used to try to predict the output of sensor three. A linear regression of the data using the method of least squares was first used to accomplish this. The third sensor’s data was used as the response, while the other two sensors’ data represented the regressor variables. The coefficients of the model were found by calculating the least-squares estimator of β, for each gas, with (Montgomery, 2001:74)

$$\hat{\boldsymbol{\beta}} = \mathbf{(X'X)^{-1}X'y} \tag{44}$$

where

y = response vector

X = regressor variable matrix

The predicted values of the third sensor, $\hat{y}_i$, were calculated by finding those $\hat{\mathbf{y}} = \mathbf{X}\hat{\boldsymbol{\beta}}$ that corresponded to the actual values y_i (Montgomery, 2001:75). To assess the validity of the model, an ANOVA table was constructed and the adjusted R^2 (R^2_{Adj}) was calculated (Montgomery, 2001:90):

$$R^2_{Adj} = 1 - \frac{SS_{\mathrm{Res}}/(n-p)}{SS_T/(n-1)} \tag{45}$$

where n is the number of observations and p is the number of parameters estimated.

Since normality of the errors was assumed, a normal probability plot was developed to check this assumption. An analysis of the model residuals was then conducted to assess the validity of the constant variance and linear assumptions and examine the model's adequacy. To do this, the studentized residuals, r_i , were calculated with (Montgomery, 2001:134):

$$r_i = \frac{e_i}{\sqrt{MS_{\mathrm{Res}}(1-h_{ii})}} \qquad i = 1, 2, \ldots, n \tag{46}$$

where

$$h_{ii} = ith\ diagonal\ element\ of\ the\ hat\ matrix$$

The studentized residuals were plotted against the fitted values $\hat{y}_i$ to detect any model defects.

A neural network analysis, through SNNAP, was used to find better predictions of the sensor three data. In both methods, the first six observations were used to train and the last observation was used to test the algorithms. After both approaches were completed, a root mean square error (RMSE) was calculated to help identify which model performed best

$$RMSE = \sqrt{\frac{\sum_{i=1}^{n}(y_i - \hat{y}_i)^2}{N}} \tag{47}$$

3.3.3 *Phases three and four*

In phase three of the analysis, new data from the same sensors used in the initial data set was used to validate the models based on the initial data set. The same methods used in phases one and two were used to develop the classification and prediction models. In phase four, data from new sensors was compared to the initial data set to observe if different sensors of the same type produced different readings. To do this, the data was tested against the same models used for validation in phase three.

3.4 SNNAP Tutorial

The following tutorial shows the steps that can be used to reproduce the neural networks acquired in this thesis. After the data is formatted in a .dat file, it is input into the SNNAP software by choosing New in the File Menu. Once the file is chosen, a Choose Model Variables window, Figure 15, appears where input and output variables are selected for the neural network analysis that is needed.

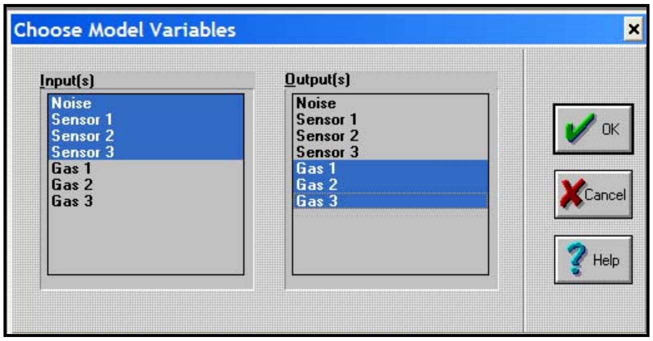

Figure 15. Choose Model Variables window

Once the model variables are accepted, a New Network window, Figure 16, will appear and Back Propagation should be used as the Network Type.

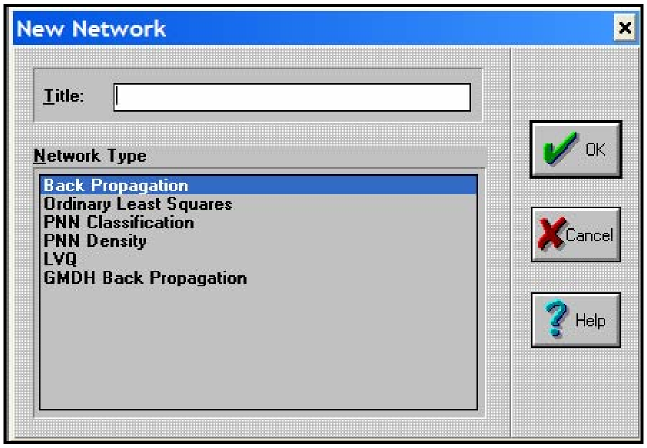

Figure 16. New Network window

After the Network type is chosen, a Structure window appears. Once the Suggest button is clicked, a Structure Suggest window will pop-up, Figure 17. After one of the output data options is selected, the Structure window, Figure 18, will appear again with the suggested structure that the program selected. The Input Layer should have a Linear Layer Type and the Layer 1 and Output Layer should be Sigmoid. Next, a Data Options window will appear where a validation sample can be chosen based on the current data using the modulus option. If modulus is selected, a Define Validation Sample box will pop-up, Figure 19, so size of the validation sample can be chosen. If separate file is selected, the software will allow the user to browse files for the data to be used for validation.

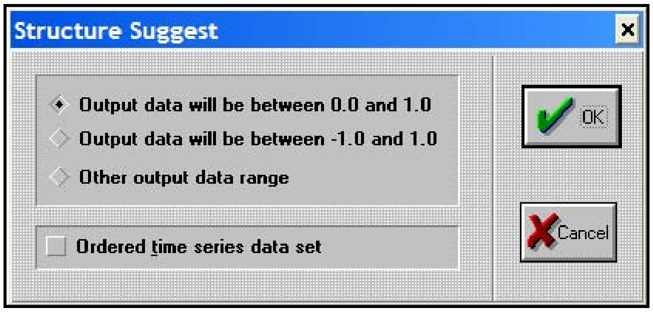

Figure 17. Structure Suggest window

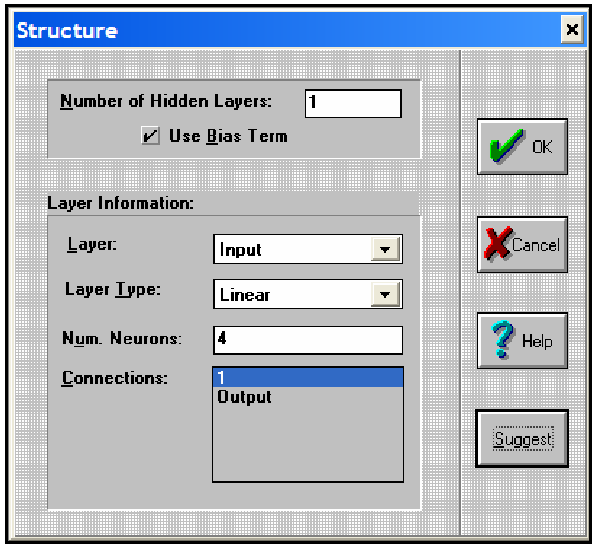

Figure 18. Structure window

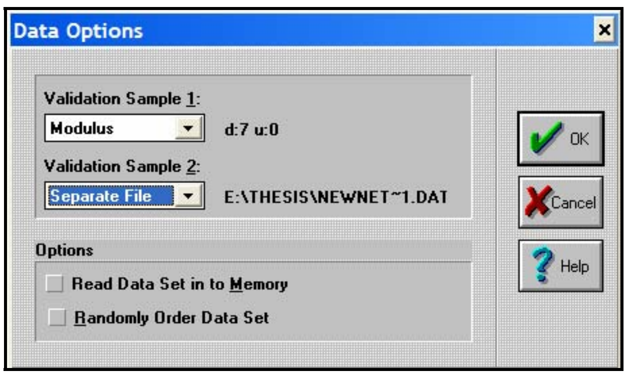

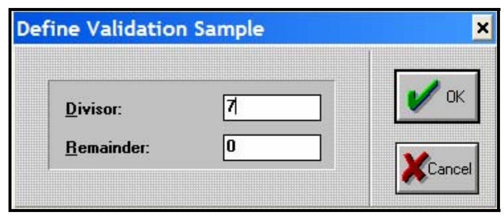

Figure 19. Data Options and Define Validation Sample windows

After data options are selected, a Data Scaling, Figure 20, window will appear where standardize input variables and no transformation on output variables should be chosen. Finally, a Parameters window, Figure 21, will appear and OK should be selected to accept the parameters given.

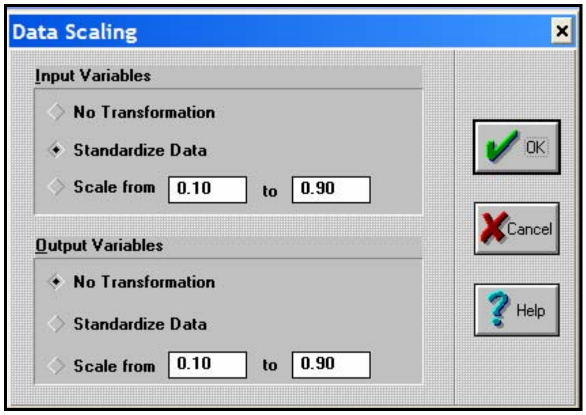

Figure 20. Data Scaling window

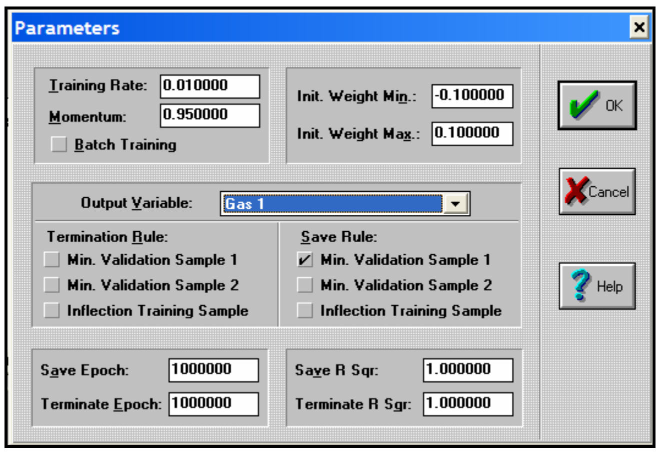

Figure 21. Parameters window

Before the neural network is trained, the weights should be saved by selecting Text Save from the Network Menu. This will allow the user to save all node weights to a specific file for use in future analysis. After this, the network can be trained by selecting Train from the Train Menu. The Stop Training option in the Train Menu allows the user to stop the training of the neural network. The Confusion Matrix option in the Network menu will produce confusion matrices for the training and validation samples. The final option needed to reproduce the outputs in this thesis is the Projection feature, Figure 22, where the user can apply the trained neural network to another file and designate a file for the output.

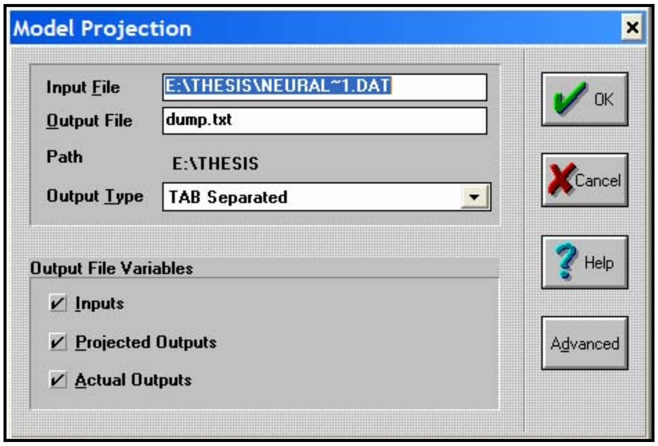

Figure 22. Model Projection window

4. Results and Analysis

In this chapter, the four phases outlined in Chapter 3 are used to analyze the experimental data. In Section 4.1, the sensor data is presented. Section 4.2 provides the numerical results of the analysis phases.

4.1 Data

During the experiment, change in relative resistance data was collected over time. Figure 23 shows the experimental data in a scaled graph matrix with equal y axes. From this set of plots, the range in the output between the gas/sensor combinations is obvious. The data was also graphed with different y axes proportional to each plot, in Figure 24, so that the changes in each gas/sensor output could be easily identified.

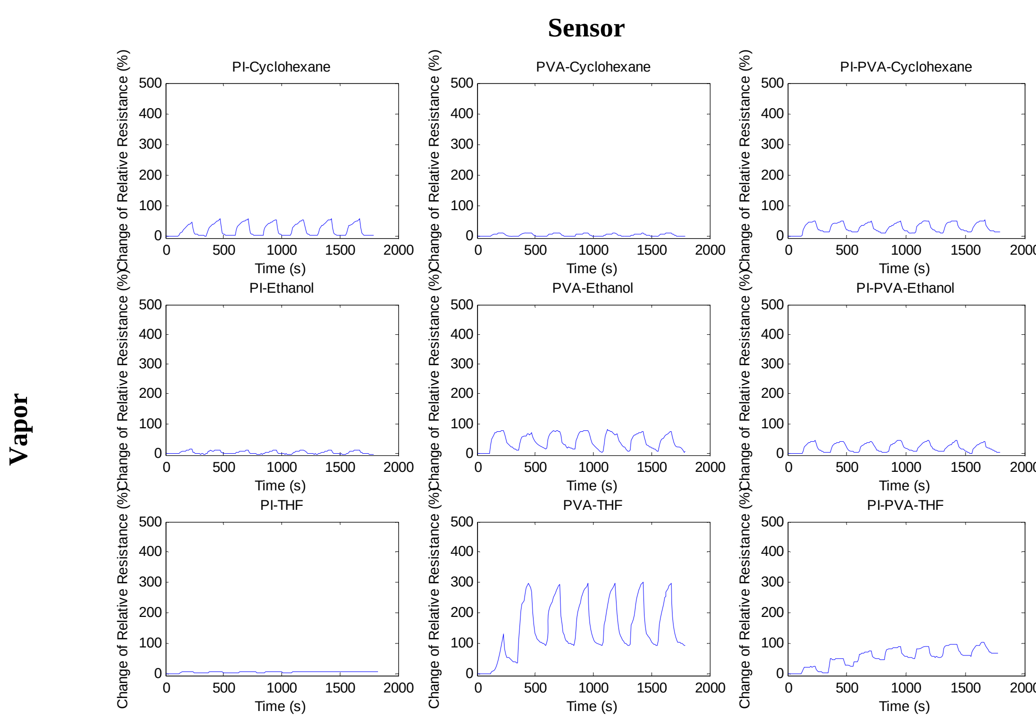

Figure 23. Data matrix by gas and sensor

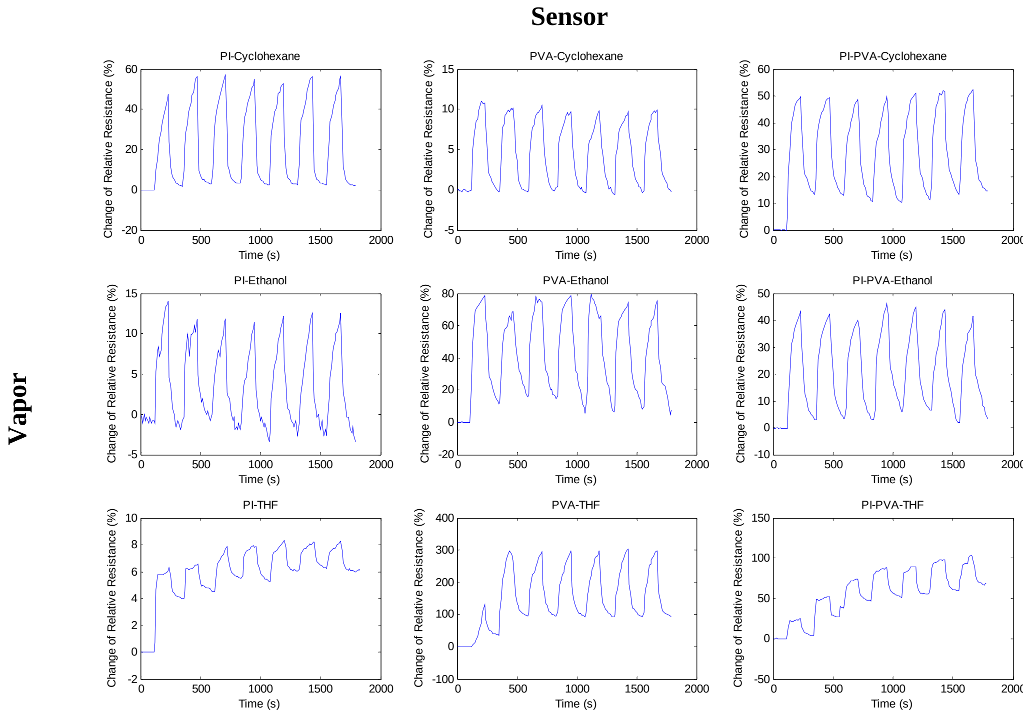

Figure 24. Scaled data matrix by gas and sensor

4.2 Analysis

Analysis was divided into four phases. The first phase consisted of taking vapor detection data from a specific set of sensors and using various techniques, including quadratic discriminant scores and neural networks, to classify the vapors. In phase two, the same data was used and sensor three data was predicted using sensor one and two data. Phase three involved using data from experiments conducted on the same set of sensors used in phases one and two. The difference was that the sensors were older at the time of these experiments and had several other experiments conducted on them. This data was used to validate classification and prediction models based on the initial data set. Finally, in phase four, data taken from new sensors of the same type were also used to validate the same models developed in phase three.

4.2.1 Phase One

During this phase, features calculated from the initial data set were used to classify the data by vapor. Table 2 shows the calculated features according to sensor and vapor. Exposures 1 through 6 were used to train the data, while exposure 7 was used to test the algorithm developed from the training.

Table 2. Data features

Exposure	Sensor 1	Sensor 2	Sensor 3	Vapor
1	1.3464947	0.83341224	0.80910072	1
2	1.21232127	0.60872578	0.95624728	1
3	1.06481227	0.87427116	1.00498005	1
4	1.0929826	0.79029322	1.25580843	1
5	1.04545194	1.07638323	0.85839787	1
6	1.08910891	0.90778385	0.73880252	1
7	1.18663325	0.82890241	0.81007631	1
1	1.12964686	0.78237425	0.96890643	2
2	0.99238041	0.84638191	0.91405588	2
3	1.3438907	0.72138031	0.91118717	2
4	1.38655643	0.75648524	1.0764978	2
5	1.24568849	0.81968627	1.16606724	2
6	1.32177839	0.77493905	1.19758733	2
7	1.20693492	1.13712767	1.12664602	2
1	0.51133845	1.79067543	0.70798521	3
2	0.696214	0.92720874	1.31292104	3
3	1.12624714	1.08751899	0.71844641	3
4	0.80396293	1.18215031	1.32391398	3
5	0.93018531	1.09438993	0.73071483	3
6	0.87240143	1.05372458	0.91074049	3
7	1.24888628	1.03326901	1.07721608	3

These features were used to calculate discriminant scores. Three scores were calculated for each observation. If the largest score was score 1, then the vapor was predicted to be cyclohexane. If the largest was score 2, the predicted vapor was ethanol. Lastly, if the largest was score 3, the vapor was predicted as THF. The Fisher's confusion matrices in Table 3 show that the training data classified fairly well with an APER of 27.8% and the method continued to perform similarly for the test data resulting in an APER of 33.3%. The quadratic analysis confusion matrices in Table 4 showed that the training data was fairly successful at identifying the correct vapor with an APER of 11.1%, performing better than Fisher's, but the test data performed poorly with an APER of 66.7%.

Table 3. Phase one Fisher's discriminant analysis confusion matrices

Training:

Actual Group	# of Cases	Predicted		
		V1	V2	V3
V1	6	4	2	0
V2	6	2	4	0
V3	6	1	0	5

Test:

Actual Group	# of Cases	Predicted		
		V1	V2	V3
V1	1	1	0	0
V2	1	0	1	0
V3	1	0	1	0

Table 4. Phase one quadratic discriminant analysis confusion matrices

Training:

Actual Group	# of Cases	Predicted		
		V1	V2	V3
V1	6	6	0	0
V2	6	1	5	0
V3	6	1	0	5

Test:

Actual Group	# of Cases	Predicted		
		V1	V2	V3
V1	1	1	0	0
V2	1	0	0	1
V3	1	1	0	0

For the neural network analysis, the data set was input in the same manner, training against the first six exposures and validating the network with the last exposure. The sensor features per vapor were the input variables and the output variables were the three vapors. The data was trained with 6 hidden nodes to 200 epochs and resulted in the confusion matrices in Table 5. These confusion matrices also showed that the neural network performed poorly for the validation sample with a similar APER of 66.7%.

Table 5. Phase one neural network analysis confusion matrices

Training:

Actual Group	**# of Cases**	**Predicted**		
		V1	**V2**	**V3**
V1	6	4	1	1
V2	6	1	5	0
V3	6	1	0	5

Test:

Actual Group	**# of Cases**	**Predicted**		
		V1	**V2**	**V3**
V1	1	0	1	0
V2	1	1	0	0
V3	1	0	0	1

Lachenbruch’s Holdout procedure was used to find an average error rate in classifying the data. To do this, the neural network was trained six more times, each time leaving a different observation out of the training data set. For this instance, there were seven holdouts (H) and three gases (G). The expected actual error rate for the training data was 12.7% and for the test data it was 52.4%. This average error confirmed the poor performance of the data. Confusion matrices for all seven procedures can be found in Appendix D.

Because the above methods performed so poorly, the data itself was closely examined and it was discovered that the single feature was not enough information to accurately classify the gases. Another feature was created based on the slopes of the plots formed when a sensor was exposed to a chemical. The following feature was calculated based on the slope of the last six readings of each observation:

$$Fs_{ijk} = \frac{\left[\left(\frac{\left(R_{\max} - R_0\right)}{R_0} * 100\right)_{ijk_l} - \left(\frac{\left(R_{\max} - R_0\right)}{R_0} * 100\right)_{ijk_{l-5}}\right]}{t_l - t_{l-5}} \tag{48}$$

where *l* is the last reading during exposure. For example, in observation one, the difference in the resistance change at 230 seconds and 180 seconds divided by 50 seconds would result in the appropriate feature for observation one. Table 6 shows the new feature according to sensor and vapor.

Table 6. Data feature based on slope

Exposure	Sensor 1	Sensor 2	Sensor 3	Vapor
1	0.3065	0.0190996	0.0846064	1
2	0.2685	0.005457	0.0916568	1
3	0.211	0.0245566	0.1222092	1
4	0.215	0.021828	0.1903644	1
5	0.1995	0.0491134	0.094007	1
6	0.222	0.0300136	0.0376028	1
7	0.232	0.0245566	0.0775558	1
1	0.0836502	0.1214098	0.1431924	2
2	0.0380228	0.1736292	0.1173708	2
3	0.0912548	-0.0639686	0.1079814	2
4	0.0912546	0.113577	0.2253522	2
5	0.0912548	-0.227154	0.2347418	2
6	0.0912548	0.1409922	0.2464788	2
7	0.068441	0.302872	0.1713616	2
1	0.0063254	1.6802412	0.043423	3
2	0.0060576	-0.325792	0.0434228	3
3	0.0160612	0.9170436	0.0374336	3
4	0.0031516	0.9773754	0.050161	3
5	0.011094	0.8687782	0.0449202	3
6	0.0064678	0.8325792	0.017968	3
7	0.0103678	0.8325792	0.074867	3

Discriminant scores were recalculated and the neural network retrained with this additional feature and the resulting confusion matrices in Tables 7, 8, and 9 show that the additional feature improves the performance of both the test and training data. Fisher's method resulted in a 0% APER for both the training and test data, while the quadratic scores method resulted in an APER of 0% for the training data and 33.3% for the test data. The neural network was trained with 10 nodes to 500 epochs and resulted in 0% APER for both data sets.

Table 7. Fisher's analysis confusion matrices for phase one with two features

Training:

Actual Group	# of Cases	Predicted V1	Predicted V2	Predicted V3
V1	6	6	0	0
V2	6	0	6	0
V3	6	0	0	6

Test:

Actual Group	# of Cases	Predicted V1	Predicted V2	Predicted V3
V1	1	1	0	0
V2	1	0	1	0
V3	1	0	0	1

Table 8. Quadratic discriminant analysis confusion matrices for phase one with two features

Training:

Actual Group	# of Cases	Predicted V1	Predicted V2	Predicted V3
V1	6	6	0	0
V2	6	0	6	0
V3	6	0	0	6

Test:

Actual Group	# of Cases	Predicted V1	Predicted V2	Predicted V3
V1	1	1	0	0
V2	1	0	0	1
V3	1	0	0	1

Table 9. Neural network confusion matrices for phase one with two features

Training:

Actual Group	# of Cases	Predicted V1	Predicted V2	Predicted V3
V1	6	6	0	0
V2	6	0	6	0
V3	6	0	0	6

Test:

Actual Group	# of Cases	Predicted V1	Predicted V2	Predicted V3
V1	1	1	0	0
V2	1	0	1	0
V3	1	0	0	1

For further analysis, noise was introduced into the data so signal-to-noise ratios could be computed. Signal to noise ratios were calculated with the following equation (Bauer, 2000:32):

$$SNR_i = 10\log_{base10}\left(\frac{\sum_{j=1}^{J}\left(w_{i,j}^1\right)^2}{\sum_{j=1}^{J}\left(w_{N,j}^1\right)^2}\right) \qquad (49)$$

$w_{i,j}^1$ = *hidden node weight*

$w_{N,j}^1$ = *noise node weight*

J = number of hidden nodes connected to each feature i

Table 10 shows the hidden node weights of the neural network along with the signal to noise ratios (SNR). Most of the ratios are similar, indicating most of the sensor data is important in distinguishing between the gases. The feature two, sensor three SNR is smaller compared to the rest indicating it may have less influence on the neural network. Because of this, another neural network was trained with all other features except for feature two of sensor three. This neural network resulted in less accuracy in classifying the data, indicating that feature two, sensor three data was needed to properly classify the vapors.

Table 10. Hidden node weights and signal-to-noise ratios for the neural network

		Feature 1			Feature 2			
	Noise	**Sensor 1**	**Sensor 2**	**Sensor 3**	**Sensor 1**	**Sensor 2**	**Sensor 3**	**Bias**
	0.015476	0.058538	0.038078	0.025285	0.038231	0.000449	-0.04065	0.035887
	0.007016	-0.07382	-0.00946	0.09303	-0.09808	0.090411	0.024747	-0.05055
	-0.01109	-0.05553	0.020847	-0.07848	-0.0941	-0.08741	0.00698	-0.01324
	-0.00542	-0.00957	0.064129	0.025578	0.071697	0.034574	-0.0665	-0.07427
	-0.0665	-0.08816	-0.00845	-0.03133	-0.0128	-0.0229	0.03621	0.015983
	-0.09698	0.048296	0.02833	-0.08473	0.080853	-0.05238	0.031864	0.043675
	0.024979	-0.02271	0.096667	0.0082	0.020847	-0.00103	-0.07241	0.02136
	0.007486	0.085345	0.083734	-0.02903	0.039396	0.012864	-0.04864	-0.09716
	0.031632	-0.03593	0.034629	-0.06489	-0.01811	-0.09142	0.007407	-0.07703
	-0.03681	0.031285	0.070367	0.092547	0.081164	0.076519	0.056743	-0.03742
sum sq	0.017304	0.032225	0.029467	0.037956	0.04068	0.034658	0.019945	0.028927
SNR		2.70041	2.311808	3.41119	3.712255	3.016482	0.616759	2.231443

Once again, Lachenbruch's Holdout procedure was conducted on the two data features to find an average error rate in classification. The expected actual error rate for the training data was 0% and for the test data it was 9.52%, so, on average, the data was able to be classified accurately. Confusion matrices for all seven holdouts can be found in Appendix D.

4.2.2 Phase Two

Phase two analysis began with a linear regression of the data to predict the sensor output of sensor three for each vapor. The **X** matrices were set up as $\mathbf{X} = [\mathbf{1}, \mathbf{x}_1, \mathbf{x}_2, \mathbf{t}]$.

The least-squares estimator of β for each vapor was

$$\hat{\boldsymbol{\beta}}_1 = \begin{bmatrix} 11.4945 \\ 0.1979 \\ 2.3821 \\ 0.0045 \end{bmatrix} \qquad \hat{\boldsymbol{\beta}}_2 = \begin{bmatrix} -2.5636 \\ 2.2863 \\ 0.1927 \\ 0.0047 \end{bmatrix} \qquad \hat{\boldsymbol{\beta}}_3 = \begin{bmatrix} 10.2563 \\ 0.4618 \\ 0.0785 \\ 0.0491 \end{bmatrix}$$

where vapor one was cyclohexane, vapor two was ethanol, and vapor three was THF.

The following models were developed:

$$\hat{y}_1 = 11.4945 + 0.1979x_1 + 2.3821x_2 + 0.0045t \tag{50}$$

$$\hat{y}_2 = -2.5636 + 2.2863x_1 + 0.1927x_2 + 0.0047t \tag{51}$$

$$\hat{y}_3 = 10.2563 + 0.4618x_1 + 0.0785x_2 + 0.0491t \tag{52}$$

where $\hat{y}$ is the predicted value of sensor three, x_1 is sensor one data, x_2 is sensor two data, and t is time. The first six exposures were used to build the models and the seventh exposure was used to validate them.

To test the significance of regression, the ANOVA tables shown in Tables 11-13, were developed.

Table 11. ANOVA table for cyclohexane

Source of Variation	Sum of Squares	Degrees of Freedom	Mean Square	F_0
Regression	6.48E+03	3	2.16E+03	193.4223
Residual	7.60E+02	68	11.17	
Total	7.24E+03	71		

Table 12. ANOVA table for ethanol

Source of Variation	Sum of Squares	Degrees of Freedom	Mean Square	F_0
Regression	9.95E+03	4	3.32E+03	240.3473
Residual	9.38E+02	68	13.7957	
Total	1.09E+04	71		

Table 13. ANOVA table for THF

Source of Variation	Sum of Squares	Degrees of Freedom	Mean Square	F_0
Regression	4.52E+04	4	1.51E+04	330.1967
Residual	3.10E+03	68	45.5798	
Total	4.83E+04	71		

The resulting p-values of approximately zero led to rejection of the null hypothesis indicating that at least one of the variables significantly contributed to all models. The R^2_{Adj} of the models were 0.8905, 0.9100, and 0.9329, respectively. These values indicated that most of the variability in the y's was explained by the models.

Since normality of the errors is required to conduct the above significance test, normal probability plots (NPP) were constructed to ensure that this assumption could be made. The NPPs, in Figures 25-27, are basically linear with some outliers present, which led to the acceptance of the normality assumption.

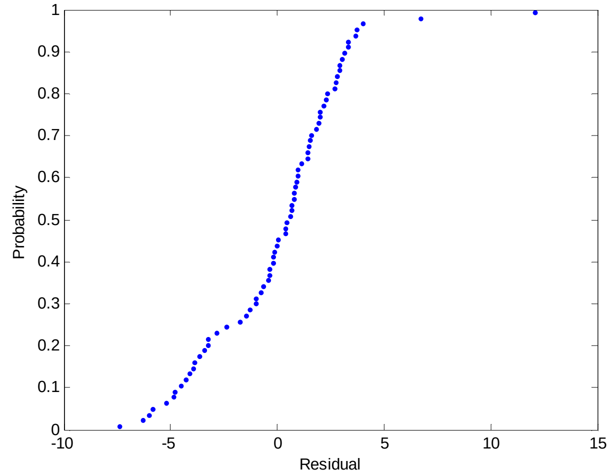

Figure 25. Normal probability plot for cyclohexane

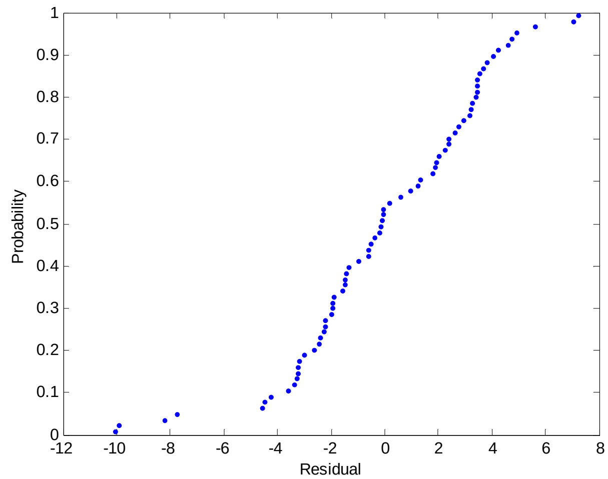

Figure 26. Normal probability plot for ethanol

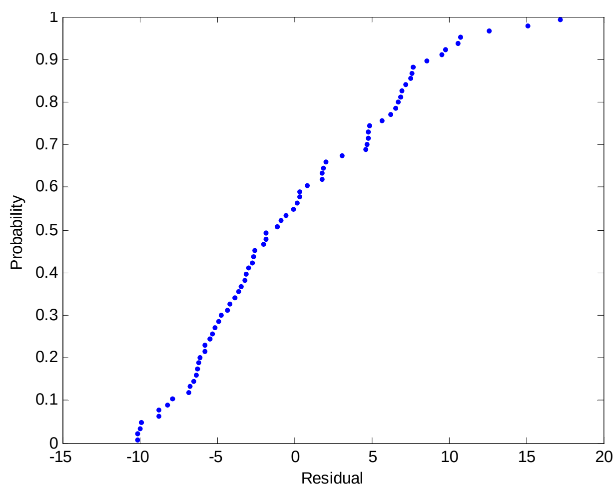

Figure 27. Normal probability plot for THF

To further assess the adequacy of the models, a residual analysis for each model was performed. The plots for cyclohexane and ethanol in Figures 28 and 29 indicated that the constant variance and linear relationship assumptions could be applied to these gases, but Figure 30 showed that they could not be applied to THF.

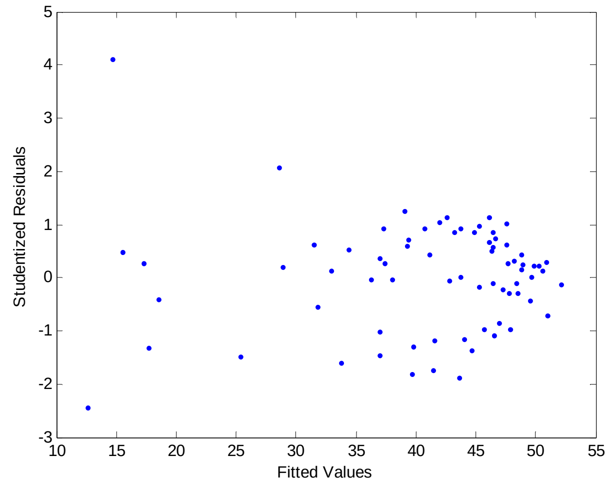

Figure 28. Sensor three residual plot for cyclohexane

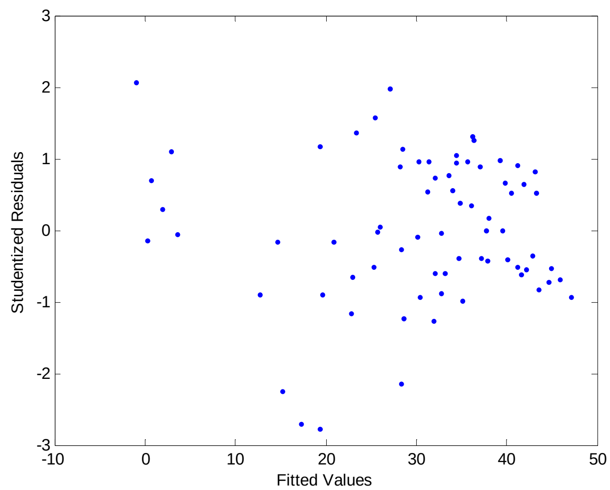

Figure 29. Sensor three residual plot for ethanol

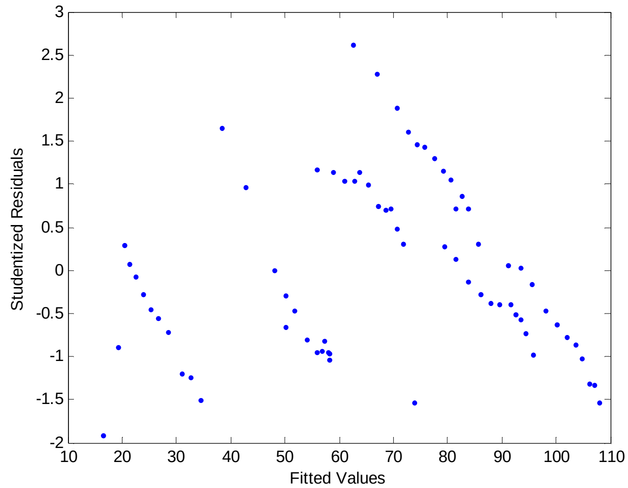

Figure 30. Sensor three residual plot for THF

Since the THF errors were found to have nonconstant variance, a weighted least squares was performed for model improvement. The variability was estimated using the moving range (MR) defined as (Montgomery, 2005:232)

$$\mathrm{MR}_i = |y_i - y_{i-1}| \tag{53}$$

From this, the weights were calculated as $\dfrac{1}{\mathrm{MR}}$ resulting in the following model:

$$y_3 = 23.3408 - 1.9601x_1 + 0.0752x_2 + 0.0535t \tag{54}$$

The residual plot, though, still indicated nonconstant variance as seen in Figure 31.

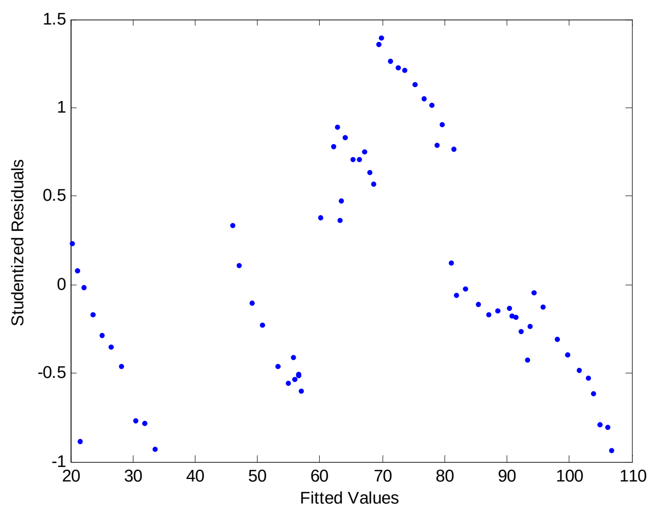

Figure 31. Weighted least squares plot for THF

Piecewise polynomial fitting (or splines) and a sinusoidal model were also used to develop a better model for THF. None of these methods succeeded in good estimates for sensor three data based on sensors one and two. This is due to the data, as seen in the y versus regressors plots in Figure 32, which would require nonlinear techniques for prediction. Because of this, the neural network served as the sole prediction method for THF.

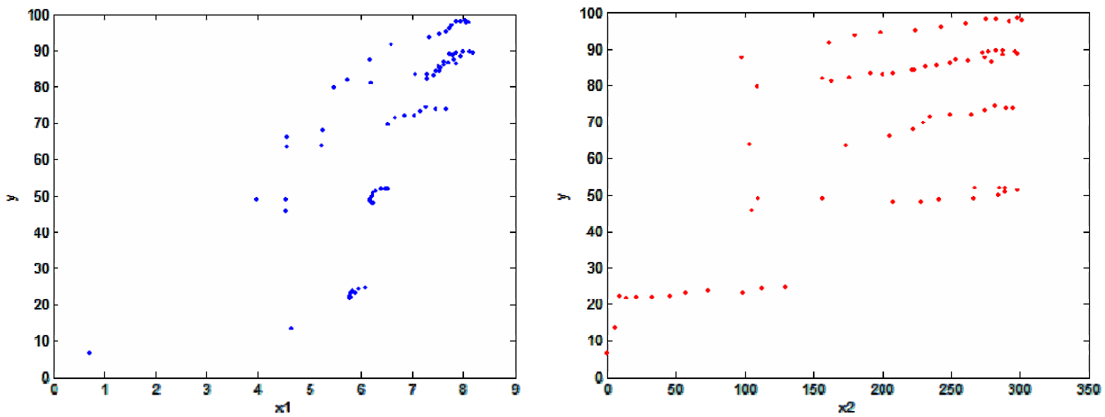

Figure 32. Plots of response, y, versus regressors, x_1 and x_2

Although the regression techniques led to adequate models for cyclohexane and ethanol, a neural network analysis was accomplished on all vapors to better predict the output of sensor three. The data of the first two sensors were used as inputs with the third sensor identified as the output. The neural network was trained with 5 nodes to 500 epochs.

The predicted values of both methods were graphed, in Figure 33, with the actual data to compare prediction capability of both models. The RMSEs, in Table 14, showed that the regression performed better than the neural network in predicting the third sensor for cyclohexane and ethanol. They also showed that the neural network performed fairly well in predicting all the vapors, including THF.

Table 14. RMSE's for sensor three models

	RMSE	
Vapor	**Neural Network**	**Regression**
Cyclohexane	2.899	1.687
Ethanol	4.824	4.380
THF	9.857	-

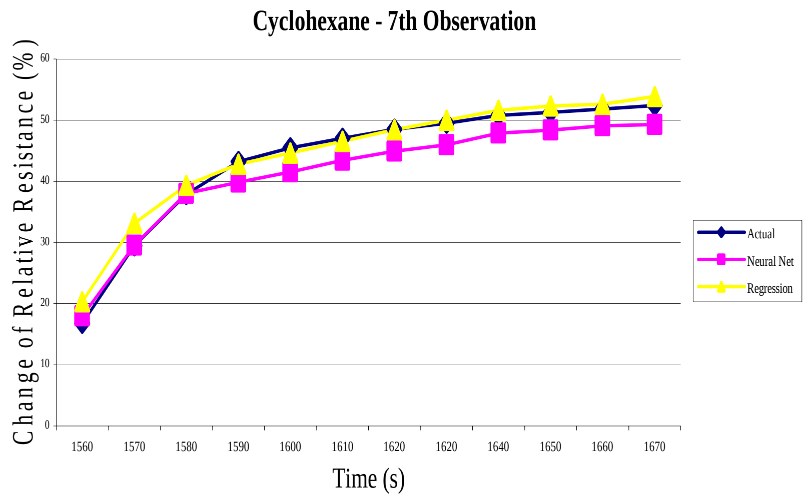

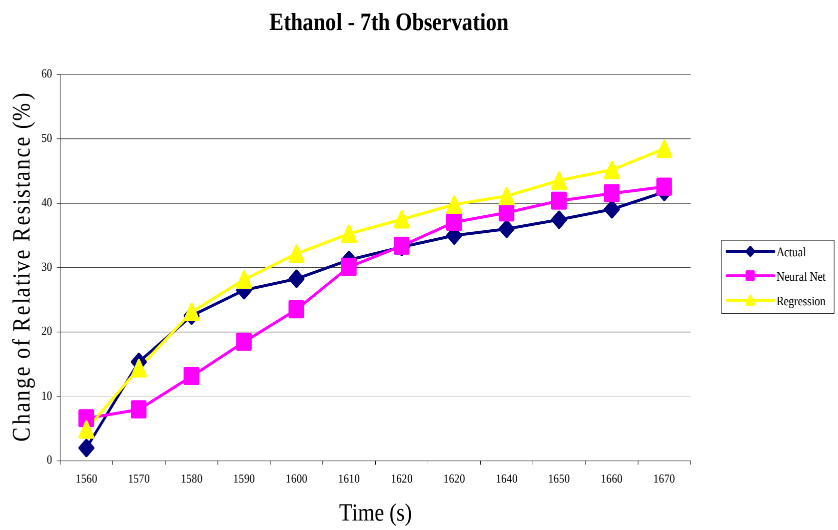

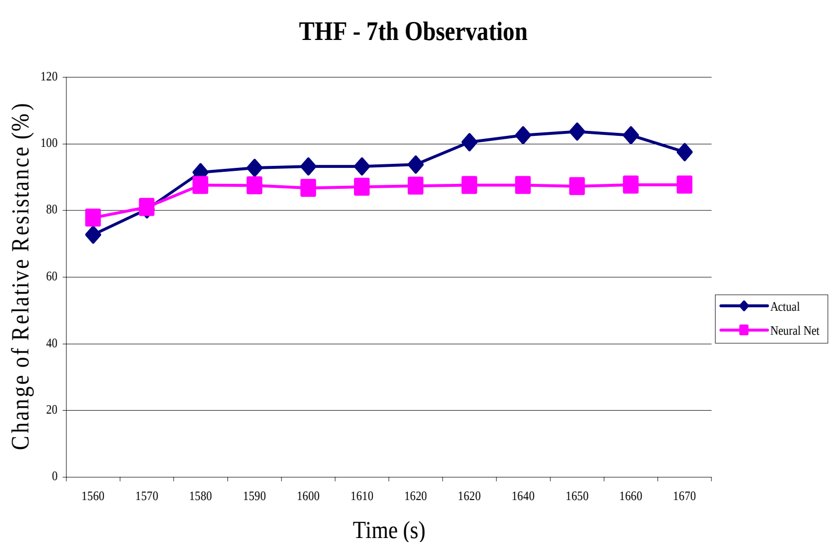

Figure 33. Predicted and actual values of sensor three by vapor

4.2.3 *Phase Three*

For phase three, data from a new set of sensors was used, as plotted in Figure 34. It was obvious that this data was different than the data in phase one, so it was not surprising if the models built on phase one data did not accurately classify this data. After discussions with Dr. Wei Chen, it was discovered that these differences were most likely due to the fact that the sensors during phase three experiments were months older than in phase one. During these months of aging, several experiments had been conducted on them which allowed for residual chemical build up in the sensors. This could have lead to different readings on specific sensors based on their chemical characteristics. Even though this was viewed as a potential issue, discriminant techniques were applied to the data to prove that sensor age impacted sensor classification.

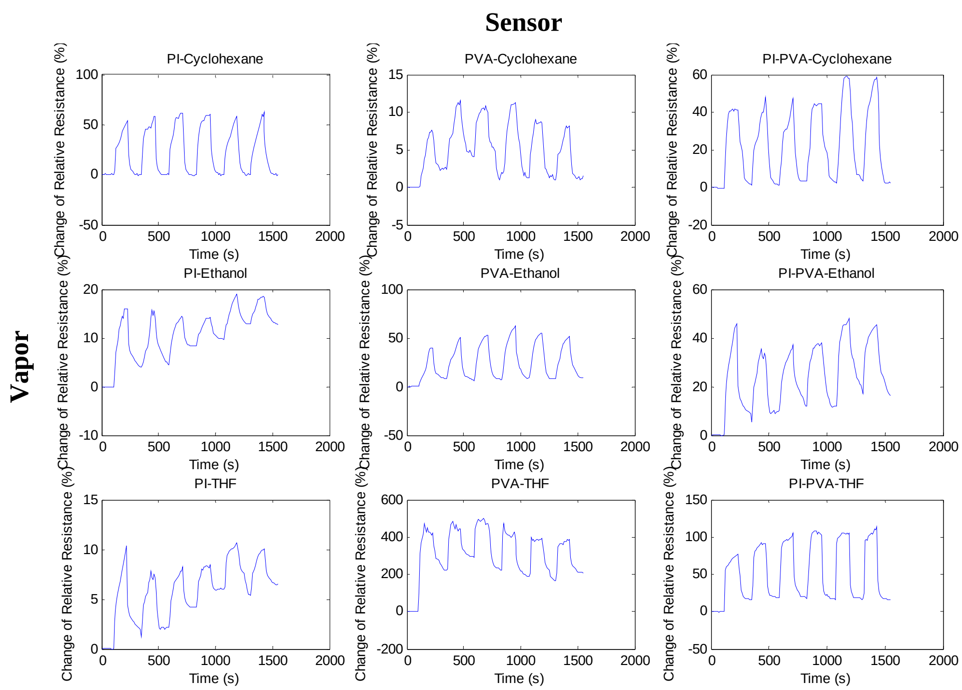

Figure 34. Phase three data matrix by vapor and sensor

Features, in Table 15, were once again calculated using Equations 41 and 48. They were then used to validate the models that were developed from the features in phase one.

Table 15. Phase three data features

	Feature 1			Feature 2			
Exposure	**Sensor 1**	**Sensor 2**	**Sensor 3**	**Sensor 1**	**Sensor 2**	**Sensor 3**	**Vapor**
1	1.175931	1.023003	0.56661	0.225396	0.020878	0.006088	1
2	1.212669	1.084147	1.538628	0.225396	0.041647	0.346308	1
3	0.971214	0.885291	1.419109	0.072459	-0.00787	0.293008	1
4	0.882484	0.978941	0.583188	0.126286	0.041264	0.021622	1
5	1.373864	0.828139	0.883084	0.315626	0.004844	0.120299	1
6	1.244025	0.989828	0.966607	0.290648	0.029388	0.180462	1
1	0.860175	1.141115	1.374607	0.032034	0.248222	-0.31358	2
2	1.236764	1.333025	1.132702	0.053152	0.284644	0.018756	2
3	1.025822	0.88837	1.151288	0.027601	0.11329	0.110866	2
4	1.063816	1.121701	0.833965	0.021488	0.242582	0.024657	2
5	1.276944	0.912194	0.797551	0.049089	0.107429	0.055433	2
6	0.879069	0.982816	0.944214	0.008892	0.123024	0.053349	2
1	1.465	1.395871	1.355226	-0.06968	-0.63253	0.145715	3
2	1.132704	0.840745	0.635177	0.004168	-0.0726	0.04204	3
3	1.151289	1.246459	0.89028	0.024637	-0.28996	0.189372	3
4	0.833969	2.735958	0.506979	0.005479	-0.16609	-0.1009	3
5	0.852657	0.507814	0.801067	0.012319	0.137248	-0.01368	3
6	0.944213	0.571045	0.679397	0.011855	0.194932	0.175784	3

The results of classification using Fisher's and quadratic discriminant analysis are shown in Tables 16 and 17. The training data were classified perfectly for both methods, but the test data performed less accurately with an APER of 55.6% for Fisher's and 38.9% for the quadratic, which was expected since the data looked so different.

Table 16. Phase three Fisher's analysis confusion matrices

Training Data:

Actual Group	# of Cases	Predicted		
		V1	V2	V3
V1	7	7	0	0
V2	7	0	7	0
V3	7	0	0	7

Test Data:

Actual Group	# of Cases	Predicted		
		V1	V2	V3
V1	6	4	2	0
V2	6	0	1	5
V3	6	0	3	3

Table 17. Phase three quadratic discriminant analysis confusion matrices

Training Data:

Actual Group	# of Cases	Predicted		
		V1	V2	V3
V1	7	7	0	0
V2	7	0	7	0
V3	7	0	0	7

Test Data:

Actual Group	# of Cases	Predicted		
		V1	V2	V3
V1	6	5	1	0
V2	6	0	4	2
V3	6	0	4	2

Table 18 shows that the neural network also performed well on the training data, but significantly misclassified the test data with an APER of 55.6%.

Table 18. Phase three neural network confusion matrices

Training Data:

Actual Group	# of Cases	Predicted V1	Predicted V2	Predicted V3
V1	7	7	0	0
V2	7	0	7	0
V3	7	0	0	7

Test Data:

Actual Group	# of Cases	Predicted V1	Predicted V2	Predicted V3
V1	6	5	1	0
V2	6	0	1	5
V3	6	0	4	2

The above results showed that the age of the sensor impacted the classification of the vapors, especially ethanol and THF.

Next, the prediction techniques used in phase two were used to develop models on the full phase two data set with no holdouts. The phase three data was then used to validate these models. The new regression models for cyclohexane and ethanol were:

$$\begin{aligned} y_1 &= 11.4133 + 0.2131x_1 + 2.3595x_2 + 0.0039t \\ y_2 &= -1.9520 + 2.0608x_1 + 0.2277x_2 + 0.0029t \end{aligned} \qquad (55)$$

These models passed the checks for adequacy and had R^2_{Adj} of 0.9052 and 0.9102, respectively. The neural network was once again trained with four nodes to 100 epochs using sensors one and two as the inputs and sensor three as the output. Table 16 shows the RMSE's of both the neural network and least squares regression for phase three data. The RMSE's show that phase one and two models were not the best prediction models for phase three data, which further shows the impact of the aged sensors. An example of a predicted values versus actual data plot is shown in Figure 35. The rest of the plots are located in Appendix E.

Table 19. Phase three RMSE's

	RMSE	
Vapor	**Neural Network**	**Regression**
Cyclohexane		
Exposure 1	4.263	6.130
Exposure 2	14.880	12.403
Exposure 3	16.489	16.981
Exposure 4	7.902	7.349
Exposure 5	14.218	15.026
Exposure 6	6.392	7.876
Ethanol		
Exposure 1	8.795	7.016
Exposure 2	7.533	5.596
Exposure 3	5.311	4.661
Exposure 4	5.190	3.732
Exposure 5	4.065	6.873
Exposure 6	1.537	6.241
THF		
Exposure 1	13.250	-
Exposure 2	21.906	-
Exposure 3	28.437	-
Exposure 4	25.909	-
Exposure 5	12.298	-
Exposure 6	15.229	-

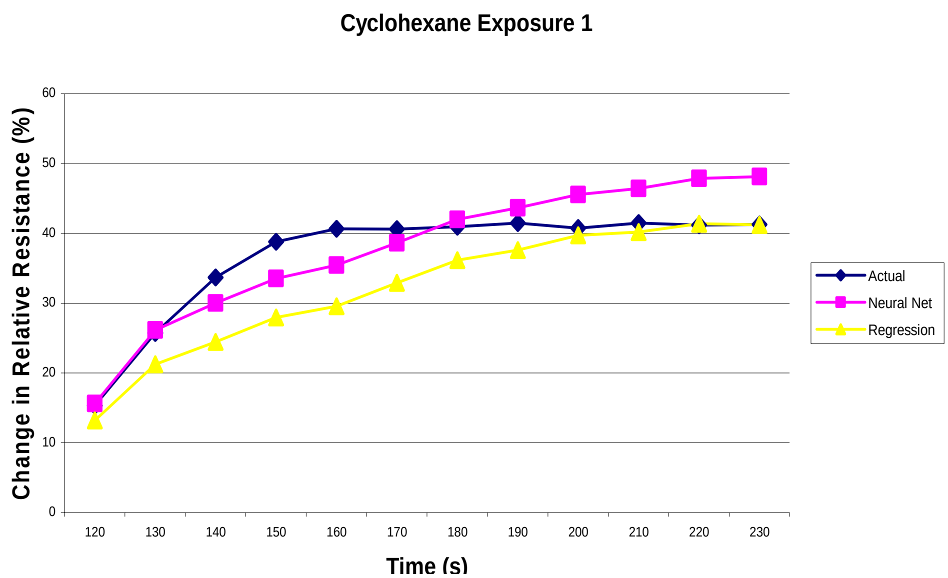

Figure 35. Predicted and actual values of sensor three for cyclohexane exposure one.

4.2.4 Phase Four

Phase four data, plotted in Figure 36, was also very different from the initial set of data. This data was collected from a newly manufactured set of PI, PVAc, and PI-PVAc sensors. It was expected that these data would also not be sufficiently classified and predicted by the models developed from the first set of data. The same methods used in phase three were used to show the inconsistencies between different sensor sets.

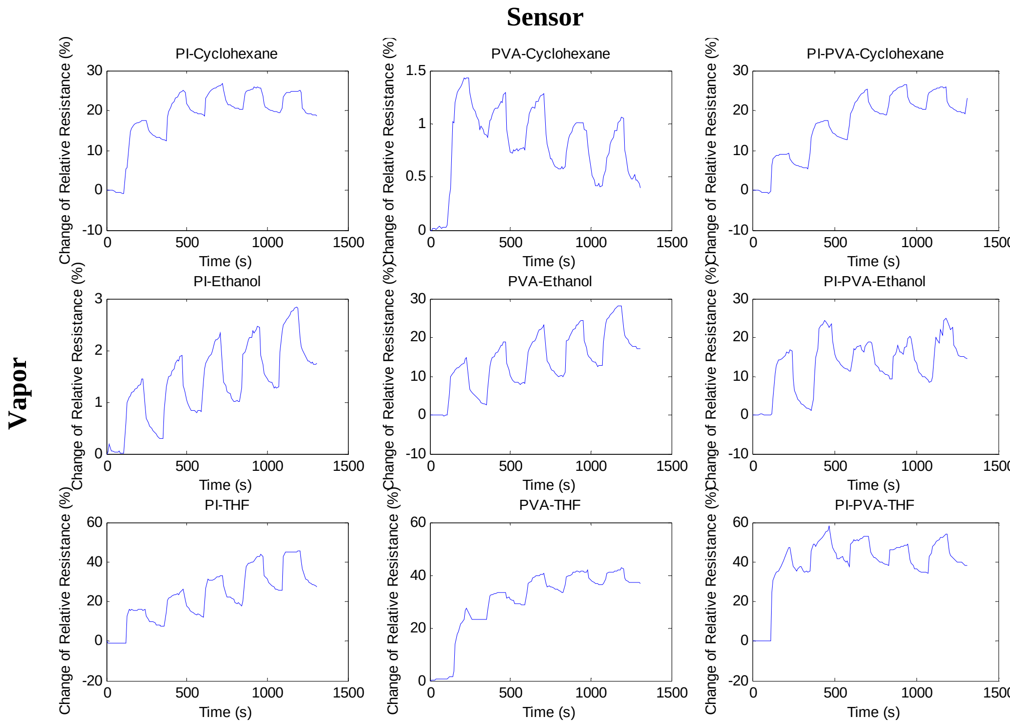

Figure 36. Phase four data matrix by vapor and sensor

Table 20 shows the data features that were calculated using Equations 41 and 48. These features were used to validate the same models developed in phase three.

Table 20. Phase four data features

	Feature 1			Feature 2			
Observation	**Sensor 1**	**Sensor 2**	**Sensor 3**	**Sensor 1**	**Sensor 2**	**Sensor 3**	**Vapor**
1	0.709334	0.780779	0.813902	0.017095	0.002395	-0.02523	1
2	0.98102	1.426941	0.862241	0.051286	0.002928	-0.02	1
3	0.819849	1.15167	1.282911	0.020083	0.001397	-0.02954	1
4	0.684759	0.707817	1.247191	0.006141	0.000133	-0.04913	1
5	0.588205	1.25645	0.640691	0.004149	0.003726	-0.06888	1
1	1.119915	1.19082	0.861281	0.004009	0.047827	0.048989	2
2	1.066997	1.007185	0.820879	0.005065	0.052047	-0.01243	2
3	1.303884	1.265177	1.022068	0.006682	0.068927	0.019174	2
4	0.889723	0.854844	1.288982	0.003869	0.037277	0.069532	2
5	0.934744	0.869599	1.102297	0.002814	0.02954	0.116308	2
1	0.420603	1.231845	1.383607	-0.00148	0.18234	0.172004	3
2	0.872359	0.556045	1.755483	0.047163	0.0074	0.127032	3
3	0.717784	0.894251	1.192714	0.050779	0.01574	0.025969	3
4	0.78837	0.787867	1.704366	0.061628	0.00834	0.037089	3
5	0.50449	1.176451	1.170101	0.007793	0.03008	0.062496	3

Tables 21 and 22 show the results from Fisher's and quadratic analysis using the features in Table 20. Fisher's approach results in an APER of 66.7% and quadratic analysis results in an APER of 73.3%, which demonstrates that the models built on the initial data are insufficient in classifying this new data. The results of the neural network, in Table 23, show further inconsistencies with an APER of 60.0%.

Table 21. Phase four Fisher's analysis confusion matrices

Training Data:

Actual Group	**# of Cases**	**Predicted V1**	**Predicted V2**	**Predicted V3**
V1	7	7	0	0
V2	7	0	7	0
V3	7	0	0	7

Test Data:

Actual Group	**# of Cases**	**Predicted V1**	**Predicted V2**	**Predicted V3**
V1	5	0	0	5
V2	5	0	1	4
V3	5	0	1	4

Table 22. Phase four quadratic discriminant analysis confusion matrices

Training Data:

Actual Group	**# of Cases**	**Predicted V1**	**Predicted V2**	**Predicted V3**
V1	7	7	0	0
V2	7	0	7	0
V3	7	0	0	7

Test Data:

Actual Group	**# of Cases**	**Predicted V1**	**Predicted V2**	**Predicted V3**
V1	5	0	2	3
V2	5	0	3	2
V3	5	0	4	1

Table 23. Phase four neural network confusion matrices

Training Data:

Actual Group	# of Cases	Predicted V1	Predicted V2	Predicted V3
V1	7	7	0	0
V2	7	0	7	0
V3	7	0	0	7

Test Data:

Actual Group	# of Cases	Predicted V1	Predicted V2	Predicted V3
V1	5	0	0	5
V2	5	0	1	4
V3	5	0	0	5

The phase two methods used to build models were also applied to this data. Using Equation 55 and a neural network, the third sensor was predicted according to vapor. Once again, THF was only predicted using a neural network. The predicted versus actual data graphs are located in Appendix E.

Table 24 includes the RMSE's that resulted from the regression analysis and neural network. When these results are compared to the results of phase three, we see that the models' prediction performance for phase three cyclohexane and THF data and phase two ethanol data is good. On average, the models predicted phase four data better.

Table 24. Phase four RMSE's

	RMSE	
Vapor	**Neural Network**	**Regression**
Cyclohexane		
Observation 1	12.110	9.422
Observation 2	6.951	3.691
Observation 3	2.859	1.456
Observation 4	1.319	3.108
Observation 5	1.682	2.638
Ethanol		
Observation 1	7.278	9.649
Observation 2	12.572	13.238
Observation 3	8.933	8.461
Observation 4	7.546	5.910
Observation 5	10.674	7.338
THF		
Observation 1	18.398	-
Observation 2	7.062	-
Observation 3	6.339	-
Observation 4	10.405	-
Observation 5	8.218	-

4.3 Summary

In phase one, Fisher's approach, quadratic discriminant scores, and neural networks were used to classify the initial data set by vapor. We were able to accurately classify the data using two data features. Phase two consisted of using the initial data set to predict sensor three output from sensors one and two. Least squares regression and neural networks were able to effectively predict the sensor three data using sensors one and two and time as variables. During phase three, the initial data set was once again used to develop classification and prediction models, but data from an "aged" sensor was used to validate these models. The models based on the initial data set poorly classified and predicted the “aged” sensor data. Lastly, in phase four, the new sensor data was used to validate the models built in phase three. These models also performed poorly for the different sensor data set.

5. Conclusions

5.1 Introduction

The goal of this thesis was to develop models that could classify carbon nanotube polymer composite sensor data by vapor. Additionally, models were built to predict sensor three data based on two other sensors (sensors one and two). Three sets of detection data from three different sensor sets were used to accomplish this:

1. PI, PVAc, PI-PVAc sensors with approximately 20 experiments conducted on them
2. Same set of sensors as 1., but seven to nine months older and about 50 experiments conducted on them
3. Different and new set of the three sensors

The data from the three sensors was generated by Dr. Wei Chen at The University of Dayton.

5.2 Literature Review Findings

The literature review began by describing the equipment that the Air Force currently uses for chemical detection, as well as the equipment that is being developed and will soon be fielded. It discussed the technology that each uses for detection along with its capability, advantages, and disadvantages.

The literature review continued with a short discussion on carbon nanotubes before moving into the topic of carbon black polymer composite sensors and their use in chemical detection research. Included in this section were several plots and other information that showed that the carbon black sensors could discriminate between various gases. Next, carbon nanotubes as sensors with polymer composites were discussed. This portion described how they were manufactured and highlighted their ability to detect different chemicals.

The literature review then described various multivariate analysis techniques. It began by describing Fisher's discriminant function and quadratic discriminant scores along with the assumptions needed to use these techniques. It continued with a description of neural networks and signal-to-noise ratios.

The literature review ended with a discussion on regression analysis. This section focused on least squares fitting, methods to ensure model accuracy and adequacy, and concluded with a discussion on weighted least squares.

5.3 Methodologies Employed

The methodology was separated into four phases based on the data and analysis technique being applied. The first phase consisted of classifying the first set of data by vapor using Fisher's method, quadratic discriminant scores, and neural networks. This was done by calculating specific features that represented each observation. It was found that a single feature was not enough to classify the data, so another feature was developed to further explain the observations. This added feature allowed the above methods to accurately classify the vapors in most instances. In the second phase, sensor one and two data were used to predict sensor three using regression analysis and neural networks. Phase three included performing the same phase one and two analysis on the second set of data. During this phase, the data was used to validate the models developed from phase one and two data. It was shown that these models could not accurately classify or predict the new data, showing that the age of the sensor had an impact on the output of the sensor. During phase four, the same analysis was conducted, but on data set three. This phase used the same techniques in phase three to prove that there were detection inconsistencies between different sets of sensors of the same types.

5.4 Relevance of the Research

This research can be applied to the Global War on Terrorism and homeland defense. The threat of chemical weapons attacks is a reality and the best way to combat it is through contamination avoidance. The technology discussed in this thesis directly contributes to avoidance through the detection and identification of a chemical vapor. Development of equipment using this technology could lead to faster and more accurate chemical detection in the field.

5.5 Recommendations for Future Research

Future research could include similar analysis conducted on much larger data sets. Currently, the models are based on small data sets, which results in great sensitivity to any changes in sensor output. A larger data set one may account for these changes and lead to the correct classification of phase three and four data sets.

Another area of research would be to analyze data on sensors that have had collected residuals removed from the sensors before each detection. The method of residual removal could be anything, such as flash heat. The important factor would be that the sensor begins fresh at each detection cycle. This method could alleviate the differences in output from new and aged sensors.

More research should also be conducted to further examine the differences in different sets of sensors. This is important in determining the detection consistencies between sensors. If the sensors have such diverse characteristics that they require different classification algorithms, this capability will be difficult to field.

The last area of research suggested is to examine the capability of the sensors to quantify the concentration of a chemical vapor. This is an important capability in the field and is one that most current USAF detectors do not have, but new generation detectors in development boast this capability. For this technology to be a viable option, it will also need to possess the ability to measure concentration.

Appendix A. Phases One and Two Raw Data

	Cyclohexane-PI	Cyclohexane-PVAc	Cyclohexane-PI/PVAc
time (s)	Change of Relative Resistance (%)	Change of Relative Resistance (%)	Change of Relative Resistance (%)
0	0	0	0
10	-0.025	0.13643	0.11751
20	-0.025	-0.13643	0.11751
30	0	-0.13643	0.11751
40	0	-0.27285	0.11751
50	-0.05	0	0.23502
60	0	0.13643	0.11751
70	-0.025	0	0
80	-0.025	-0.13643	0.23502
90	-0.05	-0.27285	0.11751
100	0	-0.13643	0.11751
110	-0.025	-0.13643	0
120	3.075	0	5.2879
130	10.1	4.7749	20.68155
140	15.75	6.95771	30.08226
150	20.675	7.63984	36.07521
160	25.325	8.45839	40.30552
170	29	8.86767	43.12573
180	32.05	9.82265	45.3584
190	35.375	10.23192	46.651
200	38.775	11.05048	47.9436
210	40.7	10.91405	48.29612
220	44.55	10.6412	49.00118
230	47.375	10.77763	49.58872
240	24.1	8.18554	39.48296
250	11.475	4.63847	27.61457
260	8.275	2.31924	22.56169
270	6.5	1.90996	20.56404
280	5.175	1.50068	19.62397
290	4.45	1.09141	18.56639
300	3.375	0.81855	17.2738
310	2.775	0.5457	15.39365
320	2.4	0.27285	14.57109
330	2.15	0.13643	14.10106
340	1.975	-0.13643	13.74853
350	1.8	-0.27285	13.2785
360	9.625	-0.13643	26.79201

	Cyclohexane-PI	Cyclohexane-PVAc	Cyclohexane-PI/PVAc
time (s)	Change of Relative Resistance (%)	Change of Relative Resistance (%)	Change of Relative Resistance (%)
370	22.35	4.63847	35.37015
380	28.8	7.77626	38.30787
390	33.25	8.18554	41.24559
400	37.8	9.27694	42.6557
410	40.2	9.41337	43.71328
420	43	9.82265	44.65335
430	47	9.95907	46.06345
440	48.45	9.68622	48.29612
450	51.275	10.0955	48.53114
460	55.075	9.95907	49.11868
470	56.425	10.0955	49.23619
480	30.575	7.77626	39.36545
490	9.425	4.7749	28.20212
500	7.075	3.54707	21.97415
510	6	1.36426	19.9765
520	5.35	0.95498	18.91892
530	4.925	0.40928	17.2738
540	4.35	0.13643	15.9812
550	3.825	0.13643	14.92362
560	3.625	0	13.98355
570	3.55	-0.13643	13.74853
580	3.125	-0.13643	13.396
590	2.95	-0.27285	13.04348
600	5.175	0.13643	17.03878
610	21.975	4.36562	29.61222
620	32.85	6.82128	33.60752
630	35.15	7.77626	35.48766
640	40.425	8.04911	37.60282
650	43.1	8.86767	40.18801
660	46.575	9.27694	42.53819
670	48.95	9.5498	44.0658
680	50.675	9.5498	46.53349
690	53.45	9.82265	47.59107
700	55.25	10.0955	48.17861
710	57.125	10.50477	48.64865
720	30.85	8.45839	37.72033
730	11.525	4.2292	25.49941
740	8.55	3.54707	21.03408
750	7.05	2.04638	18.80141
760	5.425	1.36426	16.80376
770	4.6	0.81855	15.51116

	Cyclohexane-PI	Cyclohexane-PVAc	Cyclohexane-PI/PVAc
time (s)	Change of Relative Resistance (%)	Change of Relative Resistance (%)	Change of Relative Resistance (%)
780	4.25	0.27285	13.396
790	3.725	0.13643	12.69095
800	3.525	0	12.22092
810	3.4	-0.13643	11.86839
820	3.475	0.13643	11.04583
830	3.225	0.27285	10.6933
840	5.425	0.40928	18.09636
850	24.375	5.72988	28.55464
860	30.95	6.54843	32.19741
870	36.1	7.23056	33.72503
880	39.45	7.63984	35.60517
890	42.225	8.32196	37.3678
900	44.1	8.59482	40.18801
910	46.55	9.14052	42.89072
920	48.275	9.5498	44.65335
930	50.6	9.27694	46.76851
940	52.075	9.41337	48.0611
950	54.85	9.68622	49.70623
960	29.275	7.63984	36.66275
970	12	5.45703	26.43948
980	8.05	3.13779	22.32667
990	6.625	1.90996	19.62397
1000	4.975	1.22783	17.3913
1010	4.75	0.5457	16.56874
1020	4.15	0.40928	13.74853
1030	3.45	0.13643	12.22092
1040	3.05	0.27285	11.51586
1050	2.825	-0.13643	10.92832
1060	2.625	-0.27285	10.6933
1070	2.45	-0.40928	10.34078
1080	12.175	-0.40928	13.63102
1090	27.15	4.09277	33.49001
1100	32.95	5.59345	36.07521
1110	35.375	6.13915	37.95535
1120	38.65	6.41201	41.71563
1130	40.35	6.82128	43.83079
1140	42.725	7.36698	46.29847
1150	47.8	8.04911	48.41363
1160	48.625	8.45839	49.23619
1170	50.925	9.27694	49.70623
1180	52.3	9.5498	50.52879

	Cyclohexane-PI	Cyclohexane-PVAc	Cyclohexane-PI/PVAc
time (s)	Change of Relative Resistance (%)	Change of Relative Resistance (%)	Change of Relative Resistance (%)
1190	52.7	9.82265	50.99882
1200	26.275	7.09413	40.30552
1210	10.65	5.18417	29.84724
1220	7.85	4.63847	25.3819
1230	5.925	2.72851	21.2691
1240	5.125	1.77353	19.9765
1250	4.575	1.22783	18.6839
1260	3.45	0.68213	16.21622
1270	3.1	0.13643	14.45358
1280	2.875	0.27285	13.396
1290	3.15	0	12.57344
1300	2.9	-0.40928	11.75088
1310	2.575	-0.5457	11.28085
1320	12.45	-0.5457	17.2738
1330	26.125	4.36562	33.3725
1340	34.725	5.3206	38.19036
1350	37.175	6.82128	42.53819
1360	39.25	7.50341	45.94595
1370	42.575	7.91269	47.59107
1380	45.375	8.18554	49.82374
1390	49.075	8.45839	50.88132
1400	52.275	8.73124	50.29377
1410	54.45	9.14052	50.99882
1420	55.25	9.27694	51.82139
1430	56.475	9.68622	51.70388
1440	29.675	7.09413	34.31257
1450	10.075	5.72988	30.31727
1460	6.525	4.7749	25.96945
1470	5.35	3.00136	22.56169
1480	4.525	2.18281	20.79906
1490	3.85	1.36426	19.50646
1500	3.55	0.95498	18.56639
1510	3.175	0.81855	16.92127
1520	2.875	0.40928	15.62867
1530	2.775	0.27285	14.92362
1540	2.55	0	13.98355
1550	2.425	-0.40928	13.16099
1560	10.775	-0.13643	16.80376
1570	24.55	4.09277	29.49471
1580	34.2	5.8663	37.83784
1590	36.475	7.09413	43.24324

	Cyclohexane-PI	Cyclohexane-PVAc	Cyclohexane-PI/PVAc
time (s)	Change of Relative Resistance (%)	Change of Relative Resistance (%)	Change of Relative Resistance (%)
1600	39.15	7.63984	45.47591
1610	42.025	8.18554	47.00353
1620	44.575	8.73124	48.53114
1620	46.125	9.27694	49.47121
1640	48.925	9.68622	50.76381
1650	50.475	9.82265	51.23384
1660	54.95	9.5498	51.82139
1670	56.175	9.95907	52.40893
1680	28.85	6.54843	34.78261
1690	11	5.72988	26.08696
1700	6.8	4.36562	23.14924
1710	5.275	2.45566	19.85899
1720	4.175	1.90996	18.56639
1730	3.3	1.50068	17.74383
1740	2.875	1.22783	17.03878
1750	2.725	0.81855	15.9812
1760	2.525	0.27285	15.51116
1770	2.375	0.13643	15.15864
1780	2.25	0	14.6886
1790	2.125	-0.27285	14.45358

	Ethanol-PI	Ethanol-PVAc	Ethanol-PI/PVAc
time (s)	Change of Relative Resistance (%)	Change of Relative Resistance (%)	Change of Relative Resistance (%)
0	0	0	0
10	-0.38023	-0.19582	-0.35211
20	-1.14068	0.13055	-0.23474
30	0	0.19582	0
40	-0.76046	0.32637	-0.11737
50	-0.38023	0	-0.46948
60	-0.76046	0.06527	-0.11737
70	-1.14068	-0.13055	-0.23474
80	-0.38023	-0.06527	-0.23474
90	-1.14068	0.13055	-0.23474
100	-0.76046	0.06527	-0.23474
110	-0.76046	0	-0.35211
120	-1.14068	25.2611	-0.23474
130	5.32319	47.78068	9.38967
140	7.98479	62.59791	20.65728
150	8.36502	68.60313	27.11268
160	7.22433	70.36554	31.4554
170	7.98479	71.86684	33.80282
180	9.88593	72.78068	36.26761
190	11.02662	73.49869	37.67606
200	12.54753	75.2611	39.31925
210	13.30798	76.50131	40.61033
220	13.68821	77.21932	42.01878
230	14.06844	78.85117	43.42723
240	4.56274	64.81723	31.80751
250	3.42205	53.5248	21.94836
260	1.90114	36.8799	16.43192
270	0.76046	28.39426	12.44131
280	0	26.10966	10.0939
290	-1.14068	23.62924	8.21596
300	-1.52091	21.27937	6.69014
310	-0.76046	17.55875	5.6338
320	-1.14068	15.79634	4.81221
330	-1.90114	14.68668	4.34272
340	-1.52091	12.85901	3.52113
350	-0.76046	11.6188	2.93427
360	-0.38023	12.46736	3.05164
370	6.08365	33.94256	16.43192

	Ethanol-PI	Ethanol-PVAc	Ethanol-PI/PVAc
time (s)	Change of Relative Resistance (%)	Change of Relative Resistance (%)	Change of Relative Resistance (%)
380	7.60456	47.7154	25.70423
390	9.88593	56.72324	29.57746
400	9.12548	57.63708	33.21596
410	7.22433	58.48564	34.38967
420	9.88593	60.18277	36.38498
430	9.88593	64.55614	37.9108
440	10.26616	66.12272	39.20188
450	11.02662	63.57702	40.25822
460	10.26616	68.14621	40.96244
470	11.78707	68.86423	42.25352
480	4.94297	57.04961	36.50235
490	3.42205	49.02089	29.69484
500	2.28137	39.81723	20.77465
510	1.52091	36.68407	14.78873
520	1.90114	32.3107	11.85446
530	0.76046	30.09138	9.2723
540	0.38023	26.95822	8.09859
550	0	24.08616	6.57277
560	0.38023	22.25849	5.75117
570	0	19.77807	4.81221
580	-0.76046	17.23238	4.22535
590	-0.38023	15.86162	3.28638
600	0	17.36292	3.40376
610	3.42205	47.58486	7.39437
620	4.94297	59.07311	20.65728
630	5.70342	65.20888	26.17371
640	7.22433	68.66841	29.81221
650	7.98479	72.7154	32.62911
660	7.22433	78.00261	34.74178
670	8.36502	74.21671	36.03286
680	9.12548	75.71802	37.32394
690	9.88593	76.30548	38.61502
700	11.40684	74.86945	39.31925
710	11.78707	74.80418	40.14085
720	2.6616	62.20627	36.26761
730	2.28137	38.57702	30.51643
740	1.90114	32.96345	18.30986
750	0.76046	30.8094	13.14554
760	0	28.26371	10.44601

	Ethanol-PI	Ethanol-PVAc	Ethanol-PI/PVAc
time (s)	Change of Relative Resistance (%)	Change of Relative Resistance (%)	Change of Relative Resistance (%)
770	-0.76046	24.21671	8.92019
780	-0.38023	20.43081	7.15962
790	-1.90114	20.953	5.98592
800	-1.52091	17.55875	5.16432
810	-1.90114	16.97128	4.10798
820	-1.14068	16.12272	3.28638
830	-1.90114	14.62141	2.93427
840	-1.14068	16.44909	2.93427
850	2.28137	44.58225	7.04225
860	3.42205	52.61097	23.70892
870	4.18251	63.6423	28.28638
880	4.56274	69.84334	31.10329
890	5.70342	72.06266	32.62911
900	6.84411	73.04178	34.85915
910	7.98479	74.93473	38.26291
920	8.74525	75.65274	40.96244
930	9.88593	77.08877	42.84038
940	10.64639	77.80679	44.48357
950	11.40684	78.72063	46.12676
960	3.04183	71.34465	41.19718
970	1.90114	57.5718	28.16901
980	0.76046	44.71279	22.30047
990	0	32.18016	20.07042
1000	-0.76046	30.61358	17.84038
1010	-0.38023	25.45692	15.84507
1020	-1.14068	22.25849	13.96714
1030	-1.52091	19.84334	12.55869
1040	-1.14068	16.12272	11.26761
1050	-1.90114	11.22715	9.85915
1060	-2.6616	9.46475	7.98122
1070	-3.42205	5.93995	5.98592
1080	-2.28137	9.07311	6.10329
1090	1.90114	30.15666	9.50704
1100	3.80228	60.18277	18.66197
1110	5.32319	71.80157	24.1784
1120	6.08365	79.96084	27.46479
1130	6.84411	76.82768	30.98592
1140	7.60456	75.78329	33.33333
1150	9.12548	73.89034	36.38498

	Ethanol-PI	Ethanol-PVAc	Ethanol-PI/PVAc
time (s)	Change of Relative Resistance (%)	Change of Relative Resistance (%)	Change of Relative Resistance (%)
1160	9.88593	73.2376	39.55399
1170	10.64639	68.47258	42.37089
1180	11.40684	66.44909	44.13146
1190	12.1673	64.42559	45.07042
1200	6.08365	65.99217	37.55869
1210	3.80228	52.87206	27.8169
1220	1.52091	42.10183	21.00939
1230	0.76046	36.42298	16.90141
1240	0.38023	31.52742	13.96714
1250	-0.38023	24.34726	11.73709
1260	-0.76046	23.62924	10.32864
1270	-1.14068	22.19321	9.03756
1280	-1.52091	14.42559	8.21596
1290	-0.76046	10.11749	7.62911
1300	-1.52091	7.5718	7.15962
1310	-2.6616	6.39687	6.57277
1320	-1.14068	10.11749	6.69014
1330	1.14068	43.53786	14.08451
1340	2.6616	57.50653	20.30516
1350	4.18251	62.27154	23.47418
1360	5.32319	63.90339	27.34742
1370	6.84411	65.53525	29.92958
1380	7.98479	67.29765	31.57277
1390	8.74525	68.73368	35.79812
1400	9.88593	69.97389	38.61502
1410	11.02662	70.49608	41.5493
1420	11.78707	72.32376	43.07512
1430	12.54753	74.34726	43.89671
1440	4.18251	53.91645	34.85915
1450	1.90114	43.21149	23.59155
1460	0.76046	31.39687	18.30986
1470	-0.38023	27.67624	15.96244
1480	0	22.45431	13.84977
1490	-1.14068	20.75718	11.50235
1500	-1.90114	19.38642	9.50704
1510	-0.76046	17.88512	6.80751
1520	-1.90114	15.86162	3.87324
1530	-2.6616	13.77285	3.05164
1540	-1.90114	9.8564	2.11268
1550	-2.6616	8.28982	1.87793
1560	-0.76046	9.5953	1.99531

	Ethanol-PI	Ethanol-PVAc	Ethanol-PI/PVAc
time (s)	Change of Relative Resistance (%)	Change of Relative Resistance (%)	Change of Relative Resistance (%)
1570	1.90114	27.2846	15.37559
1580	4.56274	40.46997	22.53521
1590	6.08365	48.49869	26.52582
1600	7.60456	50.91384	28.28638
1610	8.36502	57.96345	31.22066
1620	9.12548	60.05222	33.21596
1620	9.88593	63.05483	34.97653
1640	10.26616	64.81723	36.03286
1650	11.02662	68.21149	37.44131
1660	11.40684	71.99739	39.08451
1670	12.54753	75.19582	41.78404
1680	5.32319	54.37337	23.59155
1690	2.6616	39.49086	19.60094
1700	1.52091	33.68146	17.723
1710	0.76046	25.13055	15.61033
1720	-0.38023	23.89034	14.55399
1730	-0.38023	22.84595	12.55869
1740	-1.14068	22.51958	11.38498
1750	-1.90114	17.62402	8.09859
1760	-2.28137	15.4047	7.39437
1770	-1.52091	10.70496	5.39906
1780	-2.6616	4.69974	4.46009
1790	-3.42205	7.8329	3.40376

	THF-PI	THF-PVAc	THF-PI/PVAc
time (s)	Change of Relative Resistance (%)	Change of Relative Resistance (%)	Change of Relative Resistance (%)
0	0	0	0
10	0.00281	0	-0.35211
20	0.0212	0.15083	-0.23474
30	0.02238	-0.15083	0
40	0.02115	-0.15083	-0.11737
50	0.01422	-0.15083	-0.46948
60	-0.00805	0	-0.11737
70	-0.00823	-0.15083	-0.23474
80	-1.87E-04	0	-0.23474
90	-0.00299	-0.15083	-0.23474
100	0.0015	-0.15083	-0.23474
110	-0.01123	-0.15083	-0.35211
120	0.72179	0.75415	-0.23474
130	4.65948	6.03318	9.38967
140	5.78495	9.65309	20.65728
150	5.77859	14.02715	27.11268
160	5.79936	22.02112	31.4554
170	5.77316	33.33333	33.80282
180	5.76699	46.00302	36.26761
190	5.80292	57.61689	37.67606
200	5.83286	74.05732	39.31925
210	5.89181	98.4917	40.61033
220	5.95562	113.12217	42.01878
230	6.08326	130.01508	43.42723
240	6.31251	84.01207	31.80751
250	5.65002	64.55505	21.94836
260	4.86047	55.80694	16.43192
270	4.54	52.33786	12.44131
280	4.37146	49.17044	10.0939
290	4.26105	45.24887	8.21596
300	4.2122	41.93062	6.69014
310	4.1555	41.3273	5.6338
320	4.10797	39.66817	4.81221
330	4.05931	38.15988	4.34272
340	4.01234	37.40573	3.52113
350	3.9779	35.89744	2.93427
360	3.97248	110.10558	3.05164
370	4.53353	156.71192	16.43192
380	6.24682	208.29563	25.70423
390	6.21706	228.50679	29.57746

	THF-PI	THF-PVAc	THF-PI/PVAc
time (s)	Change of Relative Resistance (%)	Change of Relative Resistance (%)	Change of Relative Resistance (%)
400	6.16915	241.93062	33.21596
410	6.16635	266.36501	34.38967
420	6.2165	284.01207	36.38498
430	6.23971	289.44193	37.9108
440	6.2878	298.64253	39.20188
450	6.40159	288.98944	40.25822
460	6.48	284.91704	40.96244
470	6.51938	267.72247	42.25352
480	6.53652	200.45249	36.50235
490	5.80385	162.29261	29.69484
500	5.10094	132.73002	20.77465
510	4.9196	127.30015	14.78873
520	4.97575	113.42383	11.85446
530	4.93607	109.65309	9.2723
540	4.87862	105.42986	8.09859
550	4.81106	102.86576	6.57277
560	4.77925	101.20664	5.75117
570	4.76371	99.09502	4.81221
580	4.70476	96.98341	4.22535
590	4.61943	94.87179	3.28638
600	4.54083	105.58069	3.40376
610	4.54513	173.75566	7.39437
620	4.54363	206.33484	20.65728
630	5.25122	222.62443	26.17371
640	6.53128	230.31674	29.81221
650	6.66022	235.29412	32.62911
660	6.86155	249.62293	34.74178
670	7.03675	265.00754	36.03286
680	7.15446	274.81146	37.32394
690	7.27423	281.90045	38.61502
700	7.46287	289.74359	39.31925
710	7.66461	295.47511	40.14085
720	7.87365	190.49774	36.26761
730	7.13125	164.25339	30.51643
740	6.40963	136.80241	18.30986
750	6.15886	128.20513	13.14554
760	5.96386	115.98793	10.44601
770	5.85026	109.2006	8.92019
780	5.76025	106.03318	7.15962
790	5.67697	102.11161	5.98592
800	5.61802	100.60332	5.16432
810	5.62064	98.79336	4.10798

	THF-PI	THF-PVAc	THF-PI/PVAc
time (s)	Change of Relative Resistance (%)	Change of Relative Resistance (%)	Change of Relative Resistance (%)
820	5.58078	96.38009	3.28638
830	5.52688	94.11765	2.93427
840	5.48964	109.2006	2.93427
850	5.72581	156.56109	7.04225
860	7.07118	191.25189	23.70892
870	7.28958	208.59729	28.28638
880	7.53455	223.52941	31.10329
890	7.56636	231.97587	32.62911
900	7.62643	249.77376	34.85915
910	7.69942	262.7451	38.26291
920	7.81526	274.20814	40.96244
930	7.85849	279.63801	42.84038
940	7.9442	287.48115	44.48357
950	7.78401	298.64253	46.12676
960	7.8948	191.40271	41.19718
970	7.30455	166.66667	28.16901
980	6.55523	138.91403	22.30047
990	6.23334	124.88688	20.07042
1000	5.87029	114.93213	17.84038
1010	5.74453	108.1448	15.84507
1020	5.65507	104.67572	13.96714
1030	5.5761	102.26244	12.55869
1040	5.46924	99.09502	11.26761
1050	5.4335	96.83258	9.85915
1060	5.35078	95.32428	7.98122
1070	5.27312	93.21267	5.98592
1080	5.23812	103.92157	6.10329
1090	6.19086	163.19759	9.50704
1100	7.29107	175.86727	18.66197
1110	7.40561	200.60332	24.1784
1120	7.44977	222.17195	27.46479
1130	7.50835	239.51735	30.98592
1140	7.61913	253.39367	33.33333
1150	7.71851	273.15234	36.38498
1160	7.85699	277.37557	39.55399
1170	7.9981	282.50377	42.37089
1180	8.12105	287.17949	44.13146
1190	8.17383	296.83258	45.07042
1200	8.30614	195.77677	37.55869
1210	7.77895	160.48265	27.8169
1220	6.85541	136.95324	21.00939
1230	6.45174	125.33937	16.90141

	THF-PI	THF-PVAc	THF-PI/PVAc
time (s)	Change of Relative Resistance (%)	Change of Relative Resistance (%)	Change of Relative Resistance (%)
1240	6.27115	117.64706	13.96714
1250	6.19086	111.31222	11.73709
1260	6.13622	106.6365	10.32864
1270	6.02599	102.41327	9.03756
1280	6.13734	100	8.21596
1290	6.08619	95.77677	7.62911
1300	6.01757	93.96682	7.15962
1310	6.01813	92.76018	6.57277
1320	6.16204	98.19005	6.69014
1330	6.57432	161.99095	14.08451
1340	7.32532	180.39216	20.30516
1350	7.54783	198.79336	23.47418
1360	7.656	224.88688	27.34742
1370	7.72805	243.13725	29.92958
1380	7.76922	260.78431	31.57277
1390	7.85531	275.41478	35.79812
1400	7.94963	282.50377	38.61502
1410	8.06023	292.60935	41.5493
1420	8.03216	298.94419	43.07512
1430	8.09261	302.41327	43.89671
1440	8.19647	194.72097	34.85915
1450	8.16765	159.57768	23.59155
1460	7.06126	133.63499	18.30986
1470	6.74106	121.26697	15.96244
1480	6.63271	117.3454	13.84977
1490	6.59004	110.55807	11.50235
1500	6.47345	105.27903	9.50704
1510	6.42311	101.5083	6.80751
1520	6.35405	98.34087	3.87324
1530	6.30951	96.53092	3.05164
1540	6.285	94.11765	2.11268
1550	6.24476	92.00603	1.87793
1560	6.57844	106.78733	1.99531
1570	7.2849	161.2368	15.37559
1580	7.49431	183.55958	22.53521
1590	7.61146	202.71493	26.52582
1600	7.70335	229.41176	28.28638
1610	7.72412	252.63952	31.22066
1620	7.76473	256.1086	33.21596
1630	7.8525	269.98492	34.97653
1640	7.97995	279.93967	36.03286
1650	8.07483	290.04525	37.44131

	THF-PI	THF-PVAc	THF-PI/PVAc
time (s)	Change of Relative Resistance (%)	Change of Relative Resistance (%)	Change of Relative Resistance (%)
1660	8.18767	294.26848	39.08451
1670	8.28312	297.73756	41.78404
1680	7.57366	195.62594	23.59155
1690	6.67968	162.59427	19.60094
1700	6.37146	138.61237	17.723
1710	6.21351	121.4178	15.61033
1720	6.18618	111.61388	14.55399
1730	6.12854	105.58069	12.55869
1740	6.22099	102.71493	11.38498
1750	6.11376	101.65913	8.09859
1760	6.12274	99.69834	7.39437
1770	6.09186	97.73756	5.39906
1780	6.0331	95.02262	4.46009
1790	5.94945	93.66516	3.40376

Appendix B. Phase Three Raw Data

	Cyclohexane-PI	Cyclohexane-PVAc	Cyclohexane-PI/PVAc
time (s)	Change of Relative Resistance (%)	Change of Relative Resistance (%)	Change of Relative Resistance (%)
0	0	0	0
10	-0.27487	0.00348	-0.14201
20	-0.00598	0.00337	-0.19112
30	0.86436	0.00532	-0.19571
40	0.5856	0.00121	-0.23577
50	0.2199	-0.0011	-0.27914
60	0.2112	-3.91E-04	-0.30082
70	0.30863	6.26E-04	-0.33815
80	-0.16433	-0.00114	-0.3304
90	0.81566	-0.00153	-0.3202
100	0.10547	0.04971	-0.32049
110	0.1712	0.00407	-0.39516
120	4.60114	0.15727	15.30917
130	27.01225	1.51934	25.75957
140	29.77592	2.6002	33.7144
150	32.18405	3.86527	38.80175
160	34.92979	4.27392	40.644
170	38.39558	5.35408	40.58513
180	43.28951	6.27392	40.97713
190	45.44368	6.67473	41.48112
200	47.32298	7.39416	40.756
210	49.40843	7.38946	41.46533
220	52.00777	7.64702	41.14943
230	54.55931	7.31783	41.28153
240	19.88647	6.14749	32.85861
250	10.84255	4.37788	24.47014
260	5.53331	3.27133	21.78072
270	3.58829	2.89596	19.24494
280	1.23693	2.60827	13.45687
290	0.34957	2.28887	4.86853
300	-0.08157	2.45835	4.22209
310	0.98895	2.54916	3.35797
320	-0.3914	2.4607	2.00895
330	0.22707	2.47166	1.82286
340	-0.33762	2.6157	1.44853
350	0.00896	2.4564	1.25784
360	20.35853	3.34766	11.75965
370	35.64386	5.18342	19.90401

	Cyclohexane-PI	Cyclohexane-PVAc	Cyclohexane-PI/PVAc
time (s)	Change of Relative Resistance (%)	Change of Relative Resistance (%)	Change of Relative Resistance (%)
380	41.51479	6.46963	22.79446
390	45.37496	6.62698	24.48019
400	46.08605	7.22663	25.34603
410	47.2931	8.51049	27.273
420	47.32596	9.41076	30.34293
430	46.93457	10.72201	38.14699
440	50.64535	11.02106	39.74944
450	54.2934	11.32911	40.08687
460	58.07888	11.01401	43.72111
470	58.59576	11.49311	47.65832
480	16.19958	9.50626	40.52626
490	8.87959	8.18757	26.23916
500	4.91485	7.12447	20.13663
510	2.85928	6.39291	9.74366
520	1.49089	5.81674	4.97995
530	0.25993	4.84523	3.1693
540	0.20317	4.6507	1.98813
550	-0.12847	4.92469	1.64481
560	0.33463	4.6049	1.51257
570	0.14341	4.24636	1.4211
580	0.88437	4.05809	1.27507
590	0.10457	4.1532	1.29704
600	25.4885	5.89815	9.1133
610	31.08455	8.56842	14.01399
620	34.5862	9.0346	23.0802
630	38.93158	9.47338	29.53309
640	45.47356	9.87615	30.93882
650	54.61607	10.04251	30.99052
660	57.62773	10.44763	32.84568
670	56.42068	10.56466	34.54291
680	59.18733	10.2484	37.07151
690	61.54765	10.77955	40.91969
700	61.88527	10.23978	44.58982
710	61.25067	10.05425	47.49606
720	36.54019	6.82347	32.58292
730	13.01763	6.11359	18.60022
740	5.10607	5.969	8.1728
750	3.65103	5.40692	5.7605
760	1.98387	5.41514	3.78931

	Cyclohexane-PI	Cyclohexane-PVAc	Cyclohexane-PI/PVAc
time (s)	Change of Relative Resistance (%)	Change of Relative Resistance (%)	Change of Relative Resistance (%)
770	0.65432	5.07147	3.38525
780	-0.1213	4.76147	3.53071
790	0.61906	2.56756	3.39875
800	-0.5853	1.28425	3.60537
810	-0.87093	0.93886	3.37334
820	0.4389	1.49507	3.2945
830	-0.196	1.98473	3.46523
840	25.81416	1.85243	13.12949
850	36.81506	2.11625	20.86031
860	45.57813	3.29756	36.09223
870	50.76188	5.66721	41.47682
880	53.3911	7.42234	42.7246
890	54.44876	8.51597	44.56111
900	54.26352	9.21661	43.67229
910	56.92262	10.31572	43.6048
920	59.12758	10.98152	43.67229
930	58.8769	10.93377	44.56111
940	59.13953	11.15062	44.40747
950	60.57783	11.27979	44.7534
960	25.40185	9.84562	27.96366
970	17.01225	7.75818	24.6166
980	10.36719	6.53264	21.52944
990	5.73648	5.98505	19.69294
1000	3.50164	4.4041	18.31018
1010	1.81655	2.87522	14.76927
1020	1.90917	2.21058	5.92276
1030	-0.25695	1.56083	5.00235
1040	1.00388	1.92132	4.30997
1050	-0.50194	1.44035	3.7784
1060	0.08664	1.26386	3.04121
1070	0.55244	1.31568	2.75346
1080	18.72722	4.31916	2.354
1090	24.87601	5.18812	7.1088
1100	30.69615	6.54556	16.18793
1110	33.13415	7.20784	27.76981
1120	35.88288	8.47135	38.09099
1130	38.50612	8.9571	45.40397
1140	42.3663	8.41271	51.87266
1150	46.99432	8.47957	57.8876

	Cyclohexane-PI	Cyclohexane-PVAc	Cyclohexane-PI/PVAc
time (s)	Change of Relative Resistance (%)	Change of Relative Resistance (%)	Change of Relative Resistance (%)
1160	50.88886	8.59112	58.98749
1170	53.2686	8.58251	59.02338
1180	55.88497	8.74495	58.0398
1190	58.14759	8.65492	57.8876
1200	25.366	4.39745	50.76415
1210	12.17209	2.58361	39.14206
1220	6.8778	2.37459	33.66558
1230	4.42187	1.90332	21.33129
1240	2.68898	1.64929	15.45276
1250	1.83956	1.30977	11.23698
1260	0.39767	1.60788	6.85465
1270	-0.6833	1.38508	6.53301
1280	0.20795	1.6316	5.95004
1290	0.99821	1.10897	4.34184
1300	-0.3173	0.98505	3.81485
1310	0.30714	0.97002	3.40851
1320	13.80341	2.00219	10.74591
1330	22.01972	4.41232	23.07158
1340	30.23304	4.66792	31.65246
1350	35.07918	5.11688	39.07314
1360	38.91455	5.59167	42.87824
1370	43.75859	6.39878	46.73217
1380	47.67254	6.69274	49.61257
1390	49.84165	7.76444	53.64741
1400	53.87093	8.13042	55.16659
1410	59.93427	7.94411	57.66791
1420	58.63161	8.02669	57.62196
1430	62.20496	8.16213	58.63569
1440	25.35405	5.03468	52.53316
1450	19.92232	3.022	36.93653
1460	12.65611	1.81016	18.24987
1470	6.02928	1.50579	13.10938
1480	2.62324	1.2051	5.99312
1490	1.69704	1.08365	2.75949
1500	0.84255	1.21505	2.13115
1510	0.50792	1.38383	2.29398
1520	0.60353	1.0303	2.3583
1530	1.00388	1.06325	2.29225
1540	-0.57365	1.10717	2.58747

	Cyclohexane-PI	Cyclohexane-PVAc	Cyclohexane-PI/PVAc
time (s)	Change of Relative Resistance (%)	Change of Relative Resistance (%)	Change of Relative Resistance (%)
1550	0.02091	1.55817	2.12914

	Ethanol-PI	Ethanol-PVAc	Ethanol-PI/PVAc
time (s)	Change of Relative Resistance (%)	Change of Relative Resistance (%)	Change of Relative Resistance (%)
0	0	0	0
10	0	-0.09963	0.04168
20	-0.01852	0.16028	0.06252
30	-0.01852	-0.40286	0.06252
40	0	0.37687	0.08336
50	-0.01852	0.08332	0.08336
60	-0.03705	0.55014	0.04168
70	0	0.59346	0.06252
80	-0.11114	0.55014	0.04168
90	-0.05557	0.03355	0
100	-0.0741	0.01696	0
110	-0.03705	0.03032	0.02084
120	2.98237	5.40178	12.77462
130	7.00207	8.34741	20.13096
140	9.35522	11.11977	25.57008
150	11.8933	14.91423	28.07082
160	12.5243	17.17804	30.50904
170	13.52816	21.73273	33.0723
180	14.40776	26.90882	35.78144
190	14.01874	34.55491	38.42805
200	15.95392	38.71345	42.15803
210	15.99096	39.36322	43.92968
220	15.95392	39.96968	45.6805
230	16.00948	39.3199	20.10262
240	8.75852	24.72168	17.10173
250	7.60077	16.70782	15.20534
260	6.75793	13.93546	13.97581
270	6.21147	12.50596	12.82963
280	5.70206	11.76955	12.01689
290	5.34084	10.59996	11.32919
300	5.0352	9.34373	10.68317
310	4.74807	9.17046	10.1205
320	4.498	8.91055	9.74539
330	4.33128	8.21746	9.26608
340	4.11826	8.30409	8.93151
350	3.96956	8.04418	5.40963
360	4.50046	12.89582	12.84934
370	5.08396	19.65345	19.87225
380	6.14909	23.63873	21.42104
390	7.34389	27.58068	23.54667

	Ethanol-PI	Ethanol-PVAc	Ethanol-PI/PVAc
time (s)	Change of Relative Resistance (%)	Change of Relative Resistance (%)	Change of Relative Resistance (%)
400	8.25157	30.9595	25.60978
410	9.52046	33.49144	29.96524
420	11.38213	36.22049	31.56988
430	14.16073	40.58631	35.32099
440	15.79024	42.98895	32.4243
450	14.7066	45.70804	31.56988
460	15.5581	49.43513	33.84139
470	14.03972	50.45267	32.50766
480	11.57663	31.9125	26.27665
490	9.5581	20.56314	17.29751
500	8.68777	15.40827	12.58911
510	8.06751	11.46632	9.15191
520	7.58589	10.34005	8.94351
530	7.14161	9.9935	9.86045
540	6.03973	8.95387	10.02717
550	5.5584	8.60732	9.03146
560	5.14161	7.69764	9.52702
570	5.08604	7.26446	9.88129
580	4.7584	6.52805	9.90213
590	4.39168	6.27182	10.04801
600	6.47564	11.63959	14.57018
610	8.55032	23.10158	21.73897
620	9.73586	31.436	24.03132
630	10.7269	38.45354	26.90717
640	11.579	40.966	29.7205
650	12.34775	44.20836	30.84584
660	12.92199	46.73554	31.47102
670	13.30173	49.27009	32.82559
680	13.72778	51.39268	33.68001
690	14.02417	52.09682	35.0971
700	14.4317	52.86918	35.36801
710	14.30203	52.40004	37.01433
720	12.00742	36.46091	26.49571
730	10.21059	27.58068	23.36979
740	9.39554	18.6175	20.34835
750	8.89539	14.54191	19.22302
760	8.65458	11.59627	18.27287
770	8.49712	9.90687	17.20189
780	8.34893	9.0405	16.39097
790	8.32115	8.30409	15.7851
800	8.46008	7.87091	14.47342
810	8.29336	7.77691	13.02677

	Ethanol-PI	Ethanol-PVAc	Ethanol-PI/PVAc
time (s)	**Change of Relative Resistance (%)**	**Change of Relative Resistance (%)**	**Change of Relative Resistance (%)**
820	8.36746	7.40286	12.03517
830	8.33967	7.44813	11.76426
840	9.57152	13.37232	23.24475
850	10.65517	20.34655	30.20515
860	11.0627	32.82218	31.72643
870	11.39613	39.70977	33.14352
880	12.04447	43.95495	35.99853
890	12.60019	47.46372	35.74845
900	13.07255	50.66927	36.89463
910	13.42451	53.91813	37.22806
920	13.94318	56.20663	37.39811
930	14.00802	58.20663	37.64818
940	14.10064	60.67576	36.66873
950	14.14695	62.79835	38.12749
960	12.99994	35.20468	33.35525
970	12.29603	29.40004	29.24986
980	10.92555	23.42214	24.66606
990	10.74957	19.09032	20.83248
1000	10.56997	17.44423	17.43653
1010	10.35333	15.14836	15.70744
1020	10.16259	13.02577	14.895
1030	9.97186	11.59627	12.91584
1040	9.84219	9.90687	11.93668
1050	9.89776	8.82391	11.33263
1060	9.79588	8.39073	11.87416
1070	9.74957	8.79532	11.83248
1080	11.37968	14.67186	11.7911
1090	12.7406	23.50877	19.16947
1100	13.03788	31.16959	32.50379
1110	14.1299	38.23695	38.42073
1120	14.90791	43.50509	40.15011
1130	15.45437	47.85358	42.79614
1140	16.50098	49.93286	45.12957
1150	17.23267	51.57895	45.3588
1160	17.79766	53.09508	45.52552
1170	18.15887	53.44163	46.40078
1180	18.55714	54.39463	47.38023
1190	18.95541	55.30431	47.90122
1200	16.26016	33.47195	38.25253
1210	15.1302	23.85532	34.04354
1220	14.55422	15.14836	32.04295
1230	13.94496	12.33268	30.88449

	Ethanol-PI	Ethanol-PVAc	Ethanol-PI/PVAc
time (s)	Change of Relative Resistance (%)	Change of Relative Resistance (%)	Change of Relative Resistance (%)
1240	13.70415	10.45267	28.5431
1250	13.43758	8.60732	26.447
1260	13.04684	8.26078	23.60532
1270	12.95422	8.1815	22.33456
1280	12.92644	8.26446	21.2368
1290	12.98201	8.0875	20.85539
1300	12.9357	8.26078	18.9529
1310	13.00053	8.39073	17.14685
1320	14.02921	15.84146	27.56453
1330	14.94615	22.64241	34.12897
1340	15.53891	29.31341	36.62972
1350	16.30766	35.98441	38.13016
1360	16.99305	39.44986	40.21411
1370	17.92851	43.52177	41.97447
1380	18.02113	45.16786	42.70385
1390	18.19711	47.20381	43.45407
1400	18.39161	48.50336	44.05842
1410	18.42866	49.3264	44.53773
1420	18.53054	50.06281	44.93368
1430	18.46571	51.31904	45.37131
1440	17.14124	34.85813	39.88068
1450	15.74268	27.97054	33.42102
1460	14.82574	21.77605	29.35791
1470	14.22371	18.39723	26.00335
1480	13.91806	15.65086	24.31564
1490	13.61242	13.45896	22.62794
1500	13.39939	11.72623	21.14863
1510	13.13079	10.38337	19.8152
1520	13.07522	9.56032	18.35673
1530	12.95481	9.47368	17.14833
1540	12.86219	9.69028	16.93994
1550	12.7881	9.77691	16.44009

	THF-PI	THF-PVAc	THF-PI/PVAc
time (s)	Change of Relative Resistance (%)	Change of Relative Resistance (%)	Change of Relative Resistance (%)
0	0	0	0
10	0.00926	-0.09448	0.00578
20	0.01389	-0.04973	-0.14456
30	0.01389	0.17405	0.61871
40	0.01852	-0.57684	0.11998
50	0.01852	-0.04973	0.14167
60	0.00926	0.69121	-0.00578
70	0.01389	0.11935	-0.36284
80	0.00926	0.04475	-0.31369
90	0	-0.02486	0.0477
100	0	0.00497	0.17781
110	0.00463	98.93782	-0.27611
120	2.8388	313.74667	55.4889
130	4.47355	370.58519	59.87481
140	5.68224	413.04849	61.75552
150	6.23796	473.51514	63.05944
160	6.77979	447.15957	65.29143
170	7.3494	428.81012	66.79484
180	7.95143	450.24267	69.58483
190	8.53957	425.72702	71.56528
200	9.14623	426.57238	73.06869
210	9.76215	418.91435	73.76258
220	10.37344	410.26177	75.45391
230	4.46725	418.61598	76.87059
240	3.80039	354.91507	59.04649
250	3.37896	325.92394	48.69753
260	3.10574	282.31293	29.20088
270	2.85103	280.8211	24.17168
280	2.67042	270.97506	20.60252
290	2.5176	258.64264	18.60038
300	2.37404	249.44305	17.40633
310	2.249	239.84565	16.81074
320	2.16564	230.79524	16.72256
330	2.05913	223.63448	16.44935
340	1.98478	222.29184	16.21082
350	1.20214	221.4962	16.07349
360	2.85541	227.29443	34.63051
370	4.41606	386.79039	72.53383
380	4.76023	418.6677	80.73031
390	5.23259	464.74599	82.81196

	THF-PI	THF-PVAc	THF-PI/PVAc
time (s)	Change of Relative Resistance (%)	Change of Relative Resistance (%)	Change of Relative Resistance (%)
400	5.69106	483.55054	84.87915
410	6.65894	461.08326	86.83069
420	7.01553	446.01583	88.76778
430	7.84911	464.11664	92.38175
440	7.2054	446.46338	90.14109
450	7.01553	434.3796	90.82052
460	7.52031	446.06556	91.03735
470	7.22392	442.38573	90.86978
480	5.83926	362.62283	68.78975
490	3.84389	338.05745	34.38476
500	2.79758	331.99069	26.4427
510	2.03376	323.33811	21.98161
520	1.98745	316.12762	22.08136
530	2.19121	306.97776	20.10379
540	2.22826	302.40283	20.80924
550	2.00699	296.53499	19.83636
560	2.11712	296.08744	19.30149
570	2.19584	295.2918	19.12802
580	2.20047	295.24207	19.29282
590	2.23289	293.15352	18.92419
600	3.23782	443.28082	51.52943
610	4.83088	464.68473	85.09599
620	5.34029	486.17178	91.83243
630	5.97937	494.53555	94.30438
640	6.60456	490.72901	95.82225
650	6.85463	481.2583	97.06546
660	6.99356	488.91021	95.34521
670	7.29458	498.41429	96.53059
680	7.48445	486.76238	98.04846
690	7.79935	468.19628	99.45068
700	7.85956	471.92585	100.65051
710	8.22541	474.41222	104.81381
720	5.88794	455.86188	47.69429
730	5.19329	398.22771	35.34174
740	4.74408	315.97844	28.22366
750	4.494	285.84358	27.82034
760	4.38286	258.19509	24.07338
770	4.26709	245.61404	19.86816
780	4.20688	239.34837	19.81323
790	4.17447	236.46418	20.07054
800	4.1652	233.18216	19.67301
810	4.18373	227.71214	20.34087

	THF-PI	THF-PVAc	THF-PI/PVAc
time (s)	Change of Relative Resistance (%)	Change of Relative Resistance (%)	Change of Relative Resistance (%)
820	4.23004	225.02685	18.62929
830	4.16983	223.08748	17.81254
840	5.1655	408.76994	37.221
850	6.71225	470.33258	82.19729
860	7.05032	430.30195	99.03146
870	7.36523	421.54991	104.94391
880	7.99967	414.4886	106.47623
890	7.9441	408.37212	108.09529
900	8.19881	408.17321	107.6327
910	8.2729	405.18956	107.90737
920	8.31069	398.52608	103.85972
930	8.36626	402.60373	107.34551
940	8.14861	425.57783	105.93848
950	8.47278	399.86872	102.5876
960	7.41228	283.95393	38.07101
970	6.49997	254.61471	27.1944
980	6.14801	239.14946	23.39829
990	5.96277	227.86132	22.16376
1000	5.87478	218.36337	22.7497
1010	5.93499	217.41357	20.85887
1020	5.97667	205.84199	19.64361
1030	5.9813	202.75888	17.98601
1040	5.98593	199.80507	17.1813
1050	6.07392	192.65425	17.90602
1060	5.97204	189.04404	16.93555
1070	5.96277	188.7407	16.21468
1080	6.1758	204.36508	90.45141
1090	8.70433	398.67526	97.52515
1100	9.44529	382.51382	99.07675
1110	9.64905	388.77949	100.57053
1120	9.81114	376.79516	102.57507
1130	9.9547	382.21546	105.69754
1140	10.02879	387.5363	105.89029
1150	10.07973	389.22704	105.20604
1160	10.11678	383.5581	104.27177
1170	10.31128	385.74611	105.52407
1180	10.52894	387.18821	104.19413
1190	10.64472	394.3987	105.20604
1200	9.56569	307.42531	35.22898
1210	8.50056	260.97983	26.6393
1220	8.00968	243.3763	22.38927
1230	7.85222	235.9669	19.41425

	THF-PI	THF-PVAc	THF-PI/PVAc
time (s)	Change of Relative Resistance (%)	Change of Relative Resistance (%)	Change of Relative Resistance (%)
1240	7.67624	225.97168	19.00274
1250	7.5651	223.78367	19.37859
1260	6.86322	190.02367	18.82156
1270	6.51879	180.66993	18.4804
1280	5.87711	174.85181	18.17393
1290	5.52342	171.11787	17.60148
1300	5.46785	166.57716	16.53849
1310	5.36597	168.29773	16.82954
1320	6.12545	204.07169	25.05686
1330	7.58422	349.94232	95.87718
1340	8.13994	365.40757	96.59998
1350	8.47337	364.71138	95.38568
1360	8.93647	366.13578	101.55353
1370	9.32766	361.52882	104.3676
1380	9.48974	374.75634	104.64708
1390	9.65646	376.29789	104.20377
1400	9.79076	377.0438	107.26842
1410	9.89727	386.24339	110.80529
1420	9.98526	384.15483	110.05358
1430	10.08251	384.50292	113.43626
1440	8.86237	288.13104	41.90471
1450	7.87134	253.96825	27.94804
1460	7.41287	244.96758	23.38576
1470	7.11185	232.13788	20.62372
1480	6.95903	227.86132	17.63714
1490	6.80621	218.81092	17.00204
1500	6.6997	213.04253	17.53787
1510	6.6256	212.94307	17.25743
1520	6.52372	211.79934	16.25805
1530	6.47741	210.75506	15.82052
1540	6.4311	209.21351	16.53656
1550	6.54224	208.08967	15.92302

Appendix C. Phase Four Raw Data

	Cyclohexane-PI	Cyclohexane-PVAc	Cyclohexane-PI/PVAc
time (s)	Change of Relative Resistance (%)	Change of Relative Resistance (%)	Change of Relative Resistance (%)
0	0	0	0
10	-0.04979	0	-0.07054
20	-0.08299	0.01663	-0.09959
30	-0.07469	0.01996	-0.08714
40	-0.11618	0.00998	-0.12864
50	-0.21577	0.02662	-0.23237
60	-0.48133	0.0366	-0.49795
70	-0.62241	0.01331	-0.63903
80	-0.6556	0.02662	-0.66393
90	-0.6556	0.02662	-0.67223
100	-0.70539	0.02994	-0.70957
110	-0.72199	0.04658	-0.37761
120	5.48548	0.32604	6.10814
130	5.54357	0.38592	7.80945
140	11.73444	1.01803	8.37379
150	14.55602	1.01138	8.60202
160	15.48548	1.19436	8.80534
170	16.29876	1.29084	8.95888
180	16.59751	1.3108	9.02112
190	16.96266	1.34407	8.94643
200	17.03734	1.36403	9.05017
210	17.27801	1.43057	9.11241
220	17.39419	1.42391	9.2037
230	17.45228	1.43057	7.75966
240	17.47718	1.43057	7.13308
250	17.53527	1.29084	6.77207
260	15.29461	1.19103	6.4899
270	14.6805	1.14113	6.28242
280	14.18257	1.11784	6.10814
290	13.91701	1.07459	5.9878
300	13.56846	1.02801	5.86746
310	13.361	0.94151	5.74298
320	13.24481	0.97811	5.60604
330	13.17012	0.94151	5.5687
340	12.97925	0.90159	5.36122
350	12.78008	0.89494	9.37383
360	12.6805	0.87498	13.34495
370	12.45643	1.03134	15.12926

	Cyclohexane-PI	Cyclohexane-PVAc	Cyclohexane-PI/PVAc
time (s)	Change of Relative Resistance (%)	Change of Relative Resistance (%)	Change of Relative Resistance (%)
380	18.38174	1.04465	15.91352
390	19.74274	1.08457	16.50276
400	20.86307	1.1378	16.76418
410	21.56846	1.15111	17.00071
420	22.20747	1.15111	17.12934
430	22.99585	1.16442	17.30777
440	23.42739	1.20434	17.40736
450	23.9668	1.19768	17.49035
460	24.50622	1.27088	17.5277
470	24.77178	1.29749	16.1293
480	25.07884	0.94484	14.79314
490	24.41494	0.79846	14.39064
500	21.65145	0.73525	14.01303
510	20.84647	0.71861	13.72671
520	20.40664	0.75853	13.49019
530	19.9917	0.74523	13.29101
540	19.76763	0.76851	13.21632
550	19.56846	0.74523	13.09598
560	19.3112	0.76519	12.8719
570	19.17012	0.76519	12.71837
580	19.10373	0.77184	12.60218
590	19.07054	0.75188	16.28283
600	18.86307	0.97811	19.20412
610	18.71369	1.01138	20.32035
620	23.22822	1.09788	21.10461
630	24.08299	1.14445	21.84738
640	24.62241	1.15776	22.5611
650	25.07054	1.15111	23.20428
660	25.3029	1.21432	23.86406
670	25.49378	1.21099	24.23752
680	25.73444	1.24093	24.59023
690	25.92531	1.26422	24.94294
700	26.25726	1.2742	25.24586
710	26.30705	1.28418	22.38682
720	26.6888	0.90492	21.24569
730	25.12033	0.81176	20.63156
740	22.46473	0.71861	20.12117
750	21.88382	0.66871	19.8307
760	21.51867	0.67203	19.66887

	Cyclohexane-PI	Cyclohexane-PVAc	Cyclohexane-PI/PVAc
time (s)	Change of Relative Resistance (%)	Change of Relative Resistance (%)	Change of Relative Resistance (%)
770	21.29461	0.6188	19.49044
780	21.00415	0.59884	19.25391
790	20.80498	0.58553	19.16262
800	20.6805	0.57555	19.06718
810	20.54772	0.57888	18.98004
820	20.43983	0.59219	18.79331
830	20.34855	0.57555	21.31209
840	20.18257	0.59884	23.63584
850	20.22407	0.73857	24.34541
860	24.24066	0.85834	24.81431
870	24.6556	0.89161	25.05083
880	24.95436	0.92821	25.28736
890	25.17012	0.97146	25.68156
900	25.40249	0.99807	25.87244
910	25.44398	1.01138	26.03842
920	25.80083	1.00805	26.20856
930	25.71784	1.00472	26.42848
940	25.84232	1.01138	26.60276
950	25.70954	1.00472	23.41591
960	25.76763	0.94484	22.10465
970	23.78423	0.93153	21.698
980	21.72614	0.81842	21.33698
990	20.89627	0.72526	21.15026
1000	20.53942	0.58553	20.93033
1010	20.32365	0.51234	20.74775
1020	20.12448	0.46577	20.59837
1030	19.91701	0.41254	20.47388
1040	19.69295	0.41919	20.37014
1050	19.63485	0.43915	20.29545
1060	19.64315	0.40588	20.15436
1070	19.46058	0.41254	23.9346
1080	19.3527	0.49904	24.59853
1090	20.45643	0.56557	24.80601
1100	23.50207	0.68534	25.08403
1110	24.16598	0.72526	25.37865
1120	24.47303	0.80511	25.46164
1130	24.53942	0.84503	25.75626
1140	24.63071	0.87165	25.66911
1150	24.6888	0.93819	25.7936

time (s)	Cyclohexane-PI Change of Relative Resistance (%)	Cyclohexane-PVAc Change of Relative Resistance (%)	Cyclohexane-PI/PVAc Change of Relative Resistance (%)
1160	24.78838	0.93819	25.78945
1170	24.78838	1.01138	25.68571
1180	24.78008	1.02469	25.82265
1190	24.83817	1.05795	22.22499
1200	24.97925	1.0513	21.25814
1210	24.42324	0.75853	20.85149
1220	20.6722	0.69865	20.53612
1230	20	0.55559	20.30375
1240	19.49378	0.52565	20.06307
1250	19.27801	0.48573	19.8307
1260	19.11203	0.48573	19.69376
1270	19.07884	0.519	19.63152
1280	19.00415	0.47242	19.54853
1290	18.90456	0.46577	19.3784
1300	18.80498	0.43915	19.22486
1310	18.73029	0.39923	22.98436

	Ethanol-PI	Ethanol-PVAc	Ethanol-PI/PVAc
time (s)	Change of Relative Resistance (%)	Change of Relative Resistance (%)	Change of Relative Resistance (%)
0	0	0	0
10	0.03165	0.03517	0
20	0.1864	0	-0.01054
30	0.04572	0	0.05268
40	0.04572	-0.03517	0.07901
50	0.03165	-0.07033	0.14749
60	0.03869	-0.07033	0.15276
70	0.02814	-0.14067	0.13169
80	0.05276	-0.14067	0.12642
90	0.0211	-0.17583	0.04741
100	0.01055	-0.07033	0.03687
110	0.00352	-0.07033	0.02634
120	0.58735	5.486	0.33881
130	0.98477	9.84667	4.21934
140	1.10083	10.83134	10.59313
150	1.11138	11.14784	12.81079
160	1.19228	11.64017	14.17509
170	1.2169	12.09734	14.31732
180	1.25558	12.30834	14.49115
190	1.27669	12.73034	14.85988
200	1.31889	13.04684	15.27075
210	1.34703	13.39851	16.17151
220	1.45254	14.34801	16.0767
230	1.45605	14.69968	16.94058
240	0.9285	9.28401	16.48757
250	0.67879	6.752	9.22882
260	0.60141	5.908	6.32111
270	0.54162	5.41567	5.06216
280	0.49239	4.88817	4.06658
290	0.4537	4.5365	3.56089
300	0.39743	3.93867	3.03413
310	0.37632	3.72767	2.53371
320	0.33412	3.23534	2.20185
330	0.29895	2.88367	1.70143
340	0.28488	2.81334	1.64876
350	0.29191	2.60234	1.3327
360	0.83354	6.57617	1.10619
370	1.3013	12.51934	3.9981
380	1.41033	13.96118	10.09798

	Ethanol-PI	Ethanol-PVAc	Ethanol-PI/PVAc
time (s)	Change of Relative Resistance (%)	Change of Relative Resistance (%)	Change of Relative Resistance (%)
390	1.48419	14.73484	14.85461
400	1.51584	15.19201	17.04067
410	1.60377	15.82501	22.26085
420	1.64949	16.24701	23.12474
430	1.74797	16.70418	23.19848
440	1.81128	17.86468	24.26254
450	1.80424	17.97018	24.12558
460	1.88513	18.70868	23.32491
470	1.90272	18.84935	22.50316
480	1.30482	13.22268	23.43552
490	1.15359	11.53467	19.17931
500	1.03049	10.19834	15.64475
510	0.92146	9.00267	14.63864
520	0.88981	8.82684	14.09081
530	0.83354	8.44001	13.74842
540	0.84057	8.36967	12.92141
550	0.84057	8.26417	12.37885
560	0.79133	7.73667	12.05752
570	0.8265	8.15867	12.00485
580	0.84761	8.51034	11.80468
590	0.81947	8.08834	11.32533
600	1.39978	13.43368	11.24631
610	1.64597	16.14151	14.7914
620	1.74093	17.05584	17.10914
630	1.84293	18.21635	16.91424
640	1.88513	18.70868	17.67278
650	1.91679	19.09551	17.80973
660	1.99768	19.69335	17.94142
670	2.15595	21.45168	16.66667
680	2.21222	21.90885	16.11884
690	2.19815	21.94401	17.64117
700	2.25794	22.47151	18.63148
710	2.3318	23.13968	18.90013
720	1.66708	16.73934	18.85272
730	1.38571	13.89084	18.58407
740	1.31186	13.04684	15.13906
750	1.21338	12.09734	13.07944
760	1.17469	11.71051	12.61589
770	1.15711	11.42917	12.09966
780	1.07621	10.69067	11.29899
790	1.00236	10.05767	11.43595

	Ethanol-PI	Ethanol-PVAc	Ethanol-PI/PVAc
time (s)	Change of Relative Resistance (%)	Change of Relative Resistance (%)	Change of Relative Resistance (%)
800	1.00236	9.81151	11.04088
810	1.02346	10.19834	10.54572
820	1.01642	10.05767	10.32975
830	1.00939	9.88184	10.06637
840	1.27317	11.11267	9.20775
850	1.93437	18.99001	9.41846
860	1.97306	19.41201	14.9863
870	2.03637	20.25601	15.57627
880	2.19815	21.31101	16.57712
890	2.24035	22.15501	17.88348
900	2.25794	22.43635	16.12937
910	2.38104	23.28035	16.18732
920	2.32828	23.21002	15.75011
930	2.41269	23.91335	17.27771
940	2.45841	24.37052	17.78866
950	2.45138	24.30018	19.60598
960	1.89217	19.06035	20.15908
970	1.7339	17.30201	19.83776
980	1.55101	15.54368	16.1083
990	1.50881	14.98101	14.09608
1000	1.4455	14.38318	13.26907
1010	1.4033	13.99634	11.9469
1020	1.38923	13.75018	11.03561
1030	1.37516	13.75018	10.51938
1040	1.26965	12.51934	9.84513
1050	1.29075	12.73034	9.77665
1060	1.26965	12.66001	9.48694
1070	1.28372	12.83584	9.02339
1080	1.97306	18.91968	8.51243
1090	2.36697	23.52652	8.67046
1100	2.49358	24.68702	9.92941
1110	2.55689	25.32002	17.23557
1120	2.59206	25.81235	19.86936
1130	2.62723	26.09368	19.50063
1140	2.6835	26.65635	18.63148
1150	2.73977	27.21902	21.97113
1160	2.78198	27.85202	20.52255
1170	2.81012	28.02785	24.20459
1180	2.83825	28.16852	24.81563
1190	2.82418	28.13335	24.4469
1200	2.24035	22.57702	22.77708

	Ethanol-PI	Ethanol-PVAc	Ethanol-PI/PVAc
time (s)	Change of Relative Resistance (%)	Change of Relative Resistance (%)	Change of Relative Resistance (%)
1210	2.07154	20.67801	22.10282
1220	2.0012	20.00985	22.70333
1230	1.93085	19.30651	17.9941
1240	1.87458	18.53285	17.15655
1250	1.80424	17.97018	16.22419
1260	1.79017	17.79435	15.26022
1270	1.74797	17.58335	15.07585
1280	1.76204	17.54818	14.99157
1290	1.7339	17.19651	14.94943
1300	1.72687	17.02068	14.87042
1310	1.74797	17.16134	14.34893

	THF-PI	THF-PVAc	THF-PI/PVAc
time (s)	Change of Relative Resistance (%)	Change of Relative Resistance (%)	Change of Relative Resistance (%)
0	0	0	0
10	-0.72324	0.046	0.04223
20	-0.76143	0.092	0.03871
30	-0.89895	0.393	0.02815
40	-0.86839	0.532	0.02463
50	-1.03392	0.601	0.02111
60	-0.93206	0.671	0.02815
70	-0.91678	0.74	0.02815
80	-0.82765	0.532	0.0563
90	-1.21982	0.671	0.00704
100	-0.79963	0.763	-0.02463
110	-0.96007	0.555	-0.0563
120	-0.89131	1.619	24.7308
130	12.3663	1.318	30.6707
140	16.19894	1.504	33.46471
150	15.56229	3.54	34.66817
160	16.12509	13.999	35.51974
170	15.519	17.817	36.34316
180	15.64123	18.372	38.9014
190	15.67689	21.543	39.65093
200	16.1531	21.936	43.26131
210	15.91881	23.185	44.25012
220	16.06906	26.564	47.2623
230	15.56738	27.489	47.50158
240	16.03086	25.916	40.25969
250	12.35357	24.828	37.73665
260	11.02934	23.023	37.27919
270	10.04125	23.232	35.13266
280	9.68473	23.324	36.33261
290	9.55485	23.255	37.53607
300	9.00733	23.232	37.34253
310	7.89192	23.162	35.59012
320	7.93012	23.07	34.93209
330	8.06764	23	35.56197
340	7.49211	23.023	34.51334
350	7.72639	23.023	35.19248
360	7.40552	26.726	45.50285
370	14.66843	32.164	48.6593
380	20.57655	32.441	48.70153

	THF-PI	THF-PVAc	THF-PI/PVAc
time (s)	Change of Relative Resistance (%)	Change of Relative Resistance (%)	Change of Relative Resistance (%)
390	21.75817	32.696	47.7831
400	22.16563	32.997	50.04223
410	22.77172	33.112	50.71082
420	23.25558	33.228	51.70315
430	23.41347	33.298	52.34007
440	24.19273	33.459	54.08896
450	23.48222	33.436	54.96164
460	24.34298	33.436	56.01379
470	25.61373	33.598	58.05475
480	26.2351	31.469	49.8135
490	20.75227	31.493	47.31508
500	17.75491	31.03	44.95038
510	16.60385	30.636	44.40847
520	15.2949	30.336	41.77986
530	15.08353	29.156	41.82208
540	14.08017	29.109	42.11767
550	13.58613	29.248	42.44845
560	13.43333	28.97	41.26258
570	13.6065	28.762	39.66148
580	13.29072	28.6	40.57288
590	12.75848	28.67	37.85981
600	11.85189	33.344	49.08861
610	19.62412	36.653	49.98241
620	26.57635	37.069	51.16124
630	31.27228	37.833	50.53135
640	30.51085	38.92	51.24569
650	30.65855	39.268	50.49265
660	30.61781	39.707	51.62221
670	31.22135	39.962	51.97762
680	31.97005	39.985	52.71659
690	32.68819	40.101	52.85734
700	32.3826	40.147	52.62862
710	33.15677	40.494	52.92068
720	33.2841	36.63	44.98557
730	28.04319	35.704	43.71173
740	24.09086	35.82	42.38863
750	22.42284	35.403	42.11063
760	22.4483	35.426	41.29073
770	22.18855	35.079	40.38989
780	21.6232	34.755	39.71075
790	21.10624	34.732	39.61222

	THF-PI	THF-PVAc	THF-PI/PVAc
time (s)	Change of Relative Resistance (%)	Change of Relative Resistance (%)	Change of Relative Resistance (%)
800	19.23958	34.131	39.12661
810	19.13263	34.038	38.99993
820	19.33636	33.205	38.73601
830	19.02312	33.274	38.04631
840	17.98666	36.583	45.904
850	19.99847	39.43	45.8653
860	32.51502	39.615	45.93567
870	37.64388	39.661	46.85763
880	39.10818	40.077	47.05468
890	39.2839	40.887	47.48399
900	39.83396	41.049	47.21655
910	40.07334	41.327	47.52622
920	40.50117	41.466	48.0083
930	42.15392	41.258	48.37427
940	42.53336	41.35	48.25815
950	42.91535	41.466	49.07101
960	43.90853	40.934	40.94236
970	42.55883	41.096	39.1055
980	33.2077	42.114	38.30671
990	32.32148	38.897	36.50503
1000	31.36905	38.018	36.58245
1010	29.40308	37.671	36.12147
1020	28.5958	37.37	35.23119
1030	28.10686	36.722	34.93209
1040	27.12896	36.722	34.97783
1050	26.35989	36.56	34.75966
1060	26.41591	36.445	34.5802
1070	25.80218	36.329	33.9292
1080	25.7487	36.676	42.95869
1090	25.76398	38.388	44.64424
1100	42.44678	40.563	47.85347
1110	44.71071	40.864	49.06045
1120	45.24549	40.91	50.2041
1130	45.04176	41.049	50.61933
1140	44.94499	41.211	51.1542
1150	44.73108	41.327	52.2908
1160	45.14108	41.674	52.19931
1170	44.84568	41.744	52.72714
1180	45.06723	42.044	53.91653
1190	45.33462	42.715	54.27898
1200	45.76755	42.438	45.02076

	THF-PI	THF-PVAc	THF-PI/PVAc
time (s)	Change of Relative Resistance (%)	Change of Relative Resistance (%)	Change of Relative Resistance (%)
1210	40.47061	38.851	43.13463
1220	36.19232	38.111	42.1036
1230	33.06764	37.763	41.28017
1240	31.36905	37.208	40.43212
1250	30.60507	37.278	40.10486
1260	29.82836	37.162	40.04152
1270	29.01599	37.162	39.77761
1280	28.75115	37.116	39.68611
1290	28.33096	37.023	38.88732
1300	28.04319	37.023	38.37005
1310	27.38617	36.954	38.07094

Appendix D. Lachenbruch's Holdout Confusion Matrices

One Feature:

Training:

Actual Group	# of Cases	Predicted V1	Predicted V2	Predicted V3
V1	6	5	0	1
V2	6	1	5	0
V3	6	0	0	6

Test (Exposure 1):

Actual Group	# of Cases	Predicted V1	Predicted V2	Predicted V3
V1	1	0	1	0
V2	1	1	0	0
V3	1	0	0	1

Training:

Actual Group	# of Cases	Predicted V1	Predicted V2	Predicted V3
V1	6	5	0	1
V2	6	0	6	0
V3	6	0	0	6

Test (Exposure 2):

Actual Group	# of Cases	Predicted V1	Predicted V2	Predicted V3
V1	1	1	0	0
V2	1	1	0	0
V3	1	0	0	1

Training:

Actual Group	# of Cases	Predicted V1	V2	V3
V1	6	4	1	1
V2	6	1	5	0
V3	6	0	1	5

Test (Exposure 3):

Actual Group	# of Cases	Predicted V1	V2	V3
V1	1	0	1	0
V2	1	1	0	0
V3	1	1	0	0

Training:

Actual Group	# of Cases	Predicted V1	V2	V3
V1	6	5	0	1
V2	6	1	5	0
V3	6	0	0	6

Test (Exposure 4):

Actual Group	# of Cases	Predicted V1	V2	V3
V1	1	0	1	0
V2	1	0	1	0
V3	1	0	0	1

Training:

Actual Group	# of Cases	Predicted		
		V1	V2	V3
V1	6	6	0	0
V2	6	1	5	0
V3	6	0	0	6

Test (Exposure 5):

Actual Group	# of Cases	Predicted		
		V1	V2	V3
V1	1	0	0	1
V2	1	0	1	0
V3	1	1	0	0

Training:

Actual Group	# of Cases	Predicted		
		V1	V2	V3
V1	6	5	0	1
V2	6	1	5	0
V3	6	0	0	6

Test (Exposure 6):

Actual Group	# of Cases	Predicted		
		V1	V2	V3
V1	1	1	0	0
V2	1	0	1	0
V3	1	0	0	1

Training:

Actual Group	# of Cases	Predicted		
		V1	V2	V3
V1	6	4	1	1
V2	6	1	5	0
V3	6	1	0	5

Test (Exposure 7):

Actual Group	# of Cases	Predicted		
		V1	V2	V3
V1	1	0	1	0
V2	1	1	0	0
V3	1	0	0	1

Two Features:

Training:

Actual Group	# of Cases	Predicted		
		V1	V2	V3
V1	6	6	0	0
V2	6	0	6	0
V3	6	0	0	6

Test (Exposure 1):

Actual Group	# of Cases	Predicted		
		V1	V2	V3
V1	1	1	0	0
V2	1	0	1	0
V3	1	0	0	1

Training:

Actual Group	**# of Cases**	**Predicted V1**	**V2**	**V3**
V1	6	6	0	0
V2	6	0	6	0
V3	6	0	0	6

Test (Exposure 2):

Actual Group	**# of Cases**	**Predicted V1**	**V2**	**V3**
V1	1	1	0	0
V2	1	0	0	1
V3	1	0	0	1

Training:

Actual Group	**# of Cases**	**Predicted V1**	**V2**	**V3**
V1	6	6	0	0
V2	6	0	6	0
V3	6	0	0	6

Test (Exposure 3):

Actual Group	**# of Cases**	**Predicted V1**	**V2**	**V3**
V1	1	1	0	0
V2	1	0	1	0
V3	1	0	0	1

Training:

Actual Group	# of Cases	Predicted		
		V1	V2	V3
V1	6	6	0	0
V2	6	0	6	0
V3	6	0	0	6

Test (Exposure 4):

Actual Group	# of Cases	Predicted		
		V1	V2	V3
V1	1	0	1	0
V2	1	0	1	0
V3	1	0	0	1

Training:

Actual Group	# of Cases	Predicted		
		V1	V2	V3
V1	6	6	0	0
V2	6	0	6	0
V3	6	0	0	6

Test (Exposure 5):

Actual Group	# of Cases	Predicted		
		V1	V2	V3
V1	1	1	0	0
V2	1	0	1	0
V3	1	0	0	1

Training:

Actual Group	# of Cases	Predicted		
		V1	V2	V3
V1	6	6	0	0
V2	6	0	6	0
V3	6	0	0	6

Test (Exposure 6):

Actual Group	# of Cases	Predicted		
		V1	V2	V3
V1	1	1	0	0
V2	1	0	1	0
V3	1	0	0	1

Training:

Actual Group	# of Cases	Predicted		
		V1	V2	V3
V1	6	6	0	0
V2	6	0	6	0
V3	6	0	0	6

Test (Exposure 7):

Actual Group	# of Cases	Predicted		
		V1	V2	V3
V1	1	1	0	0
V2	1	0	1	0
V3	1	0	0	1

Appendix E. Predicted vs. Actual Sensor Three Values

Phase Three:

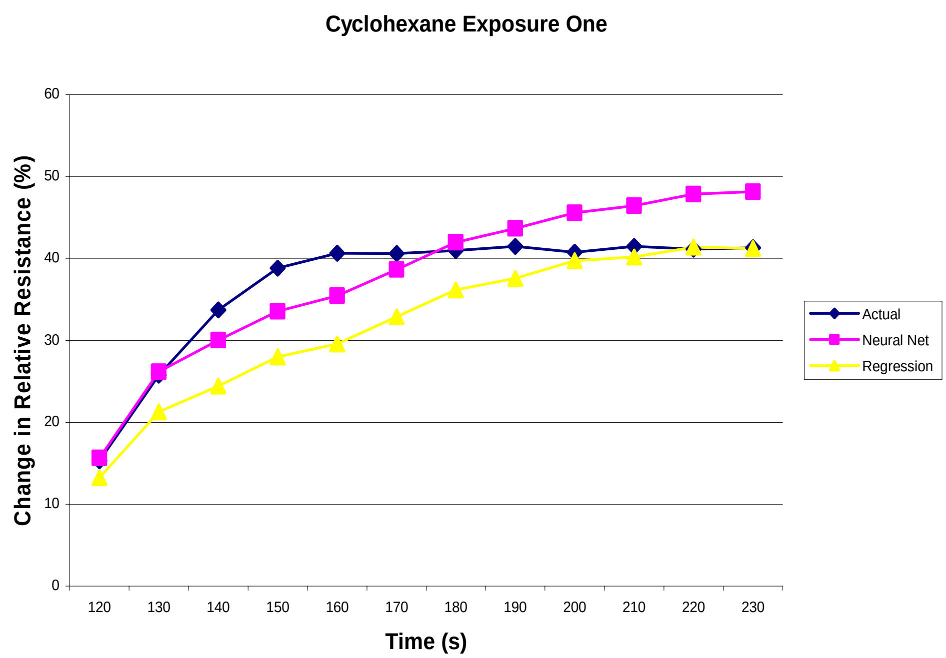

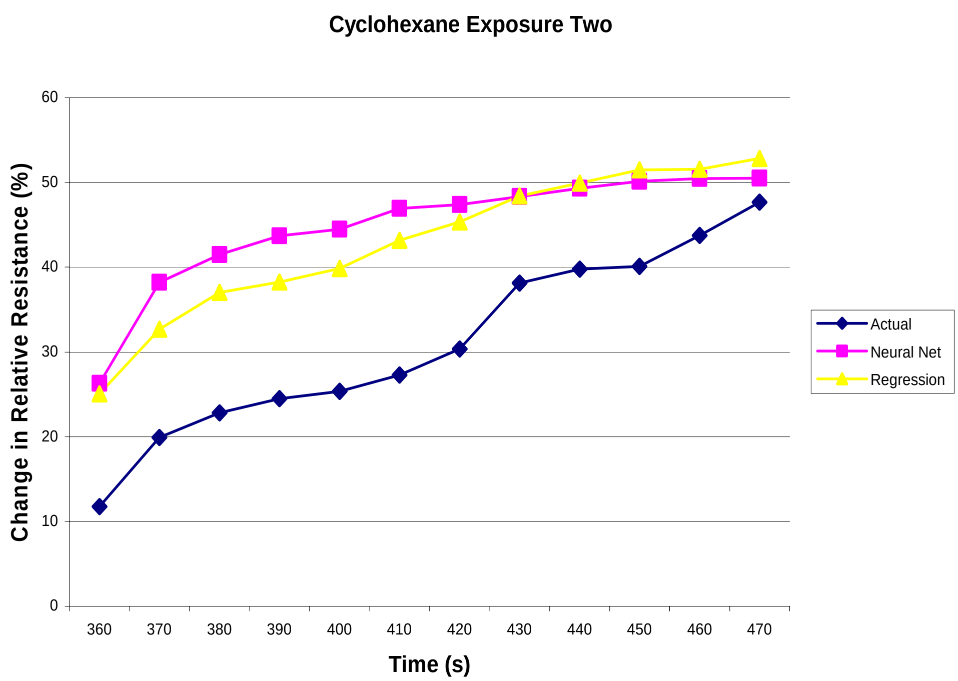

Cyclohexane Exposure Three

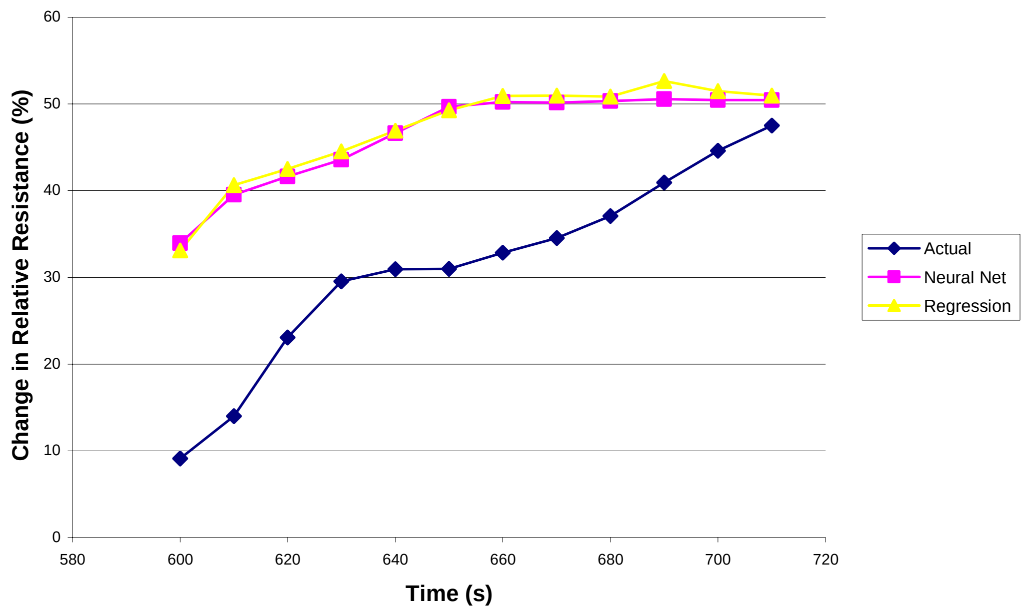

Cyclohexane Exposure Four

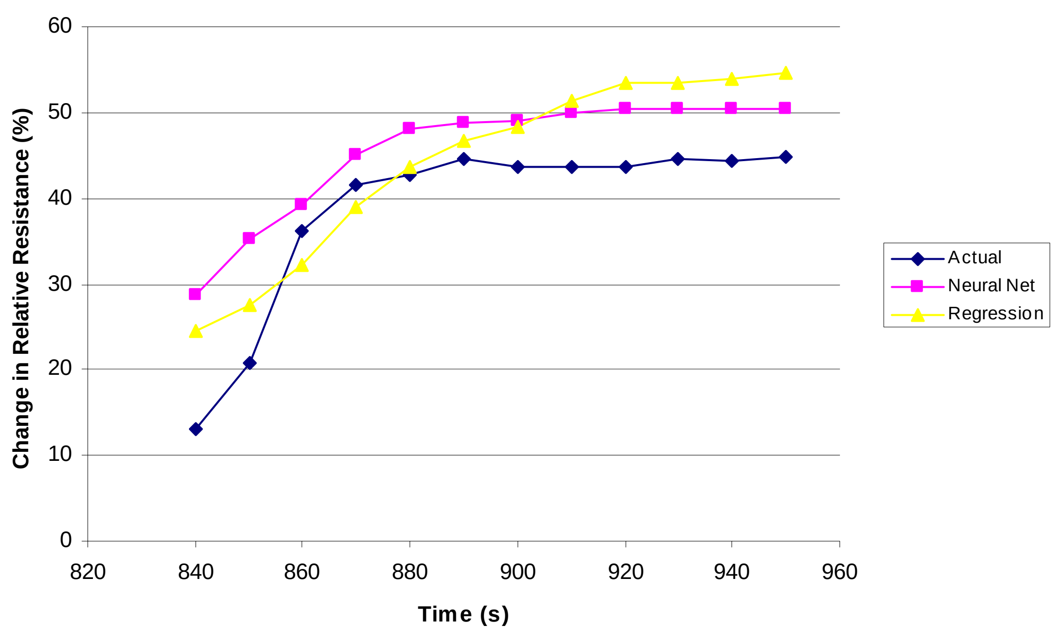

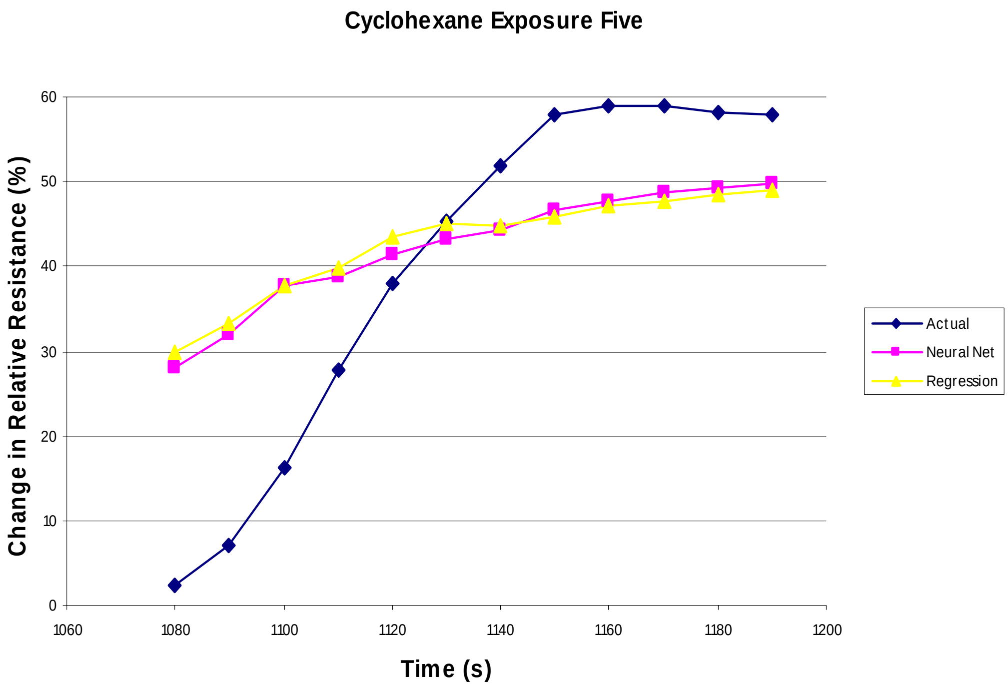
Cyclohexane Exposure Five
Change in Relative Resistance (%)
0
10
20
30
40
50
60
1060
1080
1100
1120
1140
1160
1180
1200
Time (s)
Actual
Neural Net
Regression

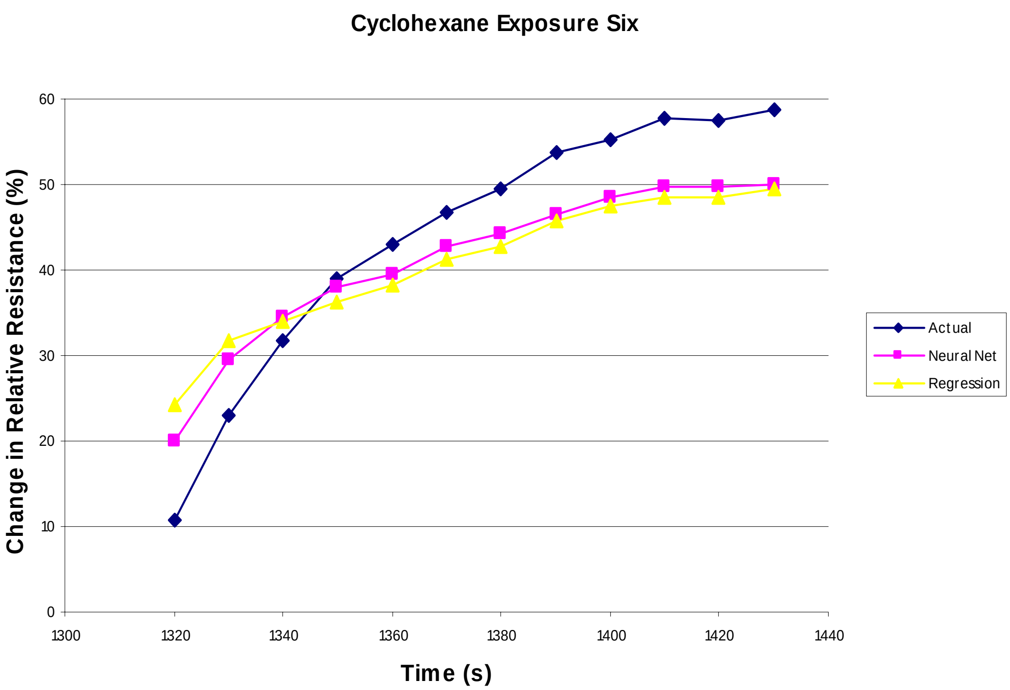
Cyclohexane Exposure Six
Change in Relative Resistance (%)
0
10
20
30
40
50
60
1300
1320
1340
1360
1380
1400
1420
1440
Time (s)
Actual
Neural Net
Regression

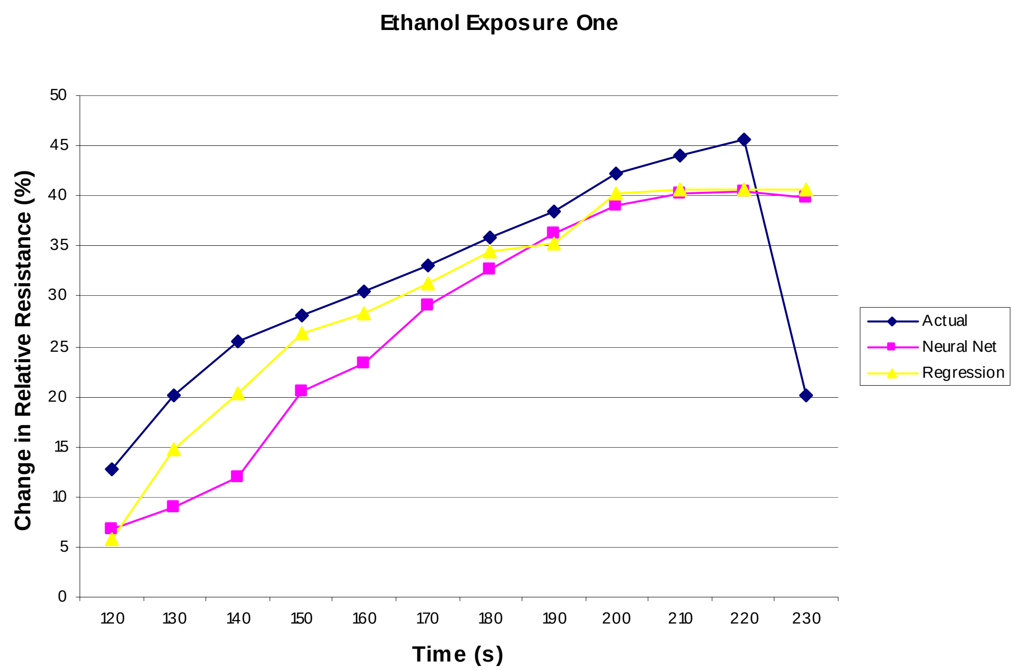
Ethanol Exposure One
50
45
40
35
30
25
20
15
10
5
0
Change in Relative Resistance (%)
120
130
140
150
160
170
180
190
200
210
220
230
Time (s)
Actual
Neural Net
Regression

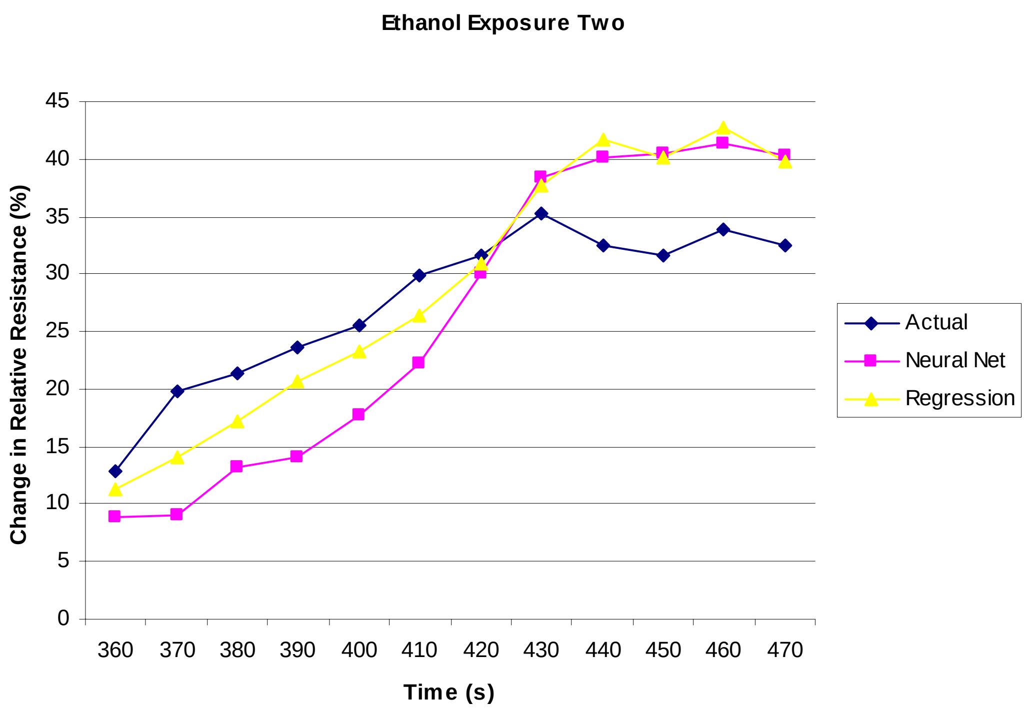
Ethanol Exposure Two
45
40
35
30
25
20
15
10
5
0
Change in Relative Resistance (%)
360
370
380
390
400
410
420
430
440
450
460
470
Time (s)
Actual
Neural Net
Regression

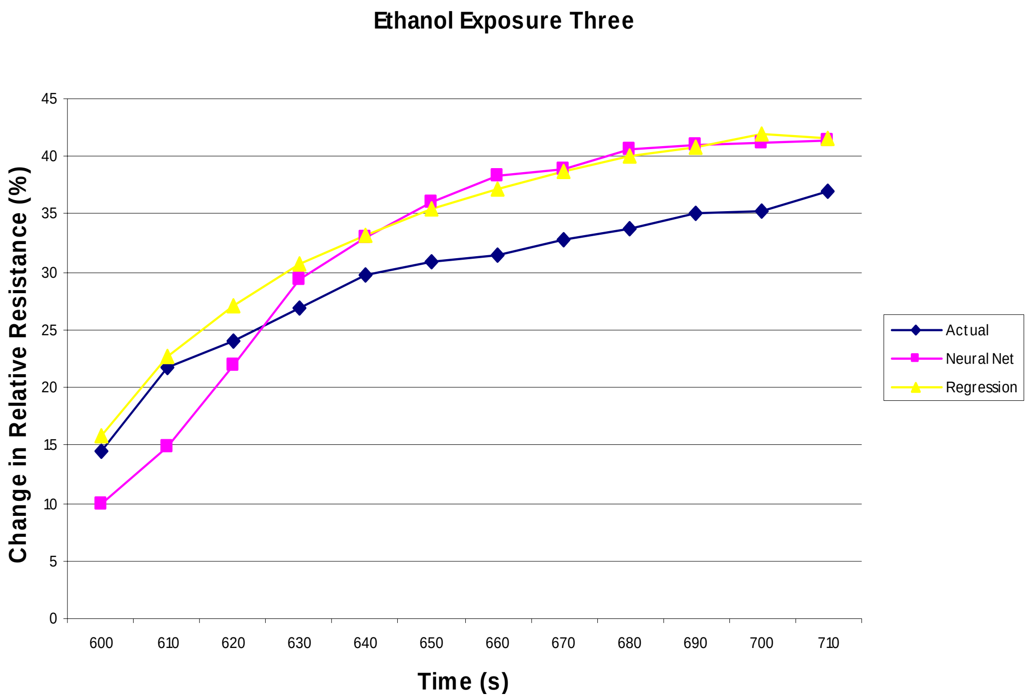
Ethanol Exposure Three
Change in Relative Resistance (%)
45
40
35
30
25
20
15
10
5
0
600
610
620
630
640
650
660
670
680
690
700
710
Time (s)
Actual
Neural Net
Regression

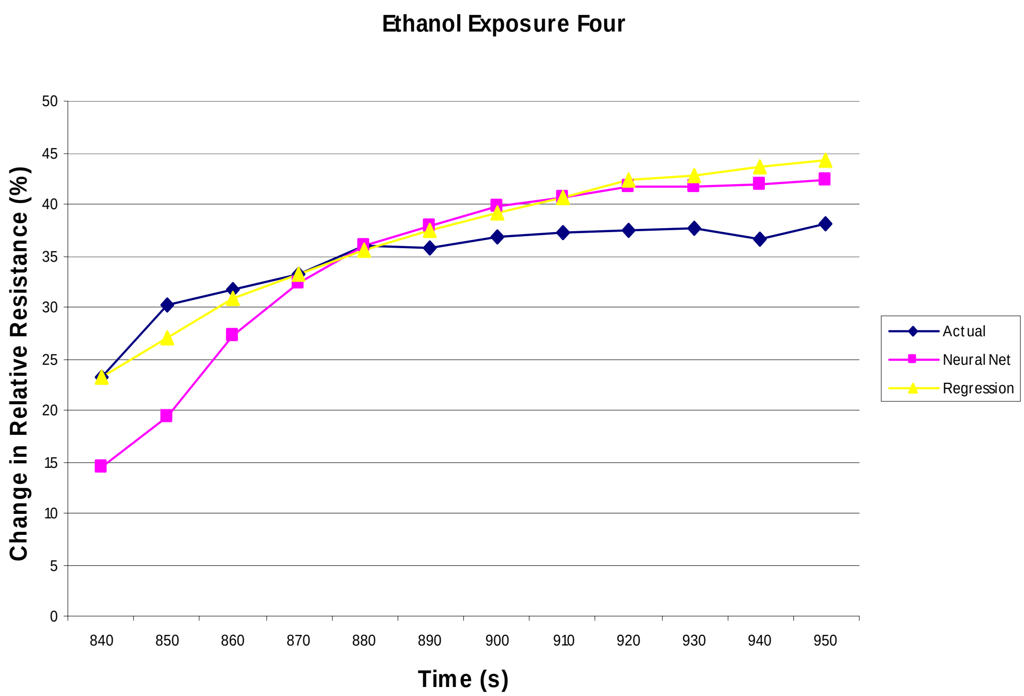
Ethanol Exposure Four
Change in Relative Resistance (%)
50
45
40
35
30
25
20
15
10
5
0
840
850
860
870
880
890
900
910
920
930
940
950
Time (s)
Actual
Neural Net
Regression

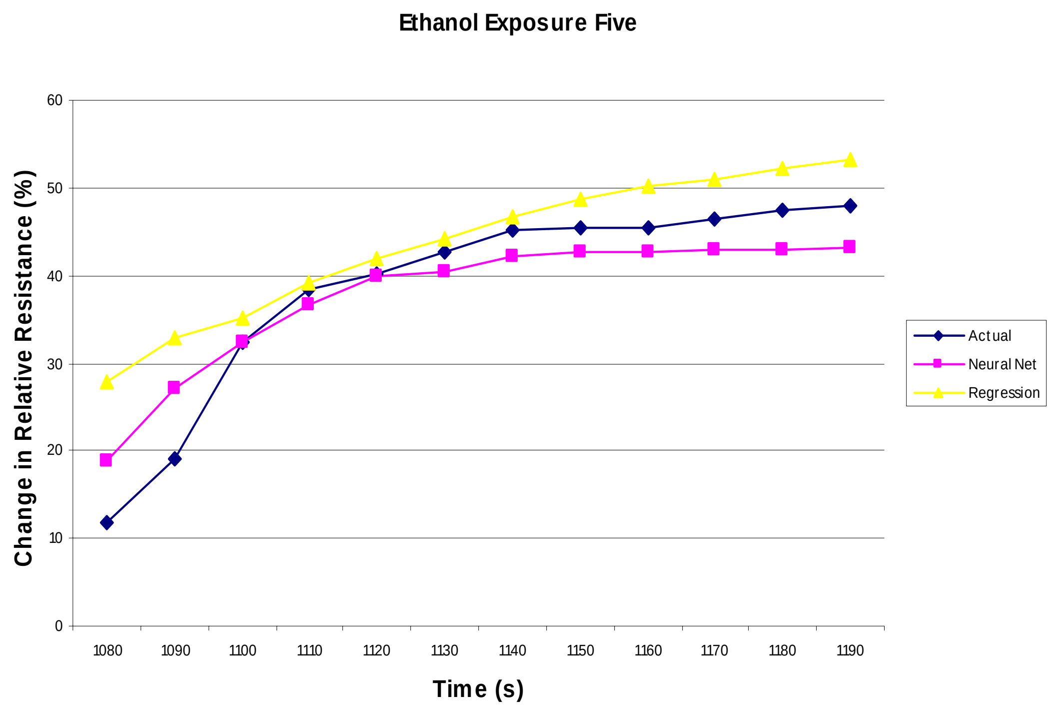
Ethanol Exposure Five
Change in Relative Resistance (%)
0
10
20
30
40
50
60
1080
1090
1100
1110
1120
1130
1140
1150
1160
1170
1180
1190
Time (s)
Actual
Neural Net
Regression

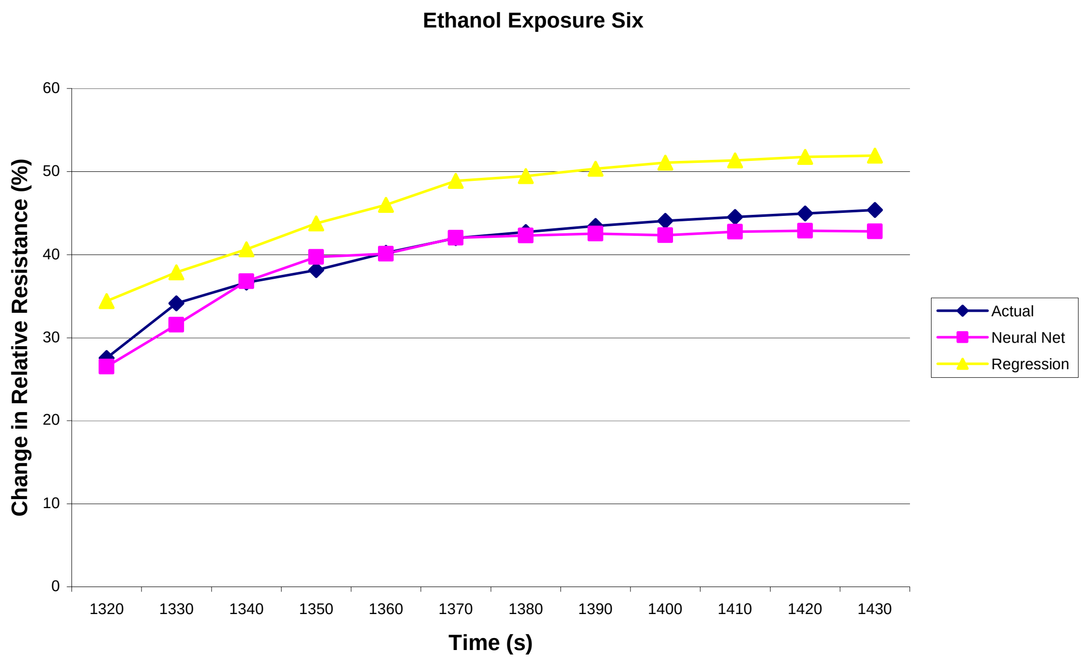
Ethanol Exposure Six
Change in Relative Resistance (%)
0
10
20
30
40
50
60
1320
1330
1340
1350
1360
1370
1380
1390
1400
1410
1420
1430
Time (s)
Actual
Neural Net
Regression

THF Exposure One

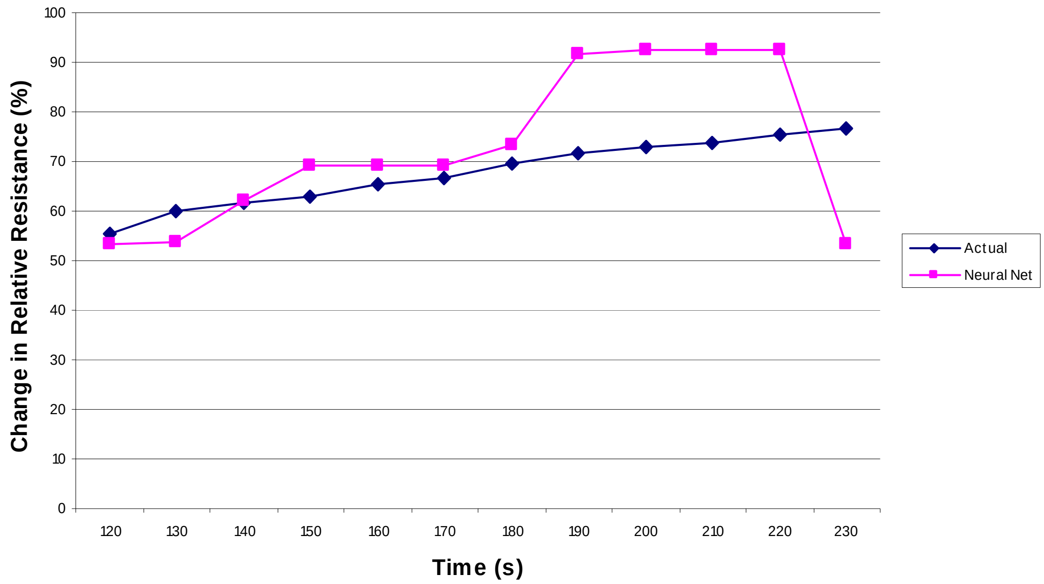

THF Exposure Two

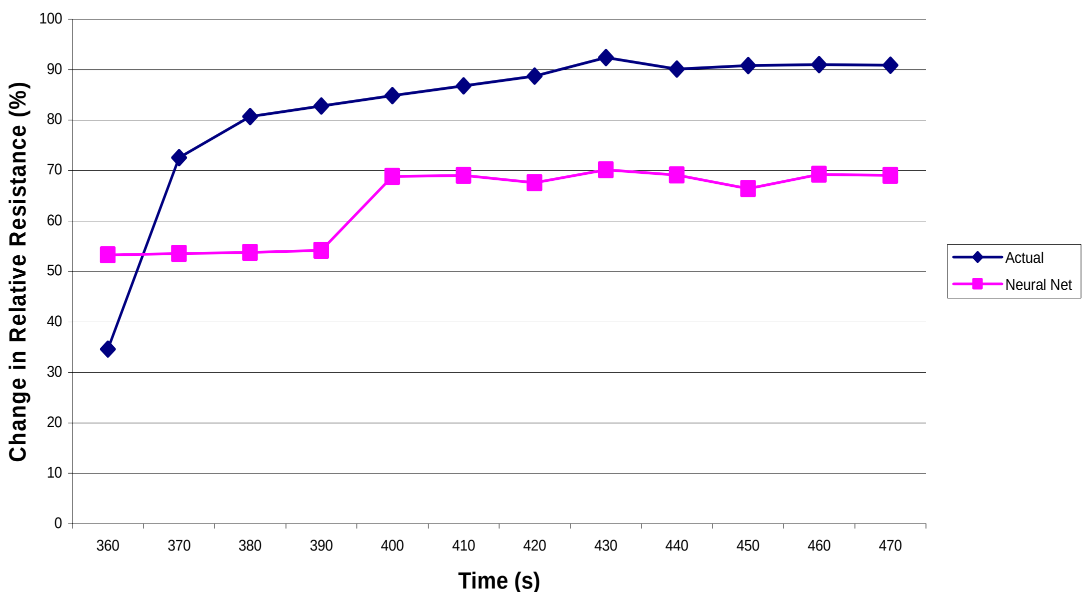

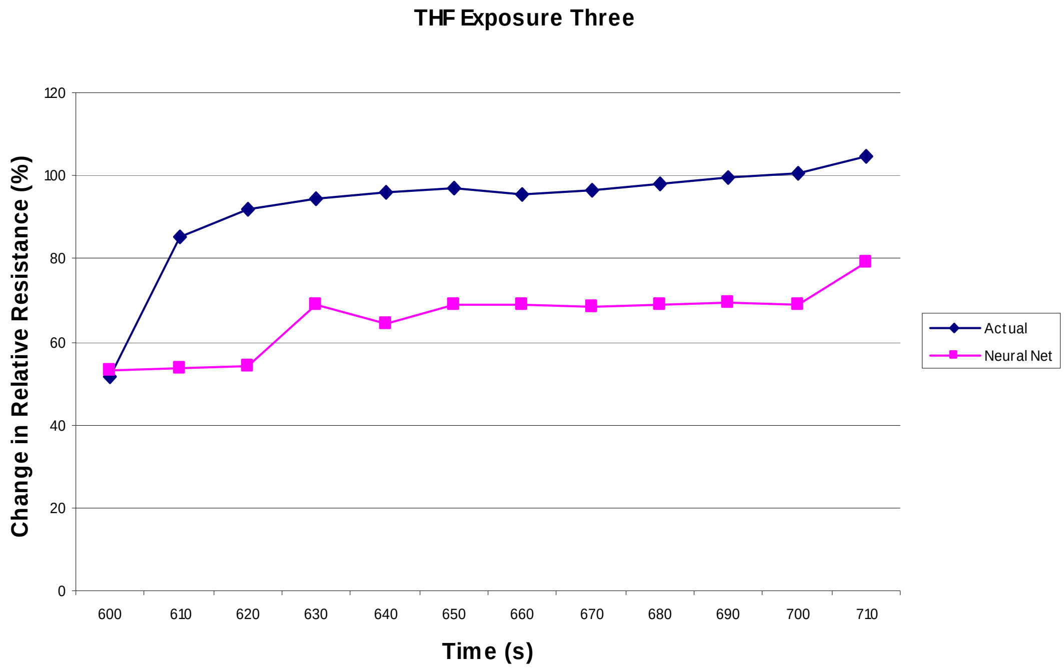
THF Exposure Three
Change in Relative Resistance (%)
0
20
40
60
80
100
120
600
610
620
630
640
650
660
670
680
690
700
710
Time (s)
Actual
Neural Net

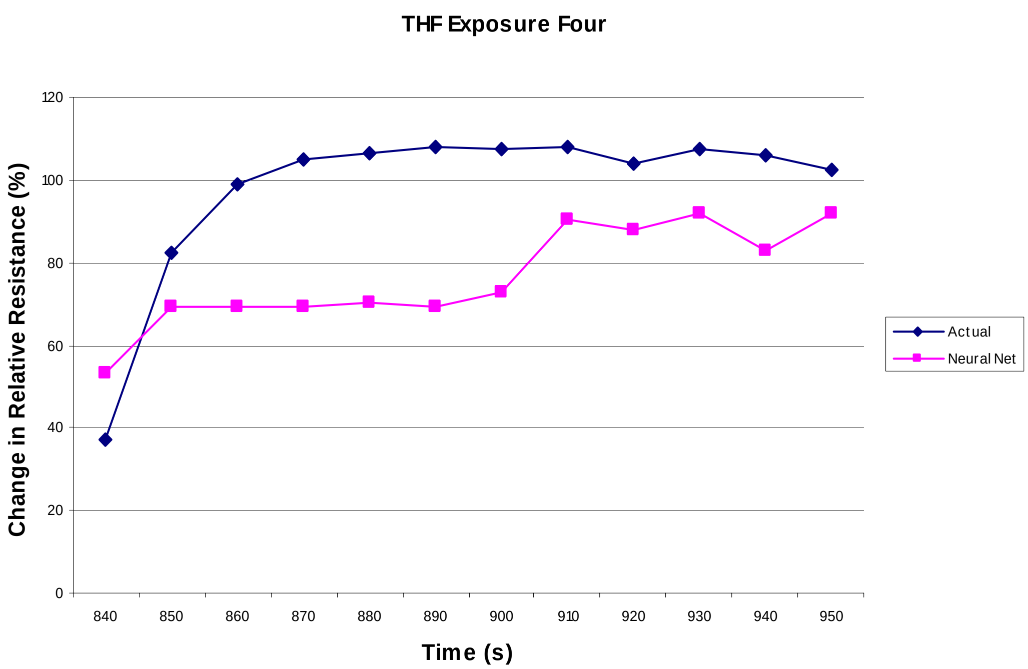
THF Exposure Four
Change in Relative Resistance (%)
0
20
40
60
80
100
120
840
850
860
870
880
890
900
910
920
930
940
950
Time (s)
Actual
Neural Net

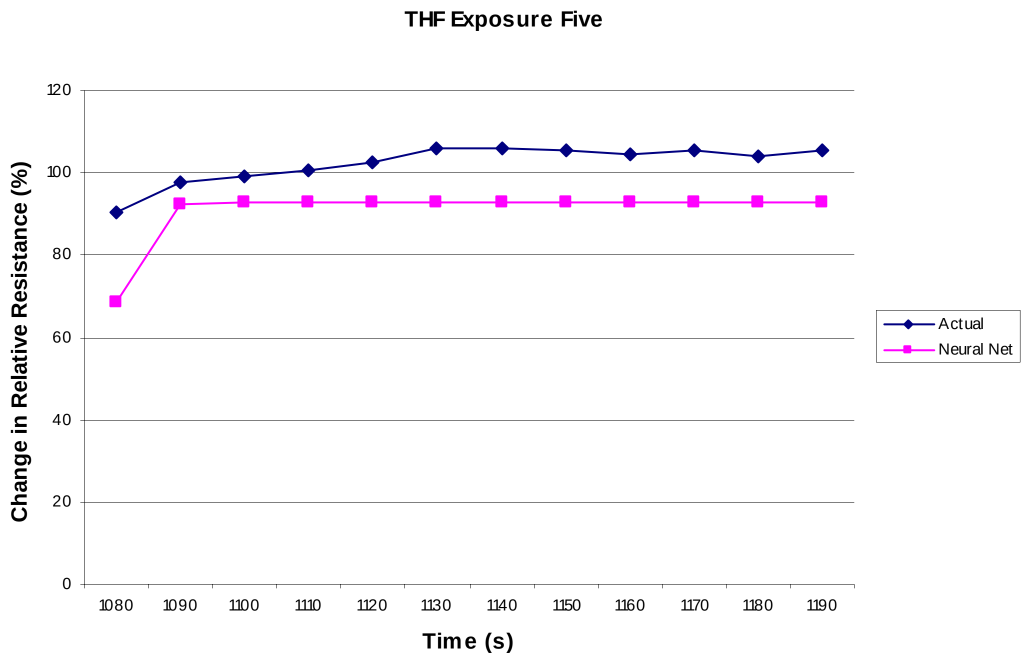
THF Exposure Five
Change in Relative Resistance (%)
120
100
80
60
40
20
0
1080
1090
1100
1110
1120
1130
1140
1150
1160
1170
1180
1190
Time (s)
Actual
Neural Net

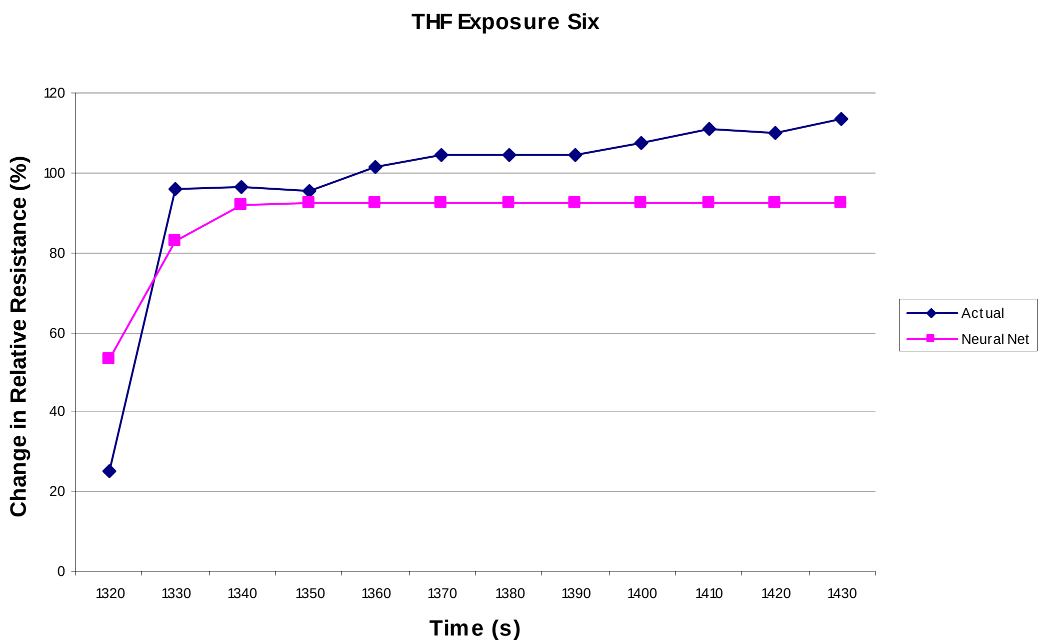
THF Exposure Six
Change in Relative Resistance (%)
120
100
80
60
40
20
0
1320
1330
1340
1350
1360
1370
1380
1390
1400
1410
1420
1430
Time (s)
Actual
Neural Net

Phase Four:

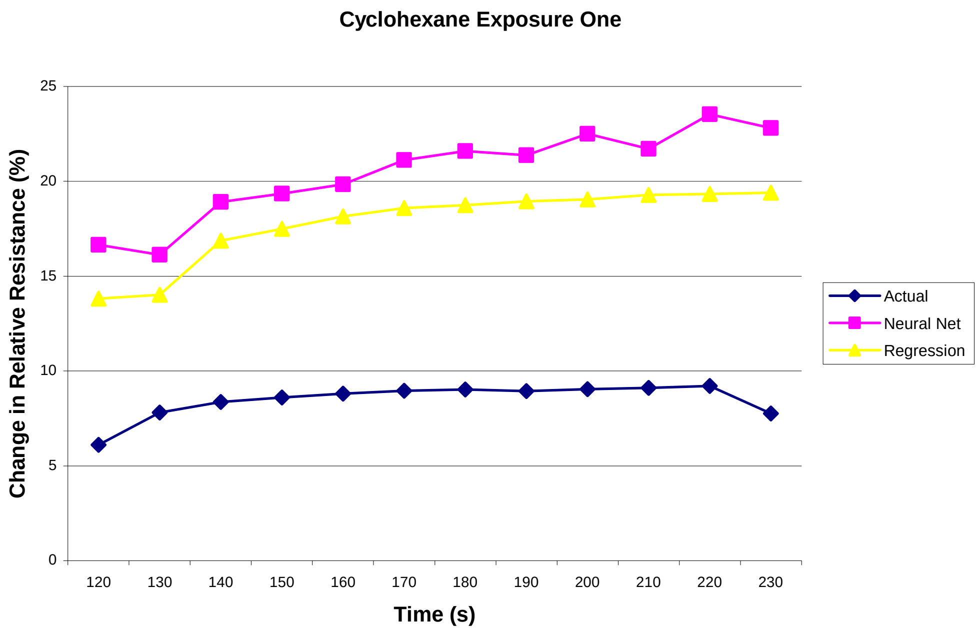

Cyclohexane Exposure One
Change in Relative Resistance (%)
25
20
15
10
5
0
120
130
140
150
160
170
180
190
200
210
220
230
Time (s)
Actual
Neural Net
Regression

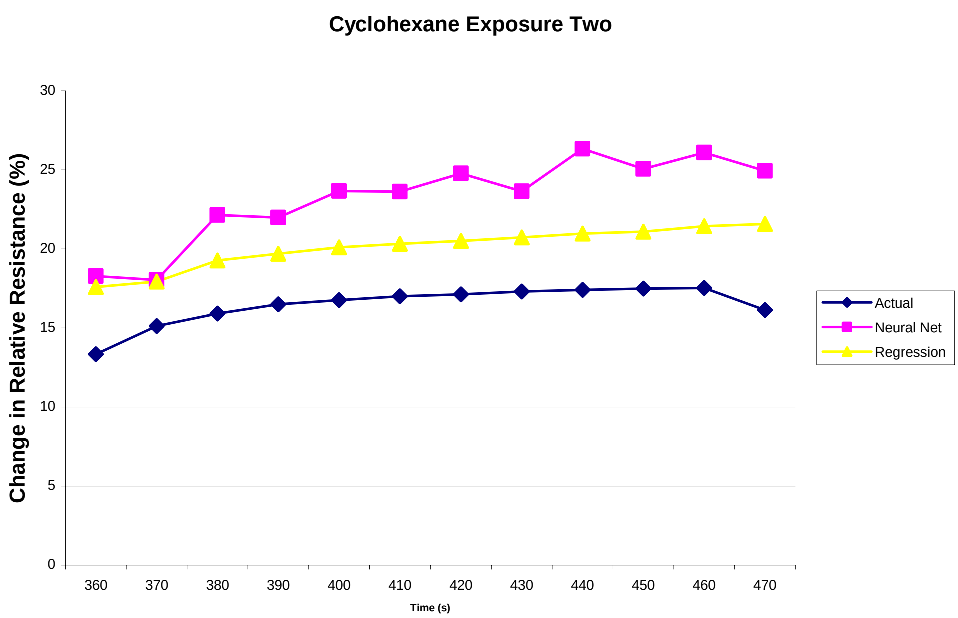

Cyclohexane Exposure Two
Change in Relative Resistance (%)
30
25
20
15
10
5
0
360
370
380
390
400
410
420
430
440
450
460
470
Time (s)
Actual
Neural Net
Regression

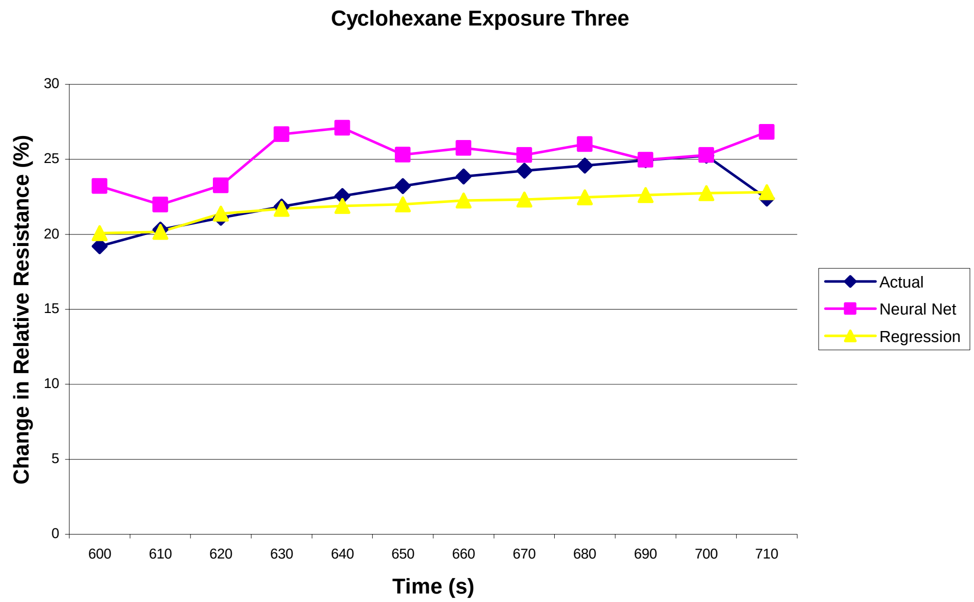
Cyclohexane Exposure Three
Change in Relative Resistance (%)
30
25
20
15
10
5
0
600
610
620
630
640
650
660
670
680
690
700
710
Time (s)
Actual
Neural Net
Regression

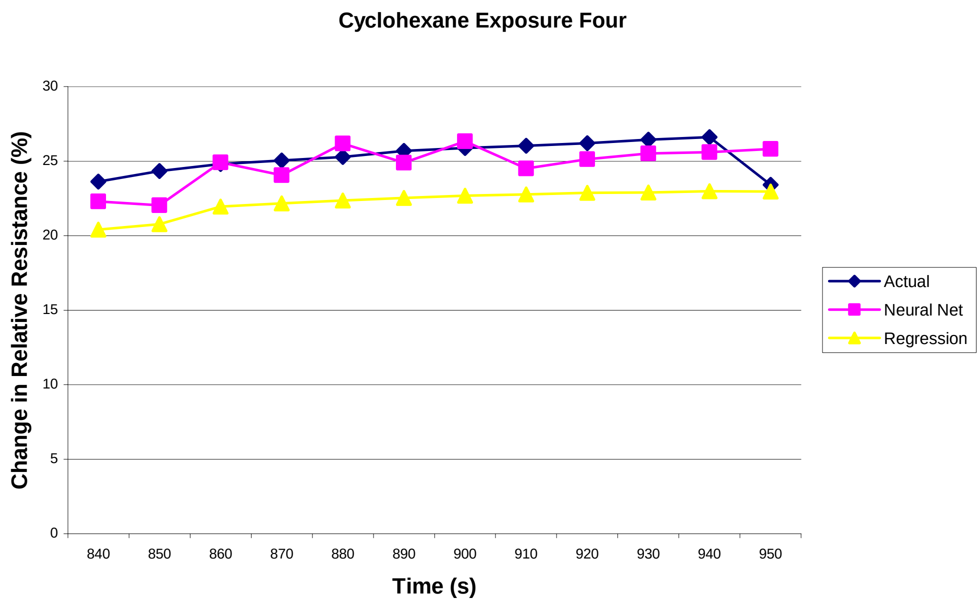
Cyclohexane Exposure Four
Change in Relative Resistance (%)
30
25
20
15
10
5
0
840
850
860
870
880
890
900
910
920
930
940
950
Time (s)
Actual
Neural Net
Regression

Cyclohexane Exposure Five

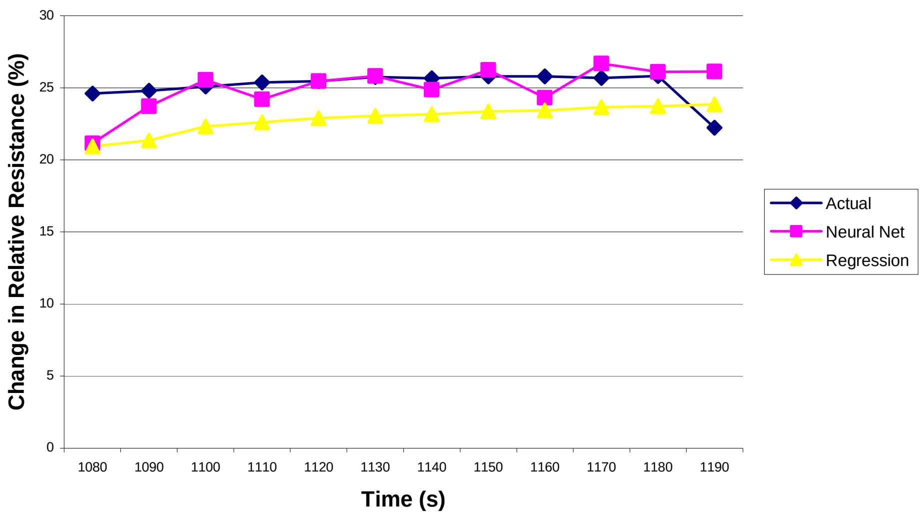

Ethanol Exposure One

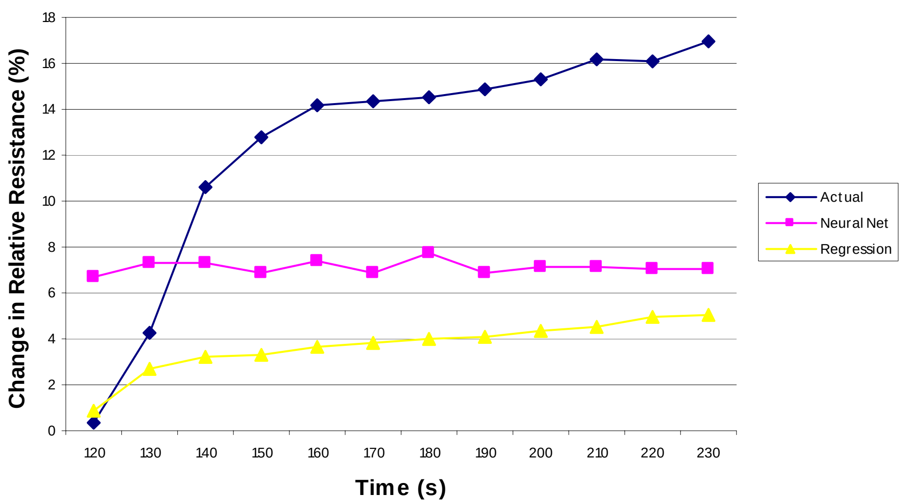

Ethanol Exposure Two

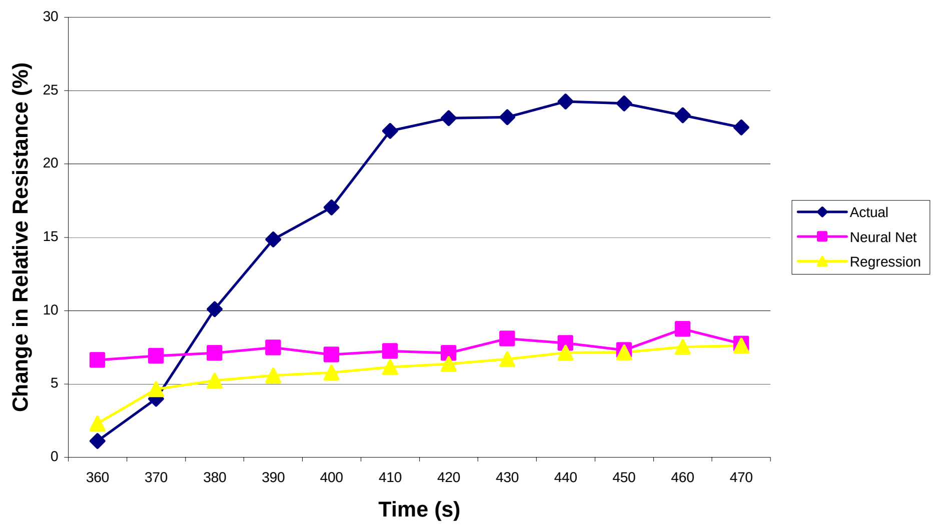

Ethanol Exposure Three

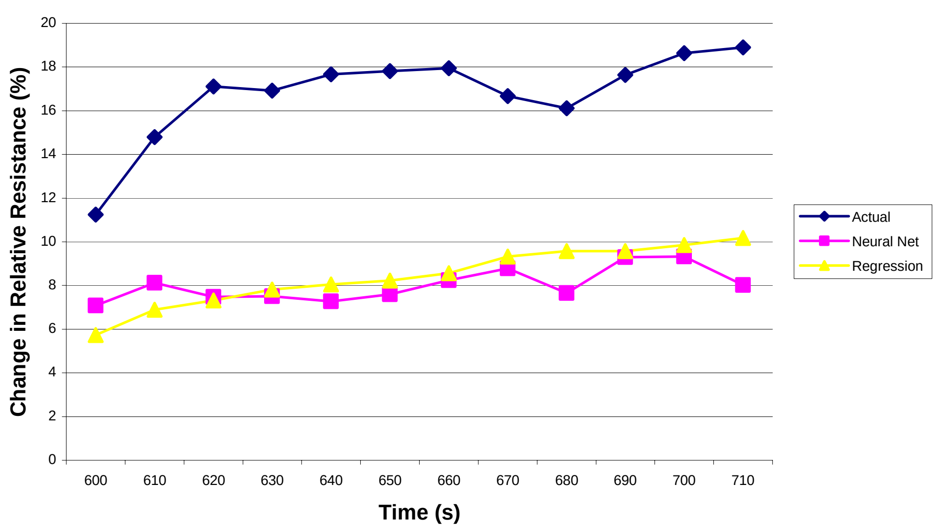

Ethanol Exposure Four

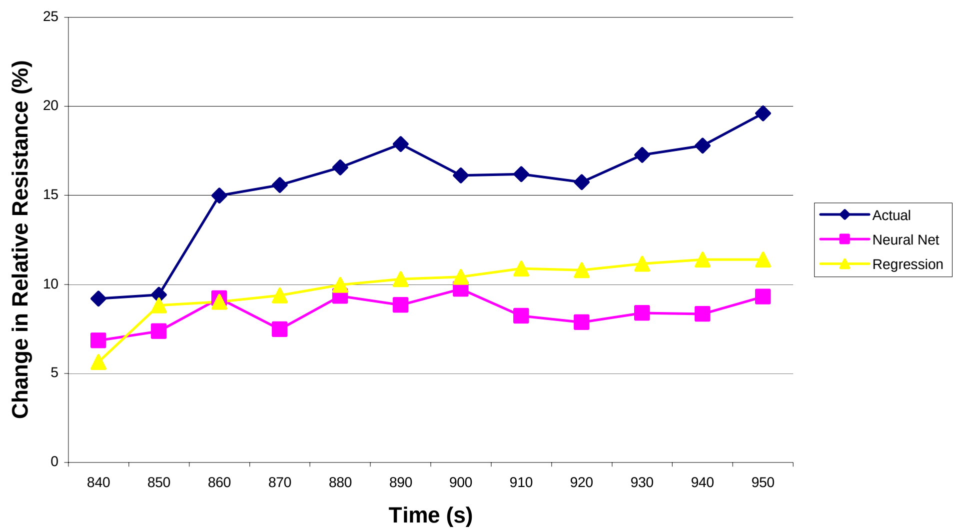

Ethanol Exposure Five

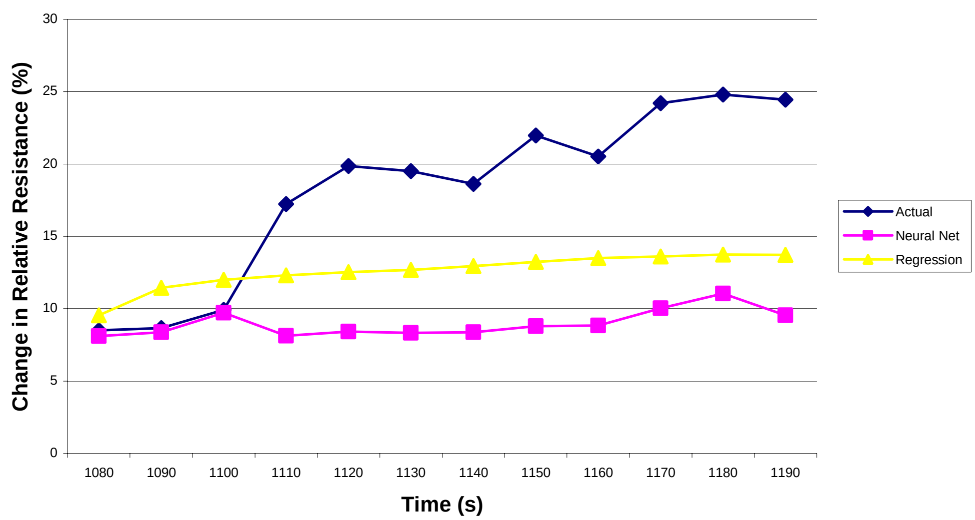

THF Exposure One

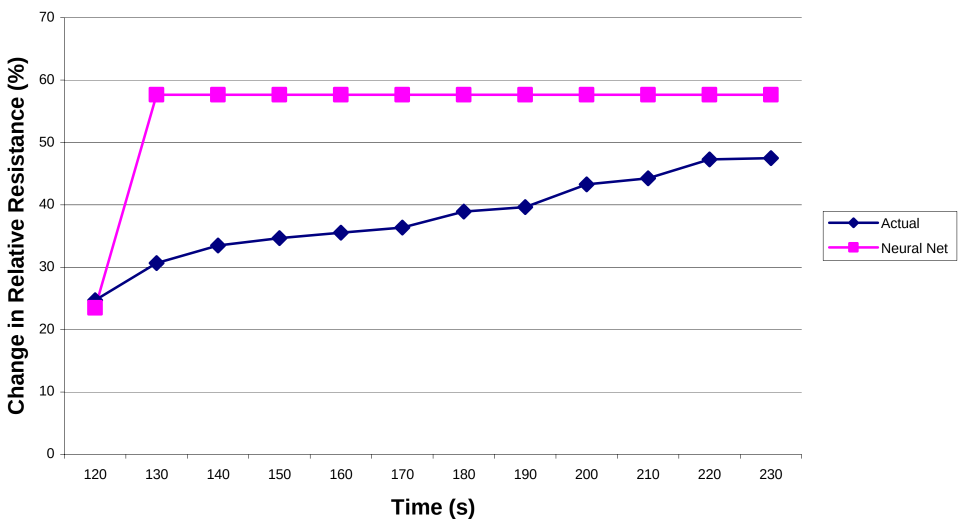

THF Exposure Two

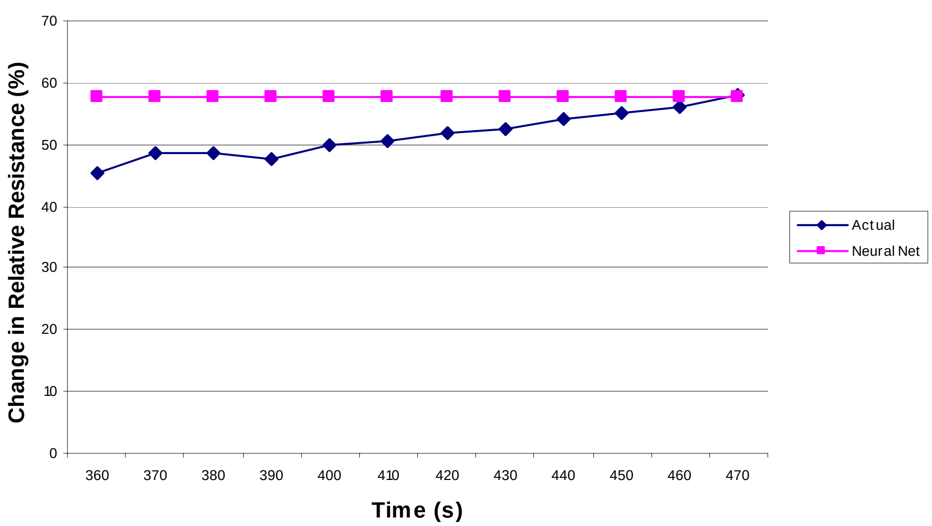

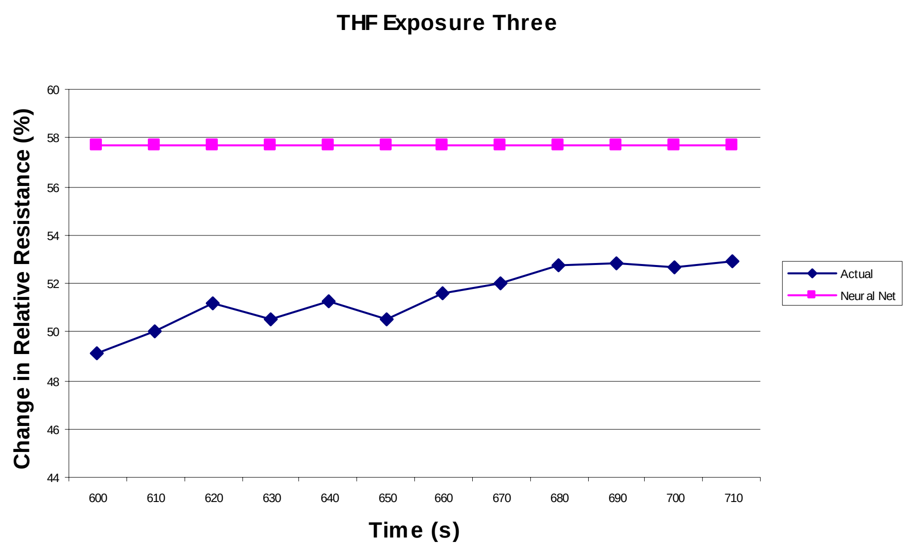
THF Exposure Three
Change in Relative Resistance (%)
60
58
56
54
52
50
48
46
44
600
610
620
630
640
650
660
670
680
690
700
710
Time (s)
Actual
Neural Net

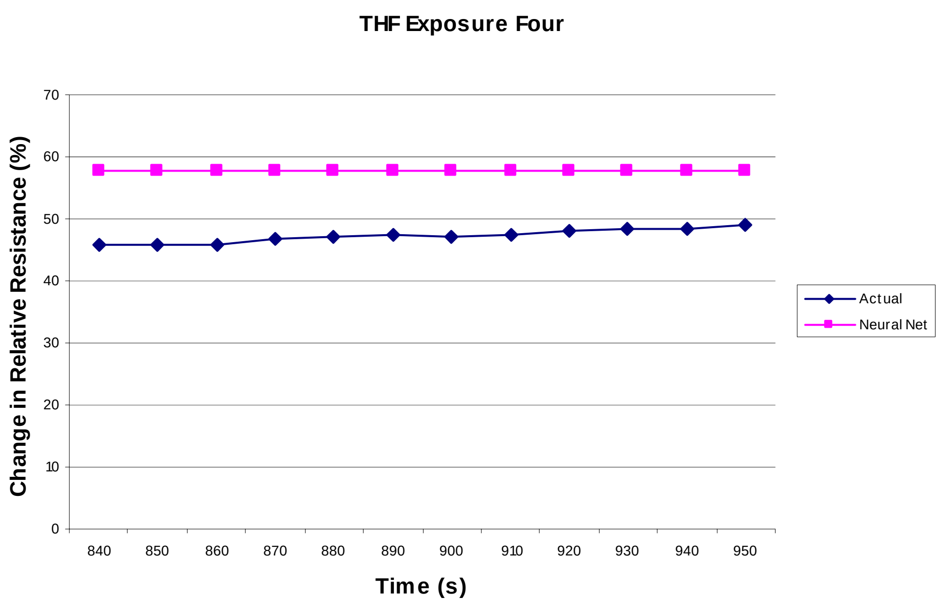
THF Exposure Four
Change in Relative Resistance (%)
70
60
50
40
30
20
10
0
840
850
860
870
880
890
900
910
920
930
940
950
Time (s)
Actual
Neural Net

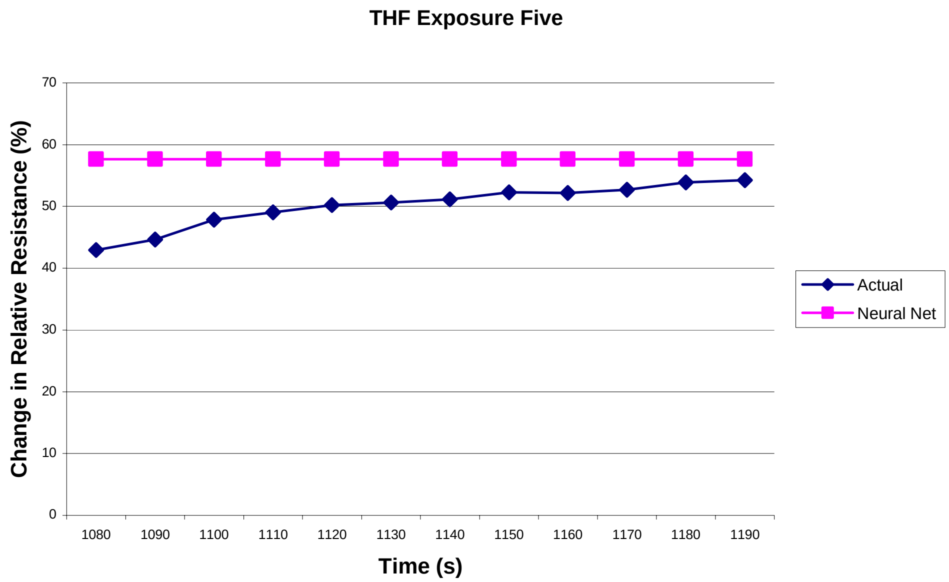

THF Exposure Five
Change in Relative Resistance (%)
70
60
50
40
30
20
10
0
1080
1090
1100
1110
1120
1130
1140
1150
1160
1170
1180
1190
Time (s)
Actual
Neural Net

Bibliography

AFCESA/CEXR. "Joint NBC Reconnaissance System Fact Sheet". Electronic Message. 1615EST, 3 January 2006.

AFRL/MLPJE. Detector Platform Photos. Electronic Message. 1124EST, 24 February 2006.

Aslan, Ismail. *Selecting Salient Features in High Feature to Exemplar Ratio Conditions*. MS Thesis, AFIT/GOR/ENS/02-02. School of Engineering and Management, Air Force Institute of Technology (AU), Wright-Patterson AFB OH, March 2002.

Bauer, Kenneth W., Jr., Stephen G. Alsing, and Kelly A. Greene. "Feature Screening using Signal-to-Noise Ratios," *Neurocomputing*, 31: 29-44 (2000).

Bauer, Kenneth W., Jr. Class Notes, OPER 685, Applied Multivariate Data Analysis. Air Force Institute of Technology, Wright Patterson AFB OH, Spring 2005a.

Bauer, Kenneth W., Jr. Class Notes, OPER 685, Applied Multivariate Data Analysis: Neural Networks. Air Force Institute of Technology, Wright Patterson AFB OH, Spring 2005b.

"Carbon Nanotube Sensors for Gas Detection". NASA: Ames Research Center. n. pag. http://www.nasa.gov/centers/ames/research/technology-onepagers/gas_detection.html. 15 November 2005.

Cook, Greg. "MINICAMS®". O.I. Analytical, CMS Field Products. Product Briefing. 6 February 2006.

Department of the Air Force (DAF). *Civil Engineer Readiness Technician's Manual for Nuclear, Biological, and Chemical Defense*. AFMAN 32-4017. Washington: HQ USAF, 29 May 2003.

Department of Defense (DoD). *Chemical and Biological Defense Program Annual Report to Congress 2005*. Annual. http://www.acq.osd.mil/cp. 15 November 2005.

Department of Defense (DoD). *M256 Series Chemical Agent Detector Kit*. Information paper. n. pag. (12 July 1999) http://www.gulflink.osd.mil/m256/index.htm. 19 November 2005.

Dillon, William R. and Matthew Goldstein. *Multivariate Analysis Methods and Applications*. New York: John Wiley & Sons, Inc., 1984.

Draeger Safety. Civil Defense Simultest (CDS) Kit. Powerpoint. n. pag. http://www.draeger.com/ST/internet/pdf/US/detection/CDSKitQI.pdf. 6 December 2005.

Doleman, Brett J., Marc C. Lonergan, Erik J. Severin, Thomas P. Vaid, and Nathan S. Lewis. "Quantitative Study of the Resolving Power of Arrays of Carbon Black-Polymer Composites in Vapor-Sensing Tasks," *Analytical Chemistry*, 70: 4177-4190 (1998).

Edgewood Chemical Biological Center (ECBC). "CBRN Unmanned Ground Reconnaissance (CUGR) Advanced Concept Technology Demonstration (ACTD)". Brochure. n. pag. http://www.edgewood.army.mil/ps/download/CUGR_Brochure.pdf. 31 January 2006.

The Foxboro Company. *TVA-1000*. Product Manual. Foxboro: The Foxboro Company. February 1995.

Harris, Peter J.F. *Carbon Nanotubes and Related Structures*. Cambridge: Cambridge University Press, 1999.

Hill, Herbert H., Jr. and Stephen J. Martin. "Conventional Analytical Methods for Chemical Warfare Agents," *Pure and Applied Chemistry*, 74: 2281-2291 (2002).

Hopkins, Alan R. and Nathan S. Lewis. "Detection and Classification Characteristics of Arrays of Carbon Black, Organic Polymer Composite Chemiresistive Vapor Detectors for the Nerve Agent Simulants Dimethylmethylphosphate and Diisopropylmethylphosponate". *Analytical Chemistry*, 73: 884-892(2001).

Huber, Richard L. AF CBRN Equipment Manager. HQ AFCESA/CEXR. Personal Interview. 31 January 2006.

Johnson, Richard A. and Dean W. Wichern. *Applied Multivariate Statistical Analysis*. Upper Saddle River: Prentice-Hall, 2002.

Joint Program Executive Office for Chemical and Biological Defense (JPEO-CBD). "M22 Automatic Chemical Agent Detection Alarm (ACADA)". Products page. n. pag. http://www.jpeocbd.osd.mil/ca_acada.htm. 19 November 2005.

Kong, Jing, Nathan R. Franklin, Chongwu Zhou, Michael G. Chapline, Shu Peng, Kyeongjae Cho, and Hongjie Dai. "Nanotube Molecular Wires as Chemical Sensors". *Science*, 287:622-625(2000).

Laljer, Charles E. *Joint Chemical Agent Detector (JCAD): The Future of Chemical Agent Detection*. Article. n. pag. http://www.dtic.mil/ndia/11ground/laljer.pdf. 15 November 2005.

Langford, R. E. *Introduction to Weapons of Mass Destruction*. Hoboken: John Wiley & Sons, Inc., 2004.

Li, Jing, Yijiang Lu, Qi Ye, Martin Cinke, Jie Han, and M. Meyyappan. "Carbon Nanotube Sensors for Gas and Organic Vapor Detection". *Nano Letters*, 3:929-933(2003).

Lonergan, Mark C., Erik J. Severin, Brett J. Doleman, Sara A. Beaber, Robert H. Grubbs, and Nathan S. Lewis. "Array-Based Vapor Sensing Using Chemically Sensitive, Carbon Black-Polymer Resistors". *Chem. Mater.*, 8:2298-2312(1996).

Marine Corps Tactical Systems Support Activity (MCTSSA). "JSLNBCRS Fact Sheet". n. pag. http://www.mctssa.usmc.mil/webserver/documents/datasheets/JSLNBCRS%20Fact%20Sheet.pdf. 31 January 2006.

Montgomery, Douglas C. *Introduction to Statistical Quality Control*. Hoboken: John Wiley & Sons, Inc., 2005.

Montgomery, Douglas C., Elizabeth A. Peck, and G. G. Vining. *Introduction to Linear Regression Analysis*. New York: John Wiley & Sons, Inc., 2001.

"Nanotube chemical sensor gains speed". *Technology Research News*. Article. n. pag. (April 2005). http://trnmag.com/Stories/2005/042005/Nanotube_chemical_sensor_gains_speed_Brief_042005.html. 15 November 2005.

Nelson, Marilyn M. and Illingworth W.T. *A Practical Guide to Neural Nets*. Reading: Addison-Wesley Publishing Company, Inc., 1991.

Organisation for the Prohibition of Chemical Weapons (OPCW). "The Chemical Weapons Convention". Fact page. n. pag. http://www.opcw.org. 3 October 2005.

Prelas, Mark A. and Tushar K. Ghosh. "Chemical Weapon Delivery, Sensors and Detection Systems," *Science and Technology of Terrorism and Counterterrorism*, Public Administration and Public Policy/101: 373-408 (2002).

Rencher, Alvin C. *Methods of Multivariate Analysis*. New York: John Wiley & Sons, Inc., 2002.

Ryan, M.A., A.V. Shevade, H. Zhou, and M.L. Homer. "Polymer-Carbon Black Composite Sensors in an Electronic Nose for Air-Quality Monitoring". *MRS Bulletin*, 29: 714-719 (2004).

Schalkoff, Robert J. *Artificial Neural Networks*. New York: The McGraw Hill Companies, Inc., 1997.

Smith, Murray. *Neural Networks for Statistical Modeling*. Boston: International Thomson Computer Press, 1996.

Sun, Yin and Kwok Y. Ong. *Detection Technologies for Chemical Warfare Agents and Toxic Vapors*. Boca Raton: CRC Press, 2005.

United States Environmental Protection Agency (EPA). *Environmental Technology Verification Program Verification Statement: Field-Portable Gas Chromatograph/Mass Spectrometer*. EPA-VS-SCM-25. Washington: US EPA, November 1998.

Utah Solid and Hazardous Waste Control Board. "CAIS Monitoring Equipment". *Resource Conservation and Recovery Act (RCRA) Hazardous Waste Treatment Part B Permit for Rapid Response System (RRS)*, Attachment 2, Appendix 3:1 (1999).

Wei, Chen. Visiting Scholar in Department of Chemical and Materials Engineering. University of Dayton, Dayton OH. Personal Interview. 23 January 2006.

Wei, Chen, Liming Dai, Ajit Roy, and Tia B. Tolle. "Multifunctional Chemical Vapor Sensors of Aligned Carbon Nanotube and Polymer Composites". *Journal of the American Chemical Society*, ASAP Article 10.1021/ja0570335. n. pag. (13 January 2006). http://pubs.acs.org/cgi-bin/abstract.cgi/jacsat/asap/abs/ja0570335.html. 24 January 2006.

Weisburg, Sanford. *Applied Linear Regression*. Hoboken: John Wiley & Sons, Inc., 2005.

Young, Ian A. *Development of a Pilot Candidate Selection Model Using Multivariate Techniques*. MS Thesis, AFIT/GOR/ENS/02-18. School of Engineering and Management, Air Force Institute of Technology (AU), Wright-Patterson AFB OH, March 2002.

REPORT DOCUMENTATION PAGE			*Form Approved* *OMB No. 074-0188*

1. REPORT DATE *(DD-MM-YYYY)*	**2. REPORT TYPE**	**3. DATES COVERED** *(From – To)*
23-03-2006	**Master's Thesis**	Jun 2005 – Mar 2006

4. TITLE AND SUBTITLE	
Detection and Classification Characteristics of Carbon Nanotube Polymer Composite Chemical Vapor Detectors	**5a. CONTRACT NUMBER**
	5b. GRANT NUMBER
	5c. PROGRAM ELEMENT NUMBER
6. AUTHOR(S)	**5d. PROJECT NUMBER**
Hinshaw, Huynh, A., Captain, USAF	**5e. TASK NUMBER**
	5f. WORK UNIT NUMBER

7. PERFORMING ORGANIZATION NAMES(S) AND ADDRESS(S)	**8. PERFORMING ORGANIZATION REPORT NUMBER**
Air Force Institute of Technology Graduate School of Engineering and Management (AFIT/EN) 2950 Hobson Way WPAFB OH 45433-7765	AFIT/GOR/ENS/06-10
9. SPONSORING/MONITORING AGENCY NAME(S) AND ADDRESS(ES) AFRL/MLPJ Attn: Dr. Rajesh Naik 3005 Hobson Way Bldg 651 WPAFB OH 45433-7702 DSN: 785-3808 x3180	**10. SPONSOR/MONITOR'S ACRONYM(S)** **11. SPONSOR/MONITOR'S REPORT NUMBER(S)**

12. DISTRIBUTION/AVAILABILITY STATEMENT
APPROVED FOR PUBLIC RELEASE; DISTRIBUTION UNLIMITED.

13. SUPPLEMENTARY NOTES

14. ABSTRACT
The first step in combating a chemical weapons threat is contamination avoidance. This is accomplished by the detection and identification of chemical agents. The Air Force has several instruments to detect chemical vapors, but is always looking for lighter, faster, and more accurate technology for a better capability.

This research is focused on using carbon nanotube polymer composite sensors for chemical detection. More specifically, models are developed to classify three sets of sensor data according to vapor using various multivariate techniques. Also, prediction models of a mixed sensor output are developed using neural networks and regression analysis. The classifiers developed are able to accurately classify three vapors for a specific set of data, but have problems when tested against data from aged sensors as well as data generated from a different set of new sensors. These results indicate that further research should be conducted to ensure accuracy in identifying chemical vapors using these types of sensors.

15. SUBJECT TERMS
Carbon Nanotubes, Chemical Detection, Multivariate Analysis, Classification, Neural Networks, Discriminant Analysis

16. SECURITY CLASSIFICATION OF:			**17. LIMITATION OF ABSTRACT**	**18. NUMBER OF PAGES**	**19a. NAME OF RESPONSIBLE PERSON**
					Kenneth W. Bauer, PhD (ENS)
REPORT	ABSTRACT	c. THIS PAGE			**19b. TELEPHONE NUMBER** *(Include area code)*
U	**U**	**U**	**UU**	169	(937) 255-6565, ext 4328; e-mail: Kenneth.Bauer@afit.edu